

PDF issue: 2025-11-02

String Regge trajectory on de Sitter space

竹内, 俊暁

(Degree) 博士 (理学) (Date of Degree) 2023-03-25 (Date of Publication) 2024-03-01 (Resource Type) doctoral thesis (Report Number) 甲第8583号 (URL) https://hdl.handle.net/20.500.14094/0100482331

※ 当コンテンツは神戸大学の学術成果です。無断複製・不正使用等を禁じます。著作権法で認められている範囲内で、適切にご利用ください。



Doctoral Dissertation

String Regge trajectory on de Sitter space

(ド・ジッター時空における弦の Regge 軌跡)

January 2023 Graduate School of Science, Kobe University

> Toshiaki Takeuchi (竹内 俊暁)

Abstract

Cosmic observations revealed that our universe experiences accelerated expansion at the present epoch and in the inflationary era. For string theory to describe our real world, accelerated expansion of the universe should be accommodated in its framework. However realizing a positive vacuum energy expanding our universe has been a challenging issue since the discovery of the cosmological constant. In this thesis, we examine this difficulty in a worldsheet perspective of string theory. More specifically, we study a consistency of a worldsheet theory on de Sitter space (a vacuum solution of Einstein equation with a positive vacuum energy).

Our main focus is on string Regge trajectories. A Regge trajectory is a higher spin tower which dominates in a certain high energy scattering process. In particular, the higher spin tower which has a leading contribution is characterized by a relation, $M^2 = 2(S-2)/\alpha'$, in flat space. Here M and S are mass and spin of higher spin fields, and α' is the inverse of the string tension. Their exchange makes high-energy behavior of scattering amplitudes mild, which is crucial to UV complete gravity in string theory.

These Regge trajectories have a possibility of violating an unitarity bound in de Sitter space. Unitarity indicates that higher spin fields within a mass range, $0 < M^2 < H^2S(S-1)$, are forbidden in de Sitter space. H is an energy scale of de Sitter space. A naive extrapolation of the flat space Regge trajectory implies that an unitarity violation may occur at a certain energy.

To discuss this potential inconsistency rigorously, we study string Regge trajectories on de Sitter space. We begin with reviewing string Regge trajectories in flat space and their importance on UV completion of gravity. We also review higher spin fields on de Sitter space involving the unitarity bound. In the main part, we derive string Regge trajectories on de Sitter space in semiclassical approximation. We also discuss UV completion by resulting Regge trajectories.

Acknowledgements

I would like to express my deepest gratitude to Noumi-san and Soda-san for their guidance. Noumi-san discussed many times with me. His feedback is always positive and is full of physics. I have learned many things from him. Soda-san made our group interactive so that I have enjoyed discussions with the member of our group. Also, his broad interest in science helped me to touch different topics. Besides, I would like to express my special thanks to my collaborators, Kato-san, Isono-san, Siyi-san, and Kanji-kun. Discussions with them were necessary to complete our works. Finally, I would like to thank the members of our group for their supporting.

My research was supported by the Iwanami Fujukai Foundation and the Kobe University SPRING Scholarship.

Contents

1	Intr	roduction	7	
2	$\mathbf{U}\mathbf{V}$	completion in string theory	10	
	2.1	Basics of worldsheet theory	11	
	2.2	String spectrum	12	
	2.3	Veneziano amplitude	20	
	2.4	Regge theory	25	
3	Hig	her spin fields in de Sitter space	2 8	
	3.1	De Sitter space	28	
	3.2	Representation of de Sitter isometry group	31	
	3.3	Higher spin field	33	
	3.4	Implication for higher spin states in string theory	39	
4	Clas	ssical strings on de Sitter space	41	
	4.1	Setup	41	
	4.2	Folded strings	44	
	4.3	Spiky strings	48	
5	Classical strings with internal motion 58			
	5.1	Folded strings with internal motion	58	
	5.2	Spiky strings with internal motion	63	
6	Con	aclusion	67	
\mathbf{A}	Spe	cial functions	69	
	A.1	Orthogonal polynomials	69	
	A.2	Spherical Harmonics	7 1	
В	More on scattering amplitudes 7			
	B.1	Unitarity bounds	76	
	B.2	Partial wave expansion	79	
	В.3	Gravity mediated amplitudes	84	

6 CONTENTS

\mathbf{C}	Massless higher spin theory	87	
	C.1 Spin two example	87	
	C.2 General spin	89	
D Details of spiky strings with internal motion			
	D.1 Derivation of Eq. (5.30)	92	
	D.2 $J = 0$ limit	93	

Chapter 1

Introduction

String theory provides a consistent and tractable formulation of quantum gravity. A study of string theory as quantum gravity started with the finding that the graviton is naturally accommodated in the string spectrum [1,2]. The graviton is represented as a ground state of superstring theory or a first excited state of bosonic string theory. Later, it was found that a UV divergence of loop amplitudes in Einstein gravity is regularized because a worldsheet symmetry introduces a minimum length of the loops [3,4]. This UV finiteness of scattering amplitudes allows us to control gravity with a few parameters. It is also worth noting that microstates of Black hole can be counted precisely in a specific setup [5]. String theory is a unique framework with these favorable properties in our current understanding. This motivates us to have a hope that string theory describes not only a quantum nature of gravity, but also everything of our real world. To investigate this possibilty, realizing observed facts of our universe has been studied extensively.

Cosmic observations revealed that our universe experiences an accelerated expansion at the present epoch and in the inflationary era [6–8]. Hence a positive vacuum energy expanding our universe has been studied in a framework of string theory since the discovery of the cosmological constant. However it remains to be a challenging issue. The difficulty of a positive vacuum energy is summarized in a no-go theorem [9]. This no-go theorem stands on some regular assumptions while a way to evade these assumptions has been developed [10,11]. These developments were combined into a single framework known as KKLT scenario [11], which is a first explicit construction of a positive vacuum energy. Later, another construction known as Large Volume Scenario [12] were also proposed.

Pieces in the scenarios are independently justified although backreactions on each other may break down their validity. This possibility has been discussed in some approximations [13–26]. These analyses indicates that generating a positive vacuum energy consistently is a difficult task (See also a nice review [27]). Also, there are some attempts [28–30] in the swampland program which try to interpret this nontriviality as an obstruction to de Sitter space in string theory.

The recent discussions are based on the supergravity approximation and approximate treatments of internal geometry. To reach a deeper understanding, we have to involve higher quantum corrections or treat six dimensional internal space explicitly, which must be a daunting task. Hence it may be reasonable to develop a complementary approach. In this thesis, we examine a realization of a positive vacuum energy in aspects of a worldsheet theory in de Sitter space.

It is well known that scattering amplitudes of Einstein gravity exhibit an unfavorable UV divergence, which leads to an unitarity violation of S matrix and a non-renormalizability. On the other hand, string theory improves this situation by introducing higher spin states. As a result, scattering amplitudes have a mild UV behavior above the scale where higher spin states appear. This is one realization of a weakly coupled UV completion of gravity. The mildness of a specific high energy scattering is achieved by a higher spin tower characterized by a relation,

$$M^2 = \frac{1}{\alpha'}(S-2). {(1.1)}$$

This higher spin tower is called a Regge trajectory. This Regge trajectory is crucial to UV complete gravity, while having a possibility to introduce an inconsistency against unitarity in de Sitter space. Unitarity indicates that higher spin states within a mass range,

$$0 < M^2 < H^2 S(S-1), (1.2)$$

are forbidden in de Sitter space. This restriction is known as the Higuchi bound [31]. In the Regge trajectory, the mass squared grows linearly as the spin increases. On the other hand, the upper bound of the Higuchi bound grows quadratically. Therefore, if we extrapolate the flat space Regge trajectory to a higher spin region, a contradiction with the Higuchi bound may occur above a certain spin.

To discuss this potential inconsistency in a rigorous way, we study semiclassical spectra of a would-be worldsheet theory in de Sitter space. Our approach is a generalization of developments on integrability in the AdS/CFT correspondence. Semiclassical spectra of worldsheet theory in various curved spacetimes have been studied since seminal works by de Vega and Sanchez in 80's [32, 33] and the followups [34–36]. Researches in this direction have been further boosted with the advent of the AdS/CFT correspondence [37], especially since the Gubser-Klebanov-Polyakov analysis [38] of folded strings [36]. As nicely reviewed in Ref. [39], various semiclassical solutions in AdS were then constructed and studied by using the integrability technique [40–79]. We also discuss high energy scattering in de Sitter space implied by semiclassical spectra.

Organization of this thesis In this thesis, we study a consistency between string Regge trajectories and the Higuchi bound, and discuss an implication for high energy scattering in de Sitter space, based on our paper [80,81]. The organization of this thesis is as follows:

• In Chap. 2, we review how an UV completion of gravity is achieved in string theory. First we summarize basics of the worldsheet theory of bosonic string in Sec. 2.1. And then, we study the string spectrum in Sec. 2.2. We show that the graviton is included in the massless spectrum. Also, infinitely many higher spin states appear above the string scale. for In Sec. 2.3, we examine a four point scattering amplitude of string theory at tree level. We show that this amplitude is milder than gravitational amplitudes in UV due to the infinitely many higher spin states. Finally, we reexamine string scattering amplitudes from the viewpoint of the Regge trajectory in Sec. 2.3. This analysis shows that the Regge trajectory plays a crucial role to make the mild UV behavior in the Regge limit.

- In Chap. 3, we review higher spin field theory in de Sitter space, mainly focusing on the Higuchi bound. First we introduce de Sitter space and its isometry group. And then we construct an irreducible representation of the de Sitter isometry in Sec. 3.2. In Sec. 3.3, we introduce higher spin fields and give a formula to calculate a norm of quantum states. We show that there is a mass range within which a negative norm state appears. This mass range is the Higuchi bound.
- In Chap. 4, we study classical strings in three dimensional de Sitter space (dS_3) , which can be regarded as a subspace of dS_4 . In Sec. 4.1, we summarize a setup of our analysis including a background metric and an ansatz on the worldsheet configuration. In Sec. 4.2, we construct folded string solutions by solving an equation of motion. And we derive a Regge trajectory by examining an energy-spin relation. This subsection is based on one of our papers [80]. Then, we generalize this solution to spiky string solutions in Sec. 4.3. This subsection is based on the other paper [81].
- In Chap. 5, we generalize the solutions in dS_3 to the solutions in $dS_3 \times S_1$, where S_1 can be regarded as a subspace of a internal space. A setup of this chapter is also summarized in Sec. 4.1. In Sec. 5.1, we study folded string solutions and derive the corresponding Regge trajectory. In Sec. 5.2, we study spiky string solutions similarly. Several technical details are written in Appendix. D. This chapter is also based on our paper [81].
- In Chap. 6, we close this thesis with concluding remarks. In particular, we discuss an implication for high energy scattering and inflation.

Chapter 2

UV completion in string theory

One obstacle to formulating quantum gravity is that Einstein gravity does not preserve unitarity in a perturbative manner. This means that we have to involve quantum corrections of all orders and non-perturbative effects if we try to quantize Einstein gravity straightforwardly. To examine this, let us consider Einstein gravity with a minimally coupled scalar field. A $2 \rightarrow 2$ scattering amplitude of identical massless scalars at tree level is given by

$$M(s,t) = \frac{1}{M_{\rm pl}^{d-2}} \left(\frac{st}{u} + \frac{su}{t} + \frac{tu}{s} \right), \qquad (2.1)$$

where $M_{\rm pl}$ is the Planck mass, and s,t,u are the Mandelstam variables. ¹ See Appendix. B.3 for the derivation. Also, d is a spacetime dimension. The amplitude exhibits a quadric divergence at the hard scattering limit,

$$s \to \infty$$
, s/t : fixed (2.3)

This behavior indicates that an unitarity bound is violated at a certain scale, which is given by,

$$M(s,t) \le C \cdot s^{\frac{4-d}{2}},\tag{2.4}$$

where C is a constant. We note that the bound (2.4) does not tell us an energy scale where Einstein gravity violates the unitarity. However, by analyzing an unitarity constraint more carefully, one can see that the unitarity is violated around the Planck scale, which we will show in Appendix. B.1.

String theory improves the high energy behavior of gravity by introducing higher spin states. In the closed string theory, higher spin states appear at the string scale $M_s = 2/\sqrt{\alpha'}$, where α' represents the inverse of the string tension. Above the string scale, these higher spin states make scattering amplitudes mild. For example, a hard scattering limit of a four point amplitude is

$$M(s,t) \simeq (\alpha' s)^{-3} e^{-\frac{\alpha'}{2} s \left(-\sin^2\frac{\theta}{2} \ln \sin^2\frac{\theta}{2} - \cos^2\frac{\theta}{2} \ln \cos^2\frac{\theta}{2}\right)}$$
 (2.5)

$$s = -(p_1 + p_2)^2, t = -(p_1 - p_3)^2, u = -(p_1 - p_4)^2,$$
 (2.2)

where p_1 and p_2 are momentums in an initial state, and p_3 and p_4 are momentums in a final state.

¹We use the mostly + convention for the metric. And, the Mandelstam variables are defined as

The amplitude is damped exponentially above the string scale, so that an unitarity violation does not occur. Another interesting high energy limit is the Regge limit, which is defined as

$$s \to \infty$$
, $t : \text{fixed}$. (2.6)

In this limit, the amplitude behaves as

$$M(s,t) \simeq (\alpha' s)^{2+\alpha' t} \,. \tag{2.7}$$

Notice that t is negative or equals to zero under a physical scattering process. In particular, for negative t, the amplitude also becomes mild above the string scale. We note that this Regge behavior respects a locality bound $M(s,t) < s^2$, which is known as the Froissart-Martin bound [82–84]. The Froissart-Martin bound is only applicable to gapped theories while respecting this bound may be also crucial for a consistency of gapless theories. As seen above, string theory achieves a mildness of scattering amplitudes by higher spin states, and makes gravitational theory consistent with fundamental requirements of quantum field theory. This is one realization of a UV completion of gravity. We comment that there is another scenario of UV completion that this mildness is achieved by quantum corrections of higher orders, which is investigated by an asymptotic safety scenario(originally proposed in [85]).

In this chapter we review the referred properties of string theory. First we summarize basics of the worldsheet theory in Sec. 2.1. For simplicity, we consider only bosonic closed string theory. In Sec. 2.2, we quantize a worldsheet theory and show its spectra. Next we study a tachyon four point amplitude in Sec. 2.3. We also study its high energy behavior in the hard scattring limit and the Regge limit. In Sec. 2.3, we reexamine the Regge limit from the viewpoint of the Regge theory. The Regge theory is an effecient tool to sum up t-channel exchanges of higher spin states. This analysis tells us that a certain higher spin tower, which is called a Regge trajectory, controls the behavior in the Regge limit.

2.1 Basics of worldsheet theory

First, we summarize basics of string worldsheet theory. A worldsheet is defined by a two dimensional surface embedded in a higher dimensional spacetime, which is called a target space. A worldsheet action of string theory is the Nambu-Goto action,

$$S_{\rm NG} = -\frac{1}{2\pi\alpha'} \int d\tau d\sigma \sqrt{-\dot{X}^2 X'^2 + (\dot{X} \cdot X')^2},$$
 (2.8)

where X represents are coordinates of a target space. τ and σ are worldsheet coordinates. The dot and the prime represents τ derivative and σ derivative respectively. And also, we defined the inner products as

$$\dot{X}^2 = G_{\mu\nu}\dot{X}^{\mu}\dot{X}^{\nu} , \quad X'^2 = G_{\mu\nu}X'^{\mu}X'^{\nu} , \quad \dot{X} \cdot X' = G_{\mu\nu}\dot{X}^{\mu}X'^{\nu} , \tag{2.9}$$

where $G_{\mu\nu}$ is the target space metric. The Nambu-Goto action calculates an area of a worldsheet. This is a natural extension of a particle whose action is given as a length of its world line. While the physical meaning of the Nambu-Goto action is manifest, the action is non-linear even in flat space. Thus, it is convenient to use a classically equivalent action, the Polyakov action,

$$S_{\rm P} = \int d\tau d\sigma \sqrt{|h|} h^{ab} \,\partial_a X \cdot \partial_b X \,, \tag{2.10}$$

where h^{ab} is the worldsheet metric. We can reproduce Eq. (2.8) from the Polyakov action by using an equation of motion for the worldsheet metric. Using this action, we can calculate a transition amplitude by the path integral formulation as,

$$\sum_{\text{topology}} \int D[X, h_{ab}] \,\Psi_{\text{in}}[X, h_{ab}] \,\Psi_{\text{out}}[X, h_{ab}] \,\exp\left[iS_p\right] \,. \tag{2.11}$$

 $\Psi_{\rm in}$ and $\Psi_{\rm out}$ represent in and out states. The intermediate string worldsheet can have various topologies. $\sum_{\rm topology}$ stands for the summation of each contribution. In the real calculation, people often use a trick of replacing the worldsheet metric with an Euclidean metric. This can be regarded as an analytic continuation to an imaginary time. In the Euclidean formulation, the transition amplitude is represented as

$$\sum_{\text{topology}} \int D[X, h_{ab}] \,\Psi_{\text{in}}[X, h_{ab}] \Psi_{\text{out}}[X, h_{ab}] \,\exp\left[-S_p\right] \,. \tag{2.12}$$

The factor in front of the action is changed due to the Wick rotation of the time. The advantage of the Euclidean theory is that we can define the metric better. For a generic topology, the metic becomes singular somewhere in the Lorentzian theory because a timelike coordinate cannot defined globally. In the Euclidean theory, we do not encounter this problem. Below, we use this Euclidean formulation.

2.2 String spectrum

To study a closed string spectrum, let us consider a cylindrical worldsheet. We parametrize the time direction by τ and the space direction by σ (see Fig. 2.1), which are

$$-\infty < \tau < \infty$$
, $0 < \sigma < 2\pi$. (2.13)

This can be regarded as a local coordinate system around an external leg. A physical spectrum should respect worldsheet symmetries. Now there are two gauge symmetries corresponding to a general coordinate transformation and a Weyl transformation. A general coordinate transformation is defined by,

$$\delta x^a = \xi^a \,, \quad \delta h_{ab} = D_a \xi_b + D_b \xi_a \,. \tag{2.14}$$

And, a Weyl transformation is defined by,

$$\delta x^a = 0 \,, \quad \delta h_{ab} = \omega(x) h_{ab} \,. \tag{2.15}$$

To deal with these gauge symmetries, we carry out BRST quantization. First we fix a gauge by choosing a worldsheet metric. A natural choice is a flat metric since a cylinder admits it globally. By introducing complex coordinates,

$$z = \tau + i\sigma, \quad \bar{z} = \tau - i\sigma,$$
 (2.16)

the line element and the action become

$$ds^2 = dz d\bar{z}, \quad S_X = \frac{1}{\pi \alpha'} \int d^2z \partial X \bar{\partial} X.$$
 (2.17)

To fix gauge symmetries in quantum field theory, we have to include a contribution from the path integral measure. This contribution is represented by Grassmann scalar fields as

$$\int D[b,c] e^{-S_{GF}}, \quad S_{GF} = \frac{1}{\pi} \int d^2z \ b\bar{\partial}c + \bar{b}\partial\bar{c}, \qquad (2.18)$$

where c is a Faddeev-Popov ghost field and b is an anti-ghost field. So far, the path integral is formally represented as

$$\int D[X, b, c] e^{-S}, \quad S = S_X + S_{GF}. \tag{2.19}$$

The resulting system has a global symmetry under the following BRST transformations instead of the fixed gauge symmetries,

$$Q_B X^{\mu} = \left(c\partial + \tilde{c}\bar{\partial}\right) X^{\mu}, \quad Q_B c = c\partial c, \quad Q_B b = T_{(m)} + T_{(g)}.$$
 (2.20)

This can be regarded as a transformation of the gauge fixing condition.

Conformal symmetry We fixed the gauge symmetries by choosing the flat metric. However, there is a residual symmetry, a conformal symmetry, which keeps the metric invariant. The conformal symmetry is defined by the holomorphic transformation,

$$z \to f(z) \,, \tag{2.21}$$

where f(z) is an arbitrary holomorphic function. Under the transformation, the metric becomes

$$h_{z\bar{z}} \to |(\partial f)|^{-2} h_{z\bar{z}}. \tag{2.22}$$

Then, we can carry out the weyl transformation to compensate the change of the metric. Finally, the metric becomes invariant. Notice that if we transform the coordinate by a non-holomorphic function, h_{zz} and $h_{\bar{z}\bar{z}}$ become nonzero. In this case, we cannot absorb the change of the metric by the Weyl transformation.

We note that this conformal symmetry is exact classically, but generically one may have an anomaly in quantum field theory. Indeed, both of the matter sector and the ghost sector have a conformal anomaly. However, if we choose the target space dimension in an appropriate way, the anomalies are cancelled each other.

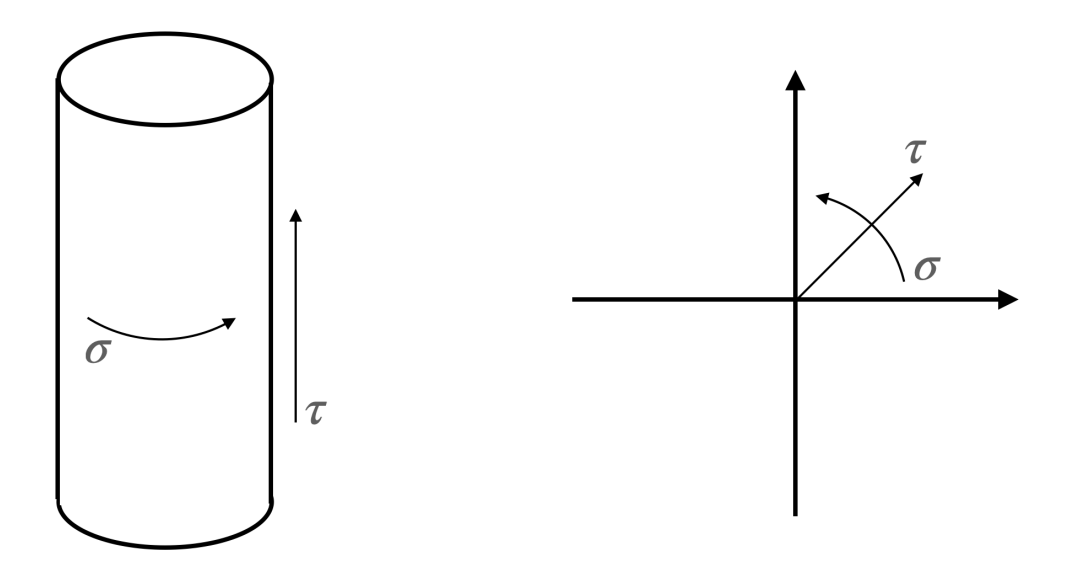


Figure 2.1: The left figure shows a freely propagating string, whose topology is a cylinder. After the conformal transformation (2.25), a cylinder is mapped to a complex plane (the right figure). The time direction corresponds to the radial direction, and the space direction corresponds to the angular direction.

2.2.1 Radial quantization

To quantize a string, it is convenient to introduce a complex plane by using a conformal transformation,

$$z = \tau + i\sigma \to e^{iz} \,. \tag{2.23}$$

The space direction and the time direction of the worldsheet are mapped to the angular direction and the radial direction as illustrated in Fig. 2.1. We quantize the fields by regarding a time coordinate as a radial direction, which is called a radial quantization. A distinctive feature of the radial quantization is that the infinite past is mapped to the origin. A state of the infinite past can be related to a local operator inserted at the origin in the vacuum state. This relation is useful to study a scattering. An interaction of strings is described by inserting a local operator into a worldsheet. For example, let us consider a four point scattering at tree level illustrated in Fig. 2.3. If we carry out the conformal transformation around the legs, the legs shrinks to points, and then this scattering amplitude is described by a sphere with four local operators.

In the rest of this subsection, we summarize quantization conditions of the fields, construct conserved charges of the worldsheet symmetries and define a vacuum state.

Quantization conditions In this paragraph, we summarize quantization conditions. First let us consider the matter sector. The equation motion $\partial \bar{\partial} X(z,\bar{z}) = 0$ indicates that $\partial X(z,\bar{z})$ is a holomorphic function and $\bar{\partial} X(z,\bar{z})$ is an anti-holomorphic function. Therefore, we can expand the

fields as

$$\partial X^{\mu}(z,\bar{z}) = -i\sqrt{\frac{\alpha'}{2}} \sum_{n} \frac{\alpha^{n}}{z^{n+1}}, \quad \bar{\partial} X^{\mu}(z,\bar{z}) = -i\sqrt{\frac{\alpha'}{2}} \sum_{n} \frac{\tilde{\alpha}^{n}}{\bar{z}^{n+1}}, \tag{2.24}$$

After integration, we obtain

$$X^{\mu}(z,\bar{z}) = x^{\mu} - i\sqrt{\frac{\alpha'}{2}}\alpha_0^{\mu} \ln z\bar{z} + i\sqrt{\frac{\alpha'}{2}} \sum_{n \neq 0} \frac{1}{n} \left(\frac{\alpha_n}{z^n} + \frac{\tilde{\alpha}_n}{\bar{z}^n} \right) , \qquad (2.25)$$

where x^{μ} is a constant. Here we imposed $\alpha_0^{\mu} = \tilde{\alpha}_0^{\mu}$ so that $(\alpha_0^{\mu} - \tilde{\alpha}_0^{\mu}) \ln(z/\bar{z})$ term vanishes. This is because this term yields an unphysical branch cut. After quantization, the coefficients are replaced by operators with the commutation relations,

$$[\alpha_m^{\mu}, \alpha_n^{\nu}] = [\tilde{\alpha}_m^{\mu}, \tilde{\alpha}_n^{\nu}] = m\delta_{m+n,0}, \quad [x^{\mu}, p^{\nu}] = i\eta^{\mu\nu},$$
 (2.26)

where we introduced a momentum as,

$$p^{\mu} = \sqrt{\frac{2}{\alpha'}} \alpha_0^{\mu} \,. \tag{2.27}$$

Next, let us consider the ghost sector. The equation of motion becomes

$$\bar{\partial}b = \bar{\partial}c = \partial\tilde{b} = \partial\tilde{c} = 0, \qquad (2.28)$$

which means that b and c are holomorphic, and also \tilde{b} and \tilde{c} are anti-holomorphic. Therefore, we can expand the operators as

$$b(z) = \sum_{n} \frac{b_n}{z^{n+2}}, \quad c(z) = \sum_{n} \frac{c_n}{z^{n-1}}, \quad \tilde{b}(z) = \sum_{n} \frac{\tilde{b}_n}{z^{n+2}}, \quad \tilde{c}(z) = \sum_{n} \frac{\tilde{c}_n}{z^{n-1}}$$
 (2.29)

Similarly to the matter sector, the commutation relations become

$$\{b_m, c_n\} = \delta_{m+n,0}, \quad \{\tilde{b}_m, \tilde{c}_n\} = \delta_{m+n,0}$$
 (2.30)

Conformal generators Let us construct conformal generators explicitly. The conformal transformation is generated by an arbitrary holomorphic function. It is convenient to consider the following conformal transformation and a corresponding generator,

$$z \to z + \epsilon z^{n+1}$$
, $G_n = z^{n+1}\partial + \bar{z}^{n+1}\bar{\partial}$. (2.31)

These generators produce an algebra,

$$[G_m, G_n] = (m-n)G_{m+n}$$
. (2.32)

Note that the holomorphic part and the anti-holomorphic part are not mixed. Hence it is often convenient to deal with these separately as,

$$L_n = z^{n+1}\partial, \quad \bar{L}_n = \bar{z}^{n+1}\bar{\partial}.$$
 (2.33)

These generators are commute each other and satisfy the same algebra as (2.32),

$$[L_m, L_n] = (m-n)L_{m+n}, \quad [\bar{L}_m, \bar{L}_n] = (m-n)\bar{L}_{m+n}.$$
 (2.34)

Next we construct a representation for operators. Let us begin with the translation (n = -1). The standard Noether's method says that its corresponding conserved current is defined through a gauged translation,

$$z \to z + \epsilon(z, \bar{z})$$
. (2.35)

A variation of the action under this transformation is given by

$$\delta S = -\int \frac{d^2z}{\pi} \,\bar{\partial}\epsilon(z,\bar{z}) \cdot T_{zz} + \partial\epsilon(z,\bar{z}) \cdot T_{z\bar{z}} + \partial\bar{\epsilon}(z,\bar{z}) \cdot T_{\bar{z}\bar{z}} + \bar{\partial}\bar{\epsilon}(z,\bar{z}) \cdot T_{z\bar{z}}, \qquad (2.36)$$

where $T_{\mu\nu}$ is the energy momentum tensor. If the parameter ϵ is a constant, the transformation reduces to just a translation and the variation vanishes. Also, the variation of the action should vanish when we use the equation of motion. This requires a conservation law,

$$\bar{\partial}T_{zz} + \partial T_{z\bar{z}} = \partial T_{\bar{z}\bar{z}} + \bar{\partial}T_{z\bar{z}} = 0. \tag{2.37}$$

To derive the conservation law, we integrated by parts. The above argument holds for any translation invariant theories but becomes simplified for a conformally invariant theory. Let us take $\epsilon(z,\bar{z}) = \epsilon(z)$, which is nothing but a conformal transformation. Hence the action should vanish under this transformation. This requires

$$T_{z\bar{z}} = 0. (2.38)$$

And consequently, the conservation law becomes

$$\bar{\partial}T_{zz} = \partial T_{\bar{z}\bar{z}} = 0. \tag{2.39}$$

Thus only T_{zz} and $T_{\bar{z}\bar{z}}$ are non-zero, and these are a holomorphic function and an anti-holomorphic function respectively. Below we use the following shorthand notation,

$$T(z) = T_{zz} \quad \bar{T}(\bar{z}) = T_{\bar{z}\bar{z}}. \tag{2.40}$$

Next let us consider a general conformal transformation,

$$z \to z + \epsilon(z, \bar{z})z^n \,. \tag{2.41}$$

A variation of the action is calculated by using Eq. (2.36) as

$$\delta S = -\int \frac{d^2 z}{\pi} \, \bar{\partial} \epsilon(z, \bar{z}) \cdot z^{n-1} T(z) + \partial \bar{\epsilon}(z, \bar{z}) \cdot \bar{z}^{n-1} \bar{T}(\bar{z}) \,. \tag{2.42}$$

Therefore, conserved currents are given by the energy momentum tensor. The conformal generators are defined as

$$L_n = \oint dz z^{n-1} T(z) , \quad \bar{L}_n = \oint d\bar{z} \bar{z}^{n-1} \bar{T}(\bar{z}) . \tag{2.43}$$

We can calculate the currents and the charges by using the definition above. First, we summarize them for the matter sector.

$$T^{(m)} = -\frac{1}{\alpha'} \eta_{\mu\nu} \partial X^{\mu} \partial X^{\nu} , \qquad (2.44)$$

$$L_n^{(m)} = \frac{1}{2} \sum_m \eta_{\mu\nu} : \alpha_m^{\mu} \alpha_{n-m}^{\nu} :, \qquad (2.45)$$

Here we introduced the normal ordering :: that creation operator are to the left of annihilation operators. Using Eq. (2.45), we can calculate the commutation relations as,

$$[L_m^{(m)}, L_n^{(m)}] = (m-n)L_{m+n}^{(m)} + \frac{D-2}{12}(m^3 - m)\delta_{m+n,0}.$$
(2.46)

Comparing the algebra, we can find the extra term which is an effect of a conformal anomaly.

For the ghost sectors,

$$T^{(g)} = -2b\partial c - \partial b \cdot c, \qquad (2.47)$$

$$L_m^{(g)} = \sum_{n} (2m - n) : b_n c_{m-n} : +a^{(g)} \delta_{m,0}, \qquad (2.48)$$

where $a^{(g)}$ is a constant coming from the normal ordering, which is fixed as $a^{(g)} = -1$ later. The commutation relations become

$$[L_m^{(g)}, L_n^{(g)}] = (m-n)L_{m+n}^{(g)} - \frac{1}{6}(m^3 - m)\delta_{m+n,0}.$$
(2.49)

The ghost theory also has a conformal anomaly. However, interestingly, the anomalies are cancelled between the matter sector and the ghost sector if we choose D=26. Bosonic string theory is defined consistently only in 26 dimensional spacetime.

Finally, we define a conformally invariant vacuum $|0\rangle$ as,

$$L_{+1}^{(m)}|0\rangle = L_0^{(m)}|0\rangle = L_{+1}^{(g)}|0\rangle = L_0^{(g)}|0\rangle = 0.$$
 (2.50)

We can introduce this vacuum since both of the matter sector and the ghost sector do not have an anomaly under these transformation. The final equality fixes $a^{(g)}$ as $a^{(g)} = -1$. Also, operators should be regular at the origin, which requires

$$p^{\mu}|0\rangle = \alpha_{n>1}^{\mu}|0\rangle = b_{n\geq -1}|0\rangle = c_{n\geq 2}|0\rangle = 0.$$
(2.51)

We note that this vacuum is not a ground state of L_0 because c_1 lowers an eigenvalue. The ground state is given by

$$|gr\rangle = c_1|0\rangle. \tag{2.52}$$

BRST charge To close this subsection, we construct the BRST charge. Noether's current is calculated by using the transformation rule (2.20) as

$$J_B = cT^{(m)} + bc\partial c. (2.53)$$

We can calculate the BRST charge using the standard Noether method as,

$$Q_B = \sum_{n} c_n L_{-n}^{(m)} + \sum_{m,n} \frac{m-n}{2} : b_{-m-n} c_m c_n : -c_0.$$
 (2.54)

2.2.2 Physical state

At last, we study physical states of the closed string. Physical state should be invariant under the conformal transformation. This requires

$$L_0|\mathrm{ph}\rangle = \bar{L}_0|\mathrm{ph}\rangle = 0.$$
 (2.55)

Notice that $L_0 + \bar{L}_0$ and $L_0 - \bar{L}_0$ are corresponding to time translation and space translation in the cylindrical coordinate system respectively. Let us assume that physical states can be represented by acting raising operators on the L_0 ground state,

(a product of
$$\alpha_{-n}$$
, b_{-n} , c_{-n}) (a product of $\tilde{\alpha}_{-n}$, \tilde{b}_{-n} , \tilde{c}_{-n}) $|k_{\mu}\rangle \otimes |gr\rangle$, (2.56)

where $|k_{\mu}\rangle$ is an eigenstate of p_{μ} defined as

$$|k_{\mu}\rangle = :e^{ikX}:|0\rangle, \quad p_{\mu}|k_{\mu}\rangle = k_{\mu}.$$
 (2.57)

Then, Eq. (2.55) are translated as,

$$\frac{\alpha'}{4}k^2 + N_{osc} - 1 = \frac{\alpha'}{4}k^2 + \tilde{N}_{osc} - 1 = 0, \qquad (2.58)$$

where N_{osc} and \bar{N}_{osc} are called a level which represents a increment of the L_0 and \bar{L}_0 eigenvalues by the creation operators. Note that -1 in Eq. (2.58) comes from the L_0 eigenvalue of the ghost ground state. We find that the mass square is quantized by $4/\alpha'$. Also, the level of the holomorphic part should be equal to the level of the anti holomorphic part, which is called a level matching condition.

The physical state should be also BRST invariant. It is important that BRST invariant states include a null state which has a form, $Q_B|\Phi\rangle$. Such a state is called a BRST exact state. A BRST exact state has a zero norm, and we cannot distinguish states which is different by a BRST exact state. Therefore, we do the following identification

$$|\Psi\rangle \sim |\Psi\rangle + Q_B|\Phi\rangle$$
. (2.59)

Along the above methodology, we study physical states of level 0, level 1 in order below. Finally, we discuss states of a higher level and show a spectrum for symmetric tensorial states.

Level 0 **state** First, let us consider the Level 0 state,

$$|\text{Lv.0}\rangle = |k^{\mu}\rangle \otimes |\text{gr}\rangle.$$
 (2.60)

The level 0 state is a tachyon,

$$\frac{\alpha'}{4}k^2 = 1. {(2.61)}$$

The condition (2.58) is automatically satisfied for the mass (2.61).

Level 1 state Level 1 states can be represented as

$$|\text{Lv. 1}\rangle = \left(e_{\mu\nu}\alpha_{-1}^{\mu}\alpha_{-1}^{\nu} + \beta_{\mu}\alpha_{-1}^{\mu}\tilde{b}_{-1} + \gamma_{\mu}\alpha_{-1}^{\mu}\tilde{c}_{-1} + \bar{\beta}_{\mu}b_{-1}\tilde{\alpha}_{-1}^{\mu} + \bar{\gamma}_{\mu}c_{-1}\tilde{\alpha}_{-1}^{\mu} + \delta b_{-1}\tilde{b}_{-1} + \lambda b_{-1}\tilde{c}_{-1} + \tilde{\lambda}c_{-1}\tilde{b}_{-1} + \kappa c_{-1}\tilde{c}_{-1}\right)|k_{\mu}\rangle \otimes |\text{gr}\rangle.$$
(2.62)

These states are massless,

$$\frac{\alpha'}{4}k^2 = 0. {(2.63)}$$

The BRST transformation for the state (2.62) is given by

 $Q_B|\text{Lv. 1}\rangle$

$$= \sqrt{\frac{\alpha'}{2}} \left[\left(\beta_{\mu} k_{\nu} + k_{\mu} \bar{\beta}_{\nu} \right) \alpha_{-1}^{\mu} \tilde{\alpha}_{-1}^{\nu} + e_{\mu\nu} k^{\mu} c_{-1} \tilde{\alpha}_{-1}^{\nu} + e_{\mu\nu} k^{\mu} \alpha_{-1}^{\nu} \tilde{c}_{-1} + \delta k_{\mu} \alpha_{-1}^{\mu} \tilde{b}_{-1} - \delta k_{\mu} b_{-1} \tilde{\alpha}_{-1}^{\mu} \right. \\ \left. + \lambda k_{\mu} \alpha_{-1}^{\mu} \tilde{c}_{-1} - \bar{\lambda} k_{\mu} c_{-1} \tilde{\alpha}_{-1}^{\mu} + \beta_{\mu} k^{\mu} c_{-1} \tilde{b}_{-1} - \bar{\beta}_{\mu} k^{\mu} b_{-1} \tilde{c}_{-1} + k_{\mu} (\gamma^{\mu} - \bar{\gamma}^{\mu}) c_{-1} \tilde{c}_{-1} \right] |k^{\mu}\rangle \otimes |gr\rangle. \quad (2.64)$$

The states are BRST closed if

$$e_{\mu\nu}k^{\mu} = \beta_{\mu} = \bar{\beta}_{\mu} = \delta = \lambda = \bar{\lambda} = k_{\mu}(\gamma^{\mu} - \bar{\gamma}^{\mu}) = 0.$$
 (2.65)

Also, we identify states which are different by the BRST exact states (2.64). Then, the following conditions are derived,

$$e_{\mu\nu} \sim e_{\mu\nu} + \beta_{\mu}k_{\nu} + k_{\mu}\bar{\beta}_{\nu} \,, \quad \kappa \sim 0 \,.$$
 (2.66)

At the second identification, we chose γ^{μ} and $\bar{\gamma}^{\mu}$ appropriately. As summarized, physical level 1 states are given by

$$|\text{Lv. 1}\rangle = e_{\mu\nu}\alpha^{\mu}_{-1}\tilde{\alpha}^{\nu}_{-1}|k_{\mu}\rangle \otimes |\text{gr}\rangle, \qquad (2.67)$$

$$e_{\mu\nu} \sim e_{\mu\nu} + \beta_{\mu}k_{\nu} + k_{\mu}\bar{\beta}_{\nu} \,, \quad e_{\mu\nu}k^{\nu} = 0 \,.$$
 (2.68)

There are two spin-2 states in level 1. One is the graviton, which is the symmetric traceless part of $e_{\mu\nu}$. Another is the antisymmetric tensorial state. The first condition of (2.68) is a gauge transformation for these states. Also, there is one scalar state, which is the traceless part of $e_{\mu\nu}$. This state is called a dilaton.

Level N state Let us generalize the above analysis to level N states. The following state is a level N state,

$$|\text{Lv. N}\rangle = e_{\mu_1 \cdots \mu_N \bar{\mu}_1 \cdots \bar{\mu}_N} \alpha_{-1}^{\mu_1} \cdots \alpha_{-1}^{\mu_N} \tilde{\alpha}_{-1}^{\bar{\mu}_1} \cdots \tilde{\alpha}_{-1}^{\bar{\mu}_N} |k_{\mu}\rangle \otimes |\text{gr}\rangle. \tag{2.69}$$

The mass square is

$$k^2 = -\frac{4}{\alpha'}(N-1) \ . \tag{2.70}$$

This state is sufficient to know the string spectrum roughly while there are many other combinations of raising operators. The BRST transformation of this state becomes

$$Q_{B}|\text{Lv. N}\rangle = \sqrt{\frac{\alpha'}{2}} c_{-1} e_{\mu_{1} \cdots \mu_{N} \bar{\mu}_{1} \cdots \bar{\mu}_{N}} k^{\mu_{1}} \alpha^{\mu_{2}} \cdots \alpha^{\mu_{N}} \tilde{\alpha}^{\bar{\mu}_{1}} \cdots \tilde{\alpha}^{\bar{\mu}_{N}} |k_{\mu}\rangle \otimes |\text{gr}\rangle$$

$$+ \frac{\alpha'}{2} c_{-2} e_{\mu_{1} \cdots \mu_{N} \bar{\mu}_{1} \cdots \bar{\mu}_{N}} \eta^{\mu_{1} \mu_{2}} \alpha^{\mu_{3}} \cdots \alpha^{\mu_{N}} \tilde{\alpha}^{\bar{\mu}_{1}} \cdots \tilde{\alpha}^{\bar{\mu}_{N}} |k_{\mu}\rangle \otimes |\text{gr}\rangle + \text{perm} + \text{h.c.}, \qquad (2.71)$$

where perm means permutation terms of holomorphic and anti-holomorphic indices, and h.c. means the Hermitian conjugation. To be BRST invariant, physical states should be transverse and traceless,

$$e_{\mu_1 \cdots \mu_N \bar{\mu}_1 \cdots \bar{\mu}_N} \eta^{\mu_1 \mu_2} = e_{\mu_1 \cdots \mu_N \bar{\mu}_1 \cdots \bar{\mu}_N} \eta^{\bar{\mu}_1 \bar{\mu}_2} = e_{\mu_1 \cdots \mu_N \bar{\mu}_1 \cdots \bar{\mu}_N} k^{\mu_1} = e_{\mu_1 \cdots \mu_N \bar{\mu}_1 \cdots \bar{\mu}_N} k^{\bar{\mu}_1} = 0.$$
 (2.72)

Their permutations also vanish. We find that this state includes higher spin states with even spin lower than 2N. The spin 2N state is a traceless part for one holomorphic index and one antiholomorphic index, which satisfy

$$\eta^{\mu_1\bar{\mu}_1} e_{\mu_1\cdots\mu_N\bar{\mu}_1\cdots\bar{\mu}_N} = \text{perm} = 0.$$
(2.73)

The spin 2N-2 state is a double traceless part for two holomorphic index and two antiholomorphic index, which satisfy

$$\eta^{\mu_1\bar{\mu}_1}\eta^{\mu_2\bar{\mu}_2}e_{\mu_1\cdots\mu_N\bar{\mu}_1\cdots\bar{\mu}_N} = \text{perm} = 0, \quad \eta^{\mu_1\bar{\mu}_1}e_{\mu_1\cdots\mu_N\bar{\mu}_1\cdots\bar{\mu}_N} = \text{perm} \neq 0$$
 (2.74)

We can identify lower spin states similarly.

Their spectrum are shown in Fig. 2.2. Massive higher spin states first appear at the scale $\frac{4}{\alpha'}$, which is of level 2. As the level increases, infinitely many higher spin states appear. In particular, the maximum spin of level N states is 2N. These states form a tower called a Regge trajectory, which is characterized by

$$M^2 = -k^2 = \frac{2}{\alpha'}(S-2) . {(2.75)}$$

This Regge trajectory controls the high energy Regge scattering and makes an amplitude mild, which we will show in Sec. 2.3.

2.3 Veneziano amplitude

String theory exhibits a mild high energy behavior due to infinitely higher spin states. This is crucial to UV complete gravity. In this section, we show how higher spin states contribute scattering amplitudes by studying a $2 \to 2$ tachyon scattering. This scattering process is described by a sphere with four legs as depicted in Fig. 2.3. If we carry out the conformal transformation of (2.25), the leg shrinks to a point, where a local operator representing the tachyon state is inserted. We can read these local operators from Eq. (2.60) as

$$e^{ikX(z,\bar{z})}, (2.76)$$

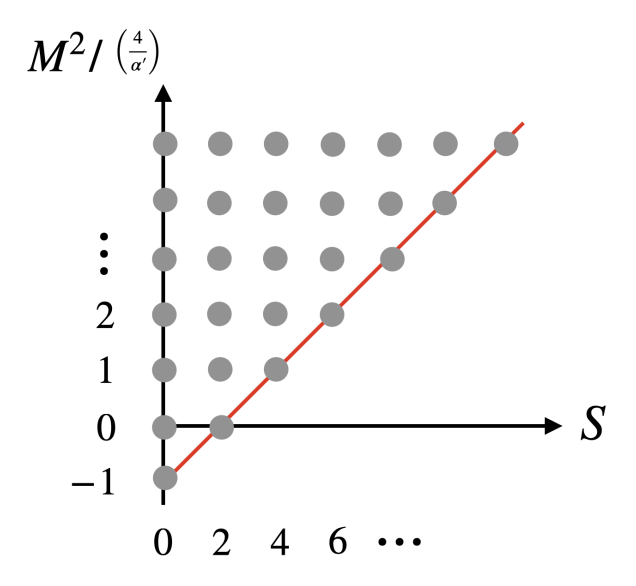


Figure 2.2: Spectrum of bosonic string theory. The vertical axis represents a mass, and the horizontal axis represents a spin. A mass is normalized by $4/\alpha'$. We illustrate only symmetric tensorial states in this figure, which have even spin. Antisymmetric tensorial states can have an odd spin. The red line represents the leading Regge trajectory.

where we used a coordinate system of the Riemann sphere. The Riemann sphere is constructed by adding a point ∞ to a complex plane (See Fig. 2.4). A tachyon four point amplitude is calculated by integrating the positions of the tachyon operators in the Riemann sphere,

$$\int \prod_{i=1}^{4} dz_i d\bar{z}_i \left\langle V_{\mathbf{k}_1}(z_1, \bar{z}_1) V_{\mathbf{k}_1}(z_2, \bar{z}_2) V_{\mathbf{k}_3}(z_3, \bar{z}_3) V_{\mathbf{k}_4}(z_4, \bar{z}_4) \right\rangle . \tag{2.77}$$

It is worth noting that there is three conformal transformations defined globally in the Riemann sphere,

$$z \to z + \epsilon$$
, $z \to z + \epsilon z$, $z \to z + \epsilon z^2$, (2.78)

where ϵ is an infinitesimal parameter. We can fix the positions of three vertex operators as $z_i = \hat{z}_i$ (i = 1, 2, 3) by using this conformal transformation (2.78). This gauge fixing can be done by adding the following gauge fixing term to the action,

$$b_i c(\hat{z}_i) + \tilde{b}_i \tilde{c}(\hat{z}_i), \qquad (2.79)$$

Integrating b_i , one obtain the position fixed four point function,

$$\int dz_4 d\bar{z}_4 \left\langle \left(\prod_{i=1}^3 c(\hat{z}_i) \tilde{c}(\hat{z}_i) V_{\mathbf{k}_i}(\hat{z}_i, \hat{\bar{z}}_i) \right) V_{\mathbf{k}_4}(z_4, \bar{z}_4) \right\rangle. \tag{2.80}$$

First, let us calculate the correlation function of the matter sector. Taking the normal ordering,

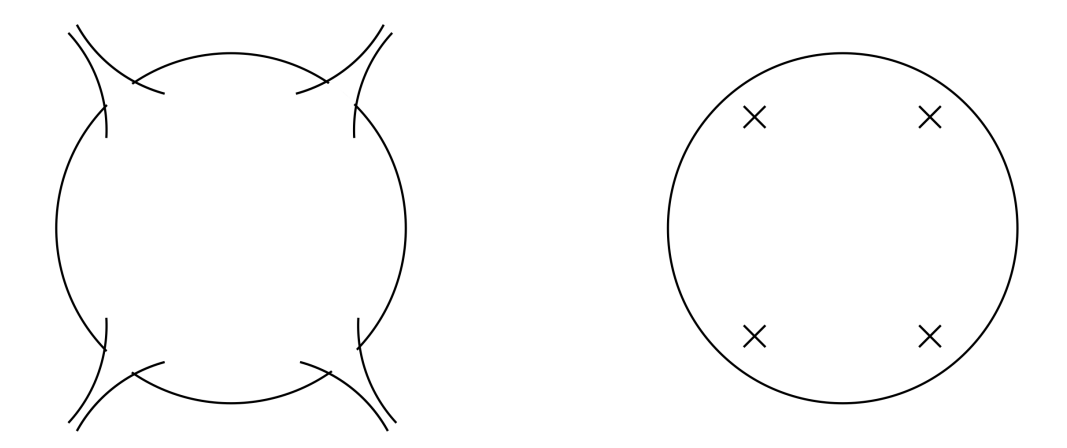


Figure 2.3: The left figure is a worldsheet representing a four body scattering at tree level. The legs represent external lines of strings. By carrying out a conformal transformation, this worldsheet transforms to a sphere (the right figure). Instead, local operators are inserted at the locations of the legs.

one obtain the following function,

$$\langle V_{\mathbf{k}_{1}}(z_{1}, \bar{z}_{1})V_{\mathbf{k}_{1}}(z_{2}, \bar{z}_{2})V_{\mathbf{k}_{3}}(z_{3}, \bar{z}_{3})V_{\mathbf{k}_{4}}(z_{4}, \bar{z}_{4})\rangle = \prod_{i < j} |z_{i} - z_{j}|^{\alpha' k_{i} \cdot k_{j}} \langle 0| : e^{i(k_{1} + k_{2} + k_{3} + k_{4})X} : |0\rangle$$

$$= \prod_{i < j} |z_{i} - z_{j}|^{\alpha' k_{i} \cdot k_{j}} \langle 0| e^{i(k_{1} + k_{2} + k_{3} + k_{4})x} |0\rangle$$

$$. \tag{2.81}$$

The final term produces a delta function as follows,

$$\langle 0|e^{i(k_1+k_2+k_3+k_4)x}|0\rangle = \int dx \ e^{i(k_1+k_2+k_3+k_4)x} = \operatorname{const} \cdot \delta^d(k_1+k_2+k_3+k_4), \qquad (2.82)$$

where the constant term comes from a path integral normalization, which we do not fix here.

The correlation function of the ghost sector is calculated by utilizing analytic properties as follows. First, the correlation function should have zeros of rank one at $z_1 = z_2$, $z_1 = z_3$, $z_2 = z_3$ since c is a fermionic operator. Next, let us consider the conformal transformation, $z \to z' = \frac{1}{z}$. The correlation function transforms as

$$\langle c(1/z_1)c(1/z_2)c(1/z_3)\rangle = \frac{1}{z_1^2 z_2^2 z_3^2} \langle c(z_1)c(z_2)c(z_3)\rangle.$$
 (2.83)

Then, a regularity at the origin means that this function can not grow faster than z_i^2 in the limit $z_i \to \infty$. Finally, one can fix a functional form from the above properties as follows,

$$\langle c(z_1)c(z_2)c(z_3)\rangle = \text{const} \cdot (z_1 - z_2)(z_2 - z_3)(z_3 - z_1).$$
 (2.84)

So far, the four point amplitude has the following form:

$$I = \int d^2 z_4 \prod_{i < j}^3 |z_i - z_j|^{2 + \alpha' k_i \cdot k_j} \prod_{i=1}^3 |z_4 - z_i|^{\alpha' k_i \cdot k_4}.$$
 (2.85)

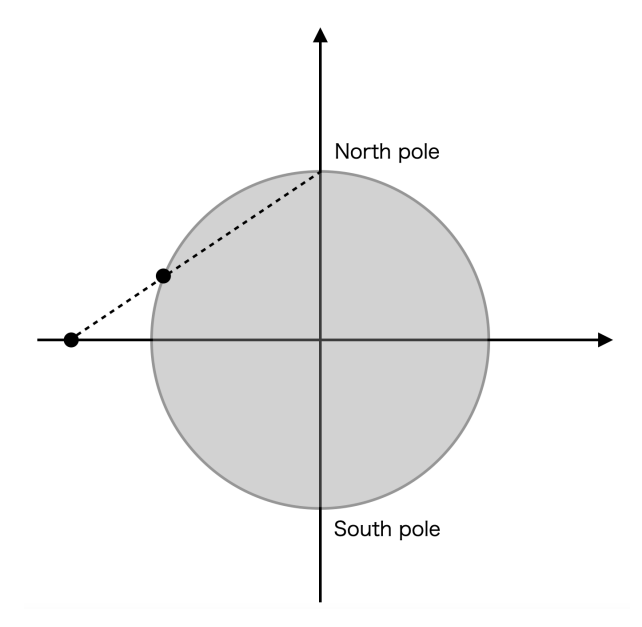


Figure 2.4: A construction of the Riemann surface. This figure represents a cross-section of a sphere embedded in three dimensional space. The horizontal line is regarded as a line of a complex plane. A point in the complex plane is mapped to a point in the sphere as follows. First we draw a line from a point in the complex plane to the north pole of the sphere. An intersection point of the line with the sphere is identified with the start point of the line. In particular, the north pole is identified with the infinity ∞ .

Carrying out the integration, we reach the following expression,

$$I = \frac{\Gamma(-\frac{\alpha's}{4} - 1)\Gamma(-\frac{\alpha't}{4} - 1)\Gamma(-\frac{\alpha'u}{4} - 1)}{\Gamma(\frac{\alpha's}{4} + 2)\Gamma(\frac{\alpha't}{4} + 2)\Gamma(\frac{\alpha'u}{4} + 2)}.$$
(2.86)

We find that s channel poles of the scattering amplitude are located at

$$s = \frac{4}{\alpha'}(N-1)\,, (2.87)$$

where N is a non-negative integer. This equals the mass square of physical string states. A summation of intermediate string states reduces to the Gamma function. t and u channel poles are similar.

High energy scattering Let us examine high energy limit of the Veneziano amplitude. In this section, we study the following two high energy limits. First let us consider the hard scattering limit,

Hard scattering limit:
$$s \to \infty$$
, $\cos \theta$: fixed, (2.88)

Here θ is the scattering angle, which is

$$\cos \theta = 1 + \frac{t}{s + \frac{16}{\alpha'}}.\tag{2.89}$$

Here the following Stirling's formula of the Gamma function is useful,

$$\Gamma(x+1) \simeq \frac{1}{\sqrt{2\pi x}} e^{x \ln x - x}. \tag{2.90}$$

The following relations of the Mandelstam variables are also useful,

$$s + t + u = -\frac{16}{\alpha'}, \quad \cos \theta = 1 + \frac{2t}{s + \frac{16}{\alpha'}}.$$
 (2.91)

First let us consider the hard scattering limit. The Mandelstam variables are parametrized as follows:

$$t = -\left(\frac{16}{\alpha'} + s\right)\sin^2\frac{\theta}{2}, \quad u = -\left(\frac{16}{\alpha'} + s\right)\cos^2\frac{\theta}{2}.$$
 (2.92)

First, we organize Eq. (2.86) by using the reflection formula of the Gamma function as,

$$I = \frac{\sin \pi (\frac{\alpha't}{4} + 2)\sin \pi (\frac{\alpha'u}{4} + 2)}{\pi \sin \pi (\frac{\alpha's}{4} + 2)} \left(\frac{\Gamma(-\frac{\alpha't}{4} - 1)\Gamma(-\frac{\alpha'u}{4} - 1)}{\Gamma(\frac{\alpha's}{4} + 2)}\right)^{2}.$$
 (2.93)

Further, using the Stirling's formula, we obtain

$$I \simeq \frac{\sin \pi (\frac{\alpha' t}{4} + 2) \sin \pi (\frac{\alpha' u}{4} + 2)}{2\pi^2 \sin \pi (\frac{\alpha' s}{4} + 2)} \frac{1}{(\frac{\alpha' s}{4})^3 \sin^{10} \frac{\theta}{2} \cos^{10} \frac{\theta}{2}} e^{-\frac{\alpha'}{2} (s + \frac{16}{\alpha'}) (-\sin^2 \frac{\theta}{2} \ln \sin^2 \frac{\theta}{2} - \cos^2 \frac{\theta}{2} \ln \cos^2 \frac{\theta}{2}) - 8}$$
(2.94)

The scattering amplitude falls off exponentially above the string scale. In particular, this behavior respect the upper bound from unitarity.

Next let us consider the Regge limit,

Regge limit:
$$s \to \infty$$
, t : fixed. (2.95)

The Mandelstam variable u is parametrized as,

$$u = -s - t - \frac{16}{\alpha'} \tag{2.96}$$

Applying the Stirling's formula to Eq. (2.93), we obtain

$$I \simeq \frac{\sin \pi (\frac{\alpha' t}{4} + 2) \sin \pi (\frac{\alpha' u}{4} + 2)}{\pi \sin \pi (\frac{\alpha' s}{4} + 2)} e^{-\frac{\alpha'}{4} t} \Gamma(-\frac{\alpha' t}{4} - 1)^2 \left(\frac{\alpha'}{4} s\right)^{2 + \frac{\alpha'}{2} t}, \tag{2.97}$$

The Mandelstam variable t is negative for a physical scattering process. Therefore, the scattering amplitude also exhibits a mild high energy behavior.

2.4. REGGE THEORY 25

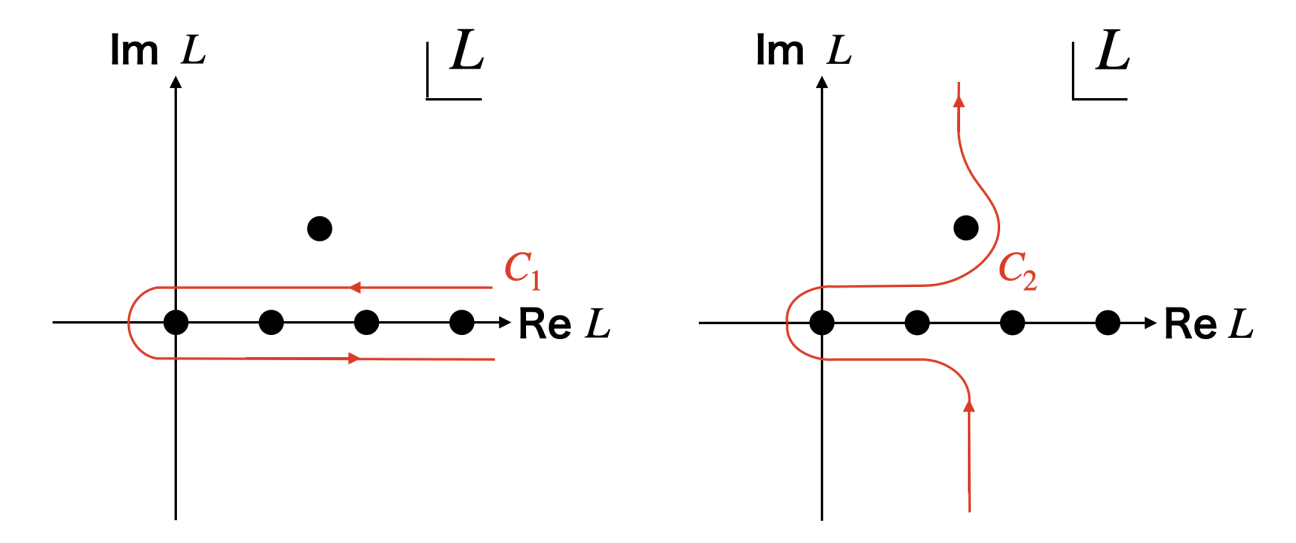


Figure 2.5: The left figure shows the integration contour of Eq. (2.101), and the right figure shows the integration contour of Eq. (2.103). The left contour is equivalent to the right contour if an integration of the infinity is negligible.

2.4 Regge theory

Infinitely many higher spin states are crucial to make the mild high energy behavior. Scattering amplitudes intermediated by higher spin states have different powers of the Mandelstam variables. If there exist only finite higher spin states, the mildness is not achieved because the power is truncated at a certain level. On the other hand, if the power continues infinitely, amplitudes may be summed up to another function beyond a convergent radius of the power expansion. From the worldsheet calculation, we find that a scattering amplitude becomes a product of the Gamma functions. In this section, we reexamine this summation by applying the Regge theory. This analysis tells us how the string spectrum controls scattering amplitudes in the Regge limit.

The Regge theory begin with expanding a scattering amplitude by a partial wave in the physical region of t channel (t > 0 and s < 0),

$$M(s,t) = \frac{\Gamma(\frac{d}{2} - \frac{3}{2})}{4\pi^{\frac{d-1}{2}}} \sum_{L=0}^{\infty} (2L + d - 3) f_L(t) C_L^{\frac{d}{2} - \frac{3}{2}}(\cos \theta), \qquad (2.98)$$

where $C_L^{\alpha}(x)$ is the Gegenbauer polynomial, a d-dimensional extension of the Legendre polynomials (See Eq. (A.4)). And, d is a spacetime dimension (d = 26 for bosonic string theory). Also, we defined a scattering angle as

$$\cos \theta = 1 + \frac{2s}{t - 4m^2},\tag{2.99}$$

where m is a mass for in and out fields. The partial wave expansion is an expansion of scattering amplitudes by angular momentum eigenstates (See Appendix .B.2.1). The partial wave amplitude

 $f_L(t)$ is calculated by using an orthogonality of the Gegenbauer polynomial,

$$f_L(t) = \frac{(4\pi)^{\frac{d-3}{2}}\Gamma(L+1)\Gamma(\frac{d-3}{2})}{\Gamma(L+d-3)} \int_1^1 dz (1-z)^{\frac{d-3}{2}} M(s,z) C_L^{\frac{d}{2}-\frac{3}{2}}(z).$$
 (2.100)

The partial wave expansion is convenient to understand t-channel physics. If there is a spin-l exchange in the t-channel, $f_l(t)$ has a pole at its mass. However, this expression cannot be applicable to the Regge limit $(t < 0, s \to \infty)$, which is our interest, because this limit is out of a convergent radius. This can be understood by an observation that Eq. (2.98) diverges at some positive s due to s-channel poles. To apply the t-channel partial wave expansion to the Regge limit, we carry out an analytic continuation. First we introduce a complex angular momentum and organized the scattering amplitude as

$$M(s,t) = \frac{\Gamma(\frac{d}{2} - \frac{3}{2})}{4\pi^{\frac{d-1}{2}}} \frac{i}{2} \int_{C_1} \frac{dL}{\sin \pi L} (2L + d - 3) f_L(t) C_L^{\frac{d}{2} - \frac{3}{2}}(-z), \qquad (2.101)$$

where C_1 is the contour depicted in Fig. 2.5. These exist poles at integer values of L due to $\frac{1}{\sin \pi L}$. This expression is not yet to be suitable because the Gegenbauer polynomial grows exponentially with l for z < -1 and z > 1,

$$C_L^{\alpha}(\cosh \chi) = e^{L\chi}, \quad C_L^{\alpha}(-\cosh \chi) = e^{i\pi L}e^{L\chi} \quad (\chi > 0), \qquad (2.102)$$

which makes the convergence of the integral worse. Next, we deform to the integral contour C_1 to C_2 . At large ImL, the Gegenbauer polynomials oscillate. Hence, the convergence are improved. This deformation is possible if the integral at the infinity is negligible. This is satisfied if $f_L(t)$ does not grow exponentially at large |L|. It is important to find such an expression of $f_L(t)$ for a complex L. The expression is constructed by the Gribov-Froissart projection, which we will show in Appendix. B.2.3. Here, we continue a discussion with assuming that we can find such a nice function for $\text{Re}L \geq L_0$. Then, the integral can be written as an integral between $L_0 - i\infty$ and $L_0 + i\infty$ plus the residues at poles where $\text{Re}L > L_0$.

$$M(s,t) = \int_{L_0 - i\infty}^{L_0 + i\infty} dL \frac{\pi}{\sin \pi L} \left(L + \frac{d-3}{2} \right) f_L(t) C_L^{\frac{d-3}{2}}(\cos \theta) + (\text{residues of poles}), \qquad (2.103)$$

In particular, the scattering amplitudes are dominated by the residue at the most right pole in the Regge limit. This is because the Gegenbaur polynomials behave as

$$C_I^{\alpha}(z) \sim z^L \quad \text{for } z \gg 1.$$
 (2.104)

If there is a pole at

$$L = f(t), (2.105)$$

this pole yields the following behavior in the Regge limit,

$$M(s,t) \simeq g(s,t) \cdot s^{f(t)}, \qquad (2.106)$$

2.4. REGGE THEORY 27

where g(s,t) is a function which are not diverge in the Regge limit. To derive this, we used a formula of the Gengenbauer polynomial,

$$C_L^{\frac{d-3}{2}}(z) \simeq \frac{2^L \Gamma\left(\frac{d-3}{2} + L\right)}{\Gamma\left(\frac{d-3}{2}\right) \Gamma(L+1)} z^L \quad (z \gg 1).$$
 (2.107)

In string theory, the Regge trajectory of Eq. (2.75) yields a pole at

$$L = f(t) = 2 + \frac{\alpha'(t - i\epsilon)}{2}$$
. (2.108)

Substituting this into Eq. (2.106), we reproduce the Regge behavior (2.97),

$$M(s,t) \sim s^{2+\frac{\alpha't}{2}}$$
. (2.109)

The above analysis showed that the Regge trajectory controls scattering amplitudes in the Regge limit and plays an important role to make the mild UV behavior. Notice that there are other Regge trajectories yielding a pole. The most leading one is Eq. (2.75).

Let us conclude this section with a summary. We constructed physical string states by adding excitations to the ground state. The first excited state includes the graviton. At the level 2 state or more, there appear infinitely many higher spin states. Their masses are quantized by the string tension. Scattering amplitudes intermediated by these higher spin states have different powers. As a result of summing up these contribution infinitely, string scattering amplitudes exhibit a mild UV behavior as seen in the tachyon four point amplitude. In particular, in the Regge limit, higher spin states on the leading Regge trajectory are important. The shape of the leading Regge trajectory controls the Regge behavior. In flat space, the leading Regge trajectory is linear so that the power of the Mandelstam variable s is modified by a linear function of the Mandelstam variable t.

Chapter 3

Higher spin fields in de Sitter space

We discussed that higher spin states are crucial to UV complete gravity in string theory. However, our main interest is the accelerating universe. Thus, it is instructive to study higher spin fields in de Sitter space. Higher spin fields have rich properties in de Sitter space which are absent in flat space or AdS space. One example is the Higuchi bound. The Higuchi bound states that higher spin fields within the following mass range produce a negative norm state,

$$0 < m^2 < H^2 S(S + d - 3), (3.1)$$

where S is the spin and H is the Hubble constant. Thus, such higher spin fields are forbidden in de Sitter space. Interestingly, this bound implies that the string spectrum should be modified in de Sitter space. On the leading Regge trajectory in flat space, the mass square grows linearly as the spin increases

$$m^2 \sim \frac{S}{\alpha'} \tag{3.2}$$

while the upper bound of the Higuchi bound grows quadratically. Therefore, the states in the leading Regge trajectory violates the Higuchi bound when $S \sim \frac{1}{\alpha' H^2}$ unless the spectrum is modified.

In this chapter, we review higher spin fields in de Sitter space, mainly focusing on the Higuchi bound. The construction of this chapter is as follows. In Sec. 3.1, we introduce de Sitter space and explain its isometry group. Utilizing the isometry group, we construct an irreducible representation in Sec. 3.2. In Sec. 3.3, we introduce higher spin fields and calculate their two point function of spinning fields by solving Ward-Takahashi identities of the de Sitter isometry. We can fix two point functions in the late time except an overall constant. Then, we show that a helicity zero mode creates a negative norm state if the mass is within the range (3.1). Finally, in Sec. 3.4, we discuss the implication of the Higuchi bound to higher spin states in string theory.

3.1 De Sitter space

d dimensional de Sitter space (dS_d) is defined by a hypersurface,

$$-Y_0^2 + Y_1^2 + \dots + Y_d^2 = R^2 = \frac{1}{H^2},$$
(3.3)

embedded into a (d+1) dimensional space with the line element,

$$ds^{2} = -dY_{0}^{2} + dY_{1}^{2} + \dots + dY_{d}^{2}.$$
(3.4)

Because the Ricci curvature is $R_{\mu\nu} = \frac{1}{H^2} g_{\mu\nu}$, dS_d is a vacuum solution of the Einstein equation with a positive cosmoligical constant,

$$R_{\mu\nu} - \frac{1}{2}g_{\mu\nu}R - \Lambda g_{\mu\nu} = 0, \quad \Lambda = \frac{(d-2)(d-1)}{2H^2}.$$
 (3.5)

Global coordinate

Let us examine a global structure of de Sitter space. It is convenient to introduce global coordinates which cover an entire spacetime:

$$Y_0 = \frac{1}{H} \sinh \eta \,, \quad Y_i = \frac{1}{H} \Omega_i \cosh \eta \,, \tag{3.6}$$

where Ω_i are coordinates of d-1 dimensinal sphere. In this coordinate, the line element becomes

$$ds^{2} = \frac{-d\eta^{2} + \cosh^{2}\eta \, d\Omega_{d-1}^{2}}{H^{2}} \,. \tag{3.7}$$

Eq. (3.7) indicates that dS_d is a d-1 dimensional unit sphere which shrinks from the past infinity to $\eta = 0$, and then expands from $\eta = 0$ to the future infinity. Next, let us introduce a conformally flat metric to understand a causal structure by defining a new time coordinate as

$$\cos T = \frac{1}{\cosh \eta} \,. \tag{3.8}$$

The corresponding line element is

$$ds^{2} = \frac{1}{H^{2}}\cos^{2}T\left(-dT^{2} + d^{2}\Omega_{d-1}\right) = \frac{1}{H^{2}}\cos^{2}T\left(-dT^{2} + d^{2}\theta + d^{2}\Omega_{d-2}\right), \qquad (3.9)$$

where, we decomposed the coordinate of S_{d-1} into an interval and S_{d-2} . These coordinates are defined within

$$-\frac{\pi}{2} \le T \le \frac{\pi}{2} \,, \qquad 0 \le \theta \le \pi \,. \tag{3.10}$$

 $\theta=0$ and $\theta=\pi$ are the north pole and the south pole of S_{d-1} respectively. Using this coordinate system, we draw a Penrose diagram (Fig. 3.1). First, one can find that $T=-\frac{\pi}{2}$ is a past null infinity, and $T=-\frac{\pi}{2}$ is a future null infinity. All null lines start at the past null infinity and end at the future null infinity. Second, there exists two cosmological horizons for an observer sitting on the north pole. One is a past cosmological horizon, which is represented by the line $\theta=T+\frac{\pi}{2}$. The observer cannot send a signal to a point beyond this horizon. The other one is a future cosmological horizon, which is represented by the line $\theta=-T+\frac{\pi}{2}$. The observer cannot receive a signal from a point beyond this horizon.

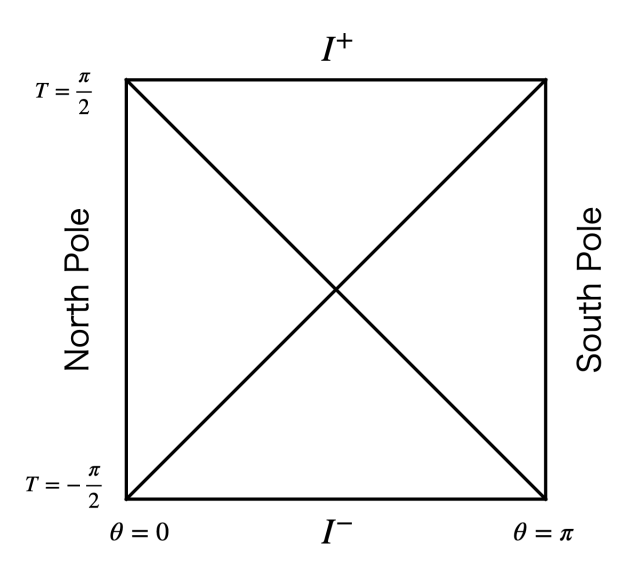


Figure 3.1: Penrose diagram of dS_d : Each point represents an S^{d-2} subspace, and the edges correspond to the north and south poles of S^{d-1} . I^+ and I^- represent a future null infinity and a past null infinity respectively.

Planar coordinate

De Sitter acceleration is manifest in the planar coordinte:

$$Y_0 = \frac{1}{H}\sinh(Ht) + \frac{H}{2}(x^i)^2 e^{Ht}, \qquad (3.11)$$

$$Y_i = x^i e^{-t} \,, \tag{3.12}$$

$$Y_d = \frac{1}{H}\cosh(Ht) - \frac{H}{2}(x^i)^2 e^{Ht}, \qquad (3.13)$$

where the line element is

$$ds^{2} = -dt^{2} + e^{2Ht} \left((dx^{1})^{2} + \dots + (dx^{d-1})^{2} \right).$$
(3.14)

The d-1 dimensional space expands exponentially in time. It is convenient to introduce conformally flat metric by defining a conformal time $\tau = -\frac{1}{H}e^{-Ht}$,

$$ds^{2} = \frac{-d\tau^{2} + (dx^{1})^{2} + \dots + (dx^{d-1})^{2}}{H^{2}\tau^{2}}.$$
(3.15)

The planar coordinates cover only half of dS_d since $Y_0 + Y_d > 0$, which is inside the past cosmological horizon as depicted in Fig. 3.2.

Static coordinate

Finally, let us introduce static coordinates,

$$Y_d + Y_0 = \frac{\sqrt{1 - r^2}e^t}{H}, \quad Y_d - Y_0 = \frac{\sqrt{1 - r^2}e^{-t}}{H}, \quad Y_i = \frac{r\Omega_{d-2}^i}{H},$$
 (3.16)

where $-\infty < t < \infty$, $0 \le r \le 1$, and Ω_{d-2}^i is a coordinate of an unit d-2 dimensional sphere. The corresponding metric is

$$ds^{2} = R^{2} \left[-(1 - r^{2})dt^{2} + \frac{dr^{2}}{1 - r^{2}} + r^{2}d\Omega_{d-2}^{2} \right].$$
 (3.17)

This metric is static in time. This coordinate system covers a quarter of the full de Sitter space since $Y_d + Y_0 > 0$ and $Y_d - Y_0 > 0$ (see Fig. 3.2). An observer sitting at the origin r = 0 has a cosmological horizon at r = 1, hence this coordinate system can be used to describe the inside of the horizon.

Isometry of de Sitter space

An isometry group of de Sitter space is SO(d, 1) since the hypersurface (3.3) does not change under the (d + 1)-dimensional rotation. In the planar coordinate, the generators are represented as ¹

$$D = \tau \frac{\partial}{\partial \tau} + x^{i} \frac{\partial}{\partial x^{i}}, \quad P_{i} = \frac{\partial}{\partial x^{i}},$$

$$M_{ij} = x_{i} \frac{\partial}{\partial x^{j}} - x_{j} \frac{\partial}{\partial x^{i}},$$

$$K_{i} = 2x_{i} \tau \frac{\partial}{\partial \tau} + (\tau^{2} - x^{2}) \frac{\partial}{\partial x^{i}} + 2x_{i} x^{j} \frac{\partial}{\partial x_{j}}.$$
(3.18)

If we define the following combination,

$$J_{0,d+1} = D$$
, $J_{ij} = M_{ij}$,
 $J_{0,i} = \frac{1}{2} (P_i - K_i)$, $J_{d+1,i} = \frac{1}{2} (P_i + K_i)$. (3.19)

the generators satisfy the Lie algebra of SO(d,1),

$$[J_{AB}, J_{CD}] = -\eta_{AC}J_{BD} - \eta_{BC}J_{AC} + \eta_{BC}J_{AD} + \eta_{AD}J_{BC}. \tag{3.20}$$

3.2 Representation of de Sitter isometry group

Let us construct an irreducible representation of SO(d,1) group. It is convenient to use D, M_{ij}, P_i and K_i as a basis of the generators. Their algebra is given by

$$[D, P_{i}] = P_{i}, \quad [D, K_{i}] = -K_{i}, \quad [P_{i}, K_{j}] = -2\delta_{ij}D - 2M_{ij},$$

$$[M_{ij}, M_{kl}] = -\delta_{jk}M_{il} + \delta_{ik}M_{jl} - \delta_{il}M_{jk} + \delta_{jl}M_{ik},$$

$$[D, M_{ij}] = 0,$$

$$[M_{ij}, P_{k}] = \delta_{jk}P_{i} - \delta_{ik}P_{j}, \quad [M_{ij}, K_{k}] = \delta_{jk}K_{i} - \delta_{ik}K_{j}.$$
(3.21)

$$I: \tau \to \frac{\tau}{\tau^2 - x^2}, \ x^i \to \frac{x^i}{\tau^2 - x^2}$$

 K_i can be decomposed as $I \cdot P_i \cdot I$. Therefore, we just check the invariance under I.

¹To check that the metric (3.15) is invariant under K_i , it is convenient to introduce the inverse transformation,

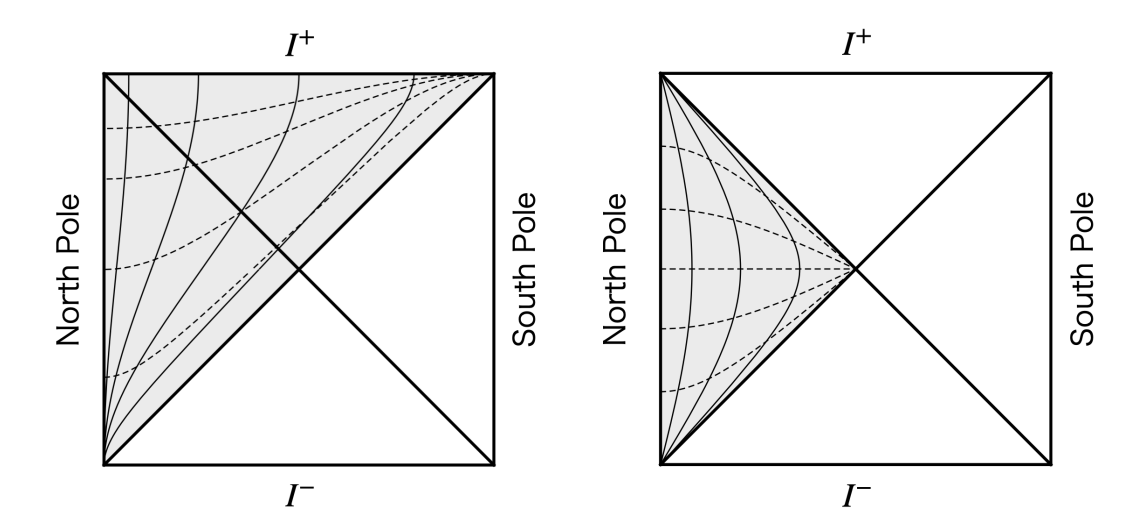


Figure 3.2: The planar coordinates cover the shaded area of the left figure. The dashed lines represent constant time slice. The black lines represent constant x^2 slices. The static coordinate covers the shaded area of the right figure. The dashed lines represent constant time slices. The black line represent constant r slices.

First, we observe that P_i is a raising operator of -D, and also K_i is a lowering operator. Thus, it is convenient to label a state by an eigenvalue of -D. Let us introduce the highest weight state as the smallest eigenvalue of -D. States with a lower eigenvalue are created by acting P_i . We note that the eigenvalue are not lower-bounded, and thus the representation space is of infinite dimension.

Further, we can classify the highest weight state by utilizing SO(d-1) subalgebra since M_{ij} commutes with D. An irreducible representation of SO(d-1) is characterized by one integer S, for which a casimir operator $M_{ij}M^{ij}$ has an eigenvalue S(S+d-3).

As a summary, we construct a highest weight representation of (Δ, S) as follows. First, we define the highest weight state as,

Highest weight state:
$$D|\Delta, S\rangle = -\Delta|\Delta, S\rangle$$
, $K_i|\Delta, S\rangle = 0$, $M_{ij}M^{ij}|\Delta, S\rangle = S(S+d-3)|\Delta, S\rangle$. (3.22)

Here S is a largest eigenvalue of M_{12} . And then, we construct descendant states by acting P_i , which have a larger eigenvalue of D. Notice that SO(d-1) has $\lfloor \frac{d-1}{2} \rfloor$ Carten operators, although we eliminate labels for an eigenvalue of these generators for simplicity.

Finally, let us comment on a quadratic Casimir operator, which commutes with all generators. It is given by

$$C_2 = \frac{1}{2} M_{AB} M^{BA} = \frac{1}{2} M_{ij} M^{ji} + D(D+d-1) - P^i K_i.$$
 (3.23)

Its eigenvalue for the representation (Δ, S) becomes ²

$$C_2 = S(S+d-3) + \Delta(\Delta+1-d). \tag{3.24}$$

²The eigenvalus are easily calculated for the highest weight state.

3.3 Higher spin field

Let us introdue a higher spin field of spin S as a representation of (Δ, S) . The generators for a spin S field $\Phi_{\mu_1\cdots\mu_S}$ are given by

$$D\Phi_{i_{1}\dots i_{N} 0\dots 0} = \left(\tau \frac{\partial}{\partial \tau} + x^{i} \frac{\partial}{\partial x^{i}} + S\right) \Phi_{i_{1}\dots i_{N} 0\dots 0},$$

$$P_{a}\Phi_{i_{1}\dots i_{N} 0\dots 0} = \frac{\partial}{\partial x^{a}} \Phi_{i_{1}\dots i_{N} 0\dots 0},$$

$$M_{ab} \Phi_{i_{1}\dots i_{N} 0\dots 0} = \left(x_{a} \frac{\partial}{\partial x^{b}} - x_{b} \frac{\partial}{\partial x^{a}}\right) \Phi_{i_{1}\dots i_{N} 0\dots 0},$$

$$(3.25)$$

$$M_{ab} \Phi_{i_1 \dots i_N 0 \dots 0} = \left(x_a \overline{\partial x^b} - x_b \overline{\partial x^a} \right) \Phi_{i_1 \dots i_N 0 \dots 0},$$

$$+ N \, \delta_{a \, (i_1} \, \Phi_{i_2 \, \cdots \, i_N) \, b \, 0 \, \cdots \, 0} - N \, \delta_{b \, (i_1} \, \Phi_{i_2 \, \cdots \, i_N) \, a \, 0 \, \cdots \, 0}$$

$$K_a \Phi_{i_1 \, \cdots \, i_N \, 0 \, \cdots \, 0} = \left(2sx_a + 2x_a \tau \frac{\partial}{\partial \tau} + 2x_a x^j \frac{\partial}{\partial x_j} + (\tau^2 - x^2) \frac{\partial}{\partial x^a} \right) \, \Phi_{i_1 \, \cdots \, i_N \, 0 \, \cdots \, 0}$$
(3.26)

$$+2Nx^{j}\,\delta_{a\,(i_{1}}\,\Phi_{i_{2}\,\cdots\,i_{N})\,j\,0\,\cdots\,0}-2Nx_{(i_{1}}\Phi_{i_{2}\,\cdots\,i_{N})\,a\,0\,\cdots\,0}$$

$$\qquad (3.27)$$

$$+2N\tau\delta_{a(i_1}\Phi_{i_2...i_N)0...0}+2(S-N)\tau\Phi_{i_1...i_Na0...0}$$
(3.28)

where the Latin indices represent spatial coordinates, and 0 represents the time τ . To consider an irrducible representation, we impose the Fierz-Pauli condition,

$$D^{\mu}\Phi_{\mu\mu_2\cdots\mu_S} = 0, \quad g^{\mu\nu}\Phi_{\mu\nu\mu_3\cdots\mu_S} = 0. \tag{3.29}$$

The quadratic Casimir operator gives a field equation.

$$\[D^{\mu}D_{\mu} + H^{2} \Big(\Delta (\Delta + 1 - d) - S \Big) \] \Phi_{\mu_{1} \dots \mu_{S}} = 0 , \tag{3.30}$$

where we used an identity, ³

$$C_2 = -\frac{1}{H^2} D_\mu D^\mu + S(S+d-2). \tag{3.31}$$

Let us remark on a relation between the dimension Δ and a mass M. A mass term is defined through a massless limit. In the massless limit, a gauge symmetry should emerge to gauge away states of small helicity. To construct a field equation of massive fields, we first construct a field equation with a gauge symmetry, and then add a mass term, which we review in Appnedix. C. A field equation of a massive field becomes

$$\left[D_{\mu}D^{\mu} + H^{2}\left(S^{2} + (d-6)S - 2d + 6\right) - m^{2}\right]\Phi_{\mu_{1}\cdots\mu_{S}} = 0.$$
(3.32)

Comparing Eq. (3.30) and Eq. (3.32), we obtain a relation,

$$\Delta = \frac{d-1}{2} \pm \sqrt{\left(S + \frac{d}{2} - \frac{5}{2}\right)^2 - \frac{m^2}{H^2}}.$$
 (3.33)

³This identity holds under the Fierz-Pauli condition (3.29).

Note that the dimension becomes imaginary when $m^2 > (S + \frac{d}{2} - \frac{5}{2})^2$. Thus fields in de Sitter space are classified into two classes as follows.

Principal series:
$$\operatorname{Im}\Delta \neq 0$$
, $m^2 > \left(S + \frac{d}{2} - \frac{5}{2}\right)^2$
Complementary series: $\operatorname{Im}\Delta = 0$, $m^2 \le \left(S + \frac{d}{2} - \frac{5}{2}\right)^2$ (3.34)

3.3.1 Quantum spinning fields

Next, let us consider quantum field theory of spinning fields. The Higuchi bound states that there exist negative norms states in the Hilbert space within the mass range (3.1). In this subsection, we give a formula to calculate inner products by using the de Sitter isometry.

In quantum field theory, a state is created by acting field operators into a vacuum state as follows,

$$\hat{\Phi}_{\mu_1 \dots \mu_S}(\tau, x) |\Omega\rangle , \qquad (3.35)$$

where $|\Omega\rangle$ is a vacuum state invariant under the de Sitter isometry. Also, $\hat{\Phi}_{\mu_1 \dots \mu_S}$ is a field operator obtained by quantizing the free field Φ . For simplicity, let us focus on the late time limit,

$$\tau \to 0$$
. (3.36)

One benefit of this limit is that only a field with S spatial indices, $\Phi_{i_1 \dots i_S}$, remains at the late time. This is because a field with a time index is damped with a higher power of τ , as indicated by the transverse condition of Eq. (3.29). Consequently, the traceless condition of Eq. (3.29) reduces to

$$\delta^{i_1 i_2} \Phi_{i_1 i_2 \dots i_S} = 0. \tag{3.37}$$

To avoid the complexity of the tensorial indices, we introduce a null vector and contract with the field as,

$$\boldsymbol{\epsilon}^s.\Phi = \epsilon^{i_1} \cdots \epsilon^{i_S} \Phi_{i_1 \cdots i_S}. \tag{3.38}$$

This vector is called a polarization vector, which satisfies

$$\epsilon_i \, \epsilon^i = 0 \,. \tag{3.39}$$

Let us expand the field as

$$\hat{\Phi}_{i_1 \dots i_S}(\tau, x) = \tau^{\Delta - S} \left(\hat{\phi}_{i_1 \dots i_S}(x) + \varepsilon(\tau) \right) + \tau^{\bar{\Delta} - S} \left(\hat{\bar{\phi}}_{i_1 \dots i_S}(x) + \varepsilon(\tau) \right) , \qquad (3.40)$$

where

$$\bar{\Delta} = d - 1 - \Delta \,. \tag{3.41}$$

The powers of τ are fixed by the field equation. The isometry generators act on the boundary fields as

$$D \epsilon^{S}.\hat{\phi} = \left(\Delta + x^{i} \frac{\partial}{\partial x^{i}}\right) \epsilon^{S}.\hat{\phi}$$

$$P_{a} \epsilon^{S}.\hat{\phi} = \frac{\partial}{\partial x^{a}} \epsilon^{S}.\hat{\phi},$$

$$M_{ab} \epsilon^{S}.\hat{\phi} = \left(x_{a} \frac{\partial}{\partial x^{b}} - x_{b} \frac{\partial}{\partial x^{a}} + \epsilon_{a} \frac{\partial}{\partial \epsilon^{b}} \epsilon^{S}.\hat{\phi} - \epsilon_{b} \frac{\partial}{\partial \epsilon^{a}}\right) \epsilon^{S}.\hat{\phi},$$

$$K_{a} \epsilon^{S}.\hat{\phi} = \left(2\Delta x_{a} + 2x_{a} x^{j} \frac{\partial}{\partial x_{j}} - x^{2} \frac{\partial}{\partial x^{a}} + 2\epsilon_{a} x \cdot \frac{\partial}{\partial \epsilon} - 2\epsilon \cdot x \frac{\partial}{\epsilon^{a}}\right) \epsilon^{S}.\hat{\phi}$$

$$(3.42)$$

Interestingly, this representation is the same as conformal generators of a primary field with a scaling dimension Δ and a spin S. Hence, we can use a techique of conformal field theory, which is a second benefit of the late time limit.

Let us calculate inner products in the Fourier space,

$$\langle \Omega | \epsilon_1^S. \hat{\Phi}(\tau, k) \epsilon_2^S. \hat{\Phi}(\tau, k') | \Omega \rangle, \qquad (3.43)$$

where the operators are defined by the Fourier transformation, e.g.,

$$\boldsymbol{\epsilon}_{2}^{S}.\hat{\Phi}(\tau,k')|\Omega\rangle = \int \frac{d^{d-1}x}{(2\pi)^{d-1}} e^{ik'\cdot x} \,\boldsymbol{\epsilon}_{2}^{S}.\hat{\Phi}(\tau,x)|\Omega\rangle. \tag{3.44}$$

Below we use the following notation,

$$\langle \boldsymbol{\epsilon}_{1}^{S}.\hat{\Phi}(\tau,k)\,\boldsymbol{\epsilon}_{2}^{S}.\hat{\Phi}(\tau,k')\rangle = \langle \Omega|\,\boldsymbol{\epsilon}_{1}^{S}.\hat{\Phi}(\tau,k)\,\boldsymbol{\epsilon}_{2}^{S}.\hat{\Phi}(\tau,k')\,|\Omega\rangle\,. \tag{3.45}$$

First, we consider a field of the principal series and $\Delta < d - \Delta$ for simplicity. In this case, the inner product is dominated by one boundary operator as

$$\langle \boldsymbol{\epsilon}_{1}^{S}.\Phi(\tau,k)\,\boldsymbol{\epsilon}_{2}^{S}.\Phi(\tau,k')\rangle = (2\pi)^{d-1}\delta^{d-1}(k+k')\,\tau^{2\Delta}\,\langle \boldsymbol{\epsilon}_{1}^{S}.\phi(k)\,\boldsymbol{\epsilon}_{2}^{S}.\phi(-k)\rangle',\tag{3.46}$$

where the delta function comes from the momentum conservation. And also, we used the primed inner products to represent a subtraction of a delta function, which is defined as,

$$\langle \boldsymbol{\epsilon}_{1}^{S}.\phi(\tau,k)\,\boldsymbol{\epsilon}_{2}^{S}.\phi(\tau,-k)\rangle = (2\pi)^{d-1}\delta^{d-1}(k+k')\,\langle \boldsymbol{\epsilon}_{1}^{S}.\phi(\tau,k)\,\boldsymbol{\epsilon}_{2}^{S}.\phi(\tau,-k)\rangle'. \tag{3.47}$$

One can fix a functional form of this inner product by soloving Ward-Takahashi identities corresponding to the de Sitter isometry, which are given by

$$\langle \Omega | [D, \epsilon_1^S . \Phi(\tau, k) \epsilon_2^S . \Phi(\tau, k')] | \Omega \rangle = 0.$$
 (3.48)

$$\langle \Omega | [b \cdot K, \epsilon_1^S \cdot \Phi(\tau, k) \epsilon_2^S \cdot \Phi(\tau, k')] | \Omega \rangle = 0.$$
 (3.49)

We introduced b_a as a parameter of a transformation K_a . The action of the generators is obtained by fourier transforming Eq. (3.42). First, Eq. (3.48) becomes

$$\left[\mathbf{k} \cdot \frac{\partial}{\partial \mathbf{k}} + d - 2\Delta - 1 \right] \langle \boldsymbol{\epsilon}_1^S.\phi(k) \, \boldsymbol{\epsilon}_2^S.\phi(-k) \rangle' = 0.$$
 (3.50)

This identity indicates that the inner product is a homogeneous function of degee $2\Delta - d$. Therefore, we can carry out the following expansion.

$$\langle \boldsymbol{\epsilon}_{1}^{S}.\phi(\boldsymbol{k})\boldsymbol{\epsilon}_{2}^{S}.\phi(-\boldsymbol{k})\rangle' = \sum_{h=0}^{S} (\boldsymbol{\epsilon}_{1}.\boldsymbol{\epsilon}_{2})^{h} (\boldsymbol{\epsilon}_{1}.\boldsymbol{k})^{s-h} (\boldsymbol{\epsilon}_{2}.\boldsymbol{k})^{s-h} \frac{A_{h}}{\mathbf{k}^{d-2\Delta+2S-2h-1}},$$
(3.51)

where

$$k = \sqrt{k^2}. (3.52)$$

Notice that neither $(\epsilon_1 \cdot \epsilon_1)$ nor $(\epsilon_2 \cdot \epsilon_2)$ appear in the expansion since the polarization vectors are null. The coefficient are fixed by Eq. (3.49), which becomes

$$\left[\boldsymbol{b} \cdot \frac{\partial}{\partial \boldsymbol{k}} \left\{ -2(\Delta - d + 2) + 2\boldsymbol{k} \cdot \frac{\partial}{\partial \boldsymbol{k}} \right\} - (\boldsymbol{b} \cdot \boldsymbol{k}) \frac{\partial^{2}}{\partial \boldsymbol{k}^{2}} + 2\boldsymbol{\epsilon} \cdot \frac{\partial}{\partial \boldsymbol{k}} \left(\boldsymbol{b} \cdot \frac{\partial}{\partial \boldsymbol{\epsilon}_{1}} \right) - 2\boldsymbol{b} \cdot \boldsymbol{\epsilon}_{1} \left(\frac{\partial}{\partial \boldsymbol{k}} \cdot \frac{\partial}{\partial \boldsymbol{\epsilon}_{1}} \right) \right] \langle \boldsymbol{\epsilon}_{1}^{S}.\phi(k) \, \boldsymbol{\epsilon}_{2}^{S}.\phi(-k) \rangle' = 0.$$
(3.53)

Eq. (3.53) gives three identities depending on a coupling with b_a . Among them, terms proportional to $b \cdot \epsilon_1$ and $b \cdot \epsilon_2$ reduce to a recursion relation,

$$A_{h-1} = \frac{2h(S - h - \Delta)}{(S - h + 1)(\Delta + h - 2)} A_h.$$
(3.54)

A term proportial to $b \cdot k$ becomes trivial. Finally, the inner product is given by

$$\langle \boldsymbol{\epsilon}_{1}^{S}.\phi(\boldsymbol{k})\boldsymbol{\epsilon}_{2}^{S}.\phi(-\boldsymbol{k})\rangle'$$

$$= A_{S} \sum_{h=0}^{S} 2^{S-h}{}_{S}C_{h} \frac{\Gamma(S-h-\Delta+\frac{d}{2}-\frac{1}{2})\Gamma(\Delta+h-1)}{\Gamma(-\Delta+\frac{d}{2}-\frac{1}{2})\Gamma(\Delta+S-1)} \cdot \frac{(\boldsymbol{\epsilon}_{1}.\boldsymbol{\epsilon}_{2})^{h} (\boldsymbol{\epsilon}_{1}.\boldsymbol{k})^{s-h} (\boldsymbol{\epsilon}_{2}.\boldsymbol{k})^{s-h}}{k^{d-2\Delta+2S-2h-1}} \quad (3.55)$$

Futher this can be summarized to the Jacobi polynomial as

$$\langle \boldsymbol{\epsilon}_{1}^{S}.\phi(\boldsymbol{k})\boldsymbol{\epsilon}_{2}^{S}.\phi(-\boldsymbol{k})\rangle' = \frac{A_{S}}{\mathbf{k}^{d-2\Delta-1}} \frac{S!\Gamma(\Delta-1)}{\Gamma(\Delta+S-1)} \left(-2\frac{(\boldsymbol{\epsilon}_{1}\cdot\boldsymbol{k})(\boldsymbol{\epsilon}_{2}\cdot\boldsymbol{k})}{\mathbf{k}^{2}}\right)^{S} P_{S}^{(\Delta-S-\frac{d}{2}-\frac{1}{2},\frac{d}{2}-\frac{5}{2})} \left(1 - \frac{\mathbf{k}^{2}\boldsymbol{\epsilon}_{1}.\boldsymbol{\epsilon}_{2}}{(\boldsymbol{\epsilon}_{1}.\boldsymbol{k})(\boldsymbol{\epsilon}_{2}.\boldsymbol{k})}\right),$$

$$(3.56)$$

where the Jacobi polynomial is defined as

$$P_n^{(\alpha,\beta)}(t) = \frac{\Gamma(\alpha+n+1)}{\Gamma(n+1)\Gamma(\alpha+1)} {}_2F_1\left[\begin{array}{c} -n, \alpha+\beta+n \\ \alpha+1 \end{array}; \frac{1-z}{2}\right], \tag{3.57}$$

where ${}_{2}F_{1}\left[\begin{array}{c} \alpha\,,\beta\\ \gamma\end{array};x\right]$ is the hypergeometric function,

$${}_{2}F_{1}\left[\begin{array}{c}\alpha,\beta\\\gamma\end{array};x\right]=\sum_{n=0}^{\infty}\frac{1}{n!}\frac{(\alpha)_{n}(\beta)_{n}}{(\gamma)_{n}}x^{n}.$$
(3.58)

To derive Eq. (3.56), we used the following identity,

$$\frac{\Gamma\left(s-h-\Delta+\frac{d}{2}\right)}{\Gamma\left(-\Delta+\frac{d}{2}\right)} = (-1)^{s-h} \frac{\Gamma\left(\Delta-\frac{d}{2}+1\right)}{\Gamma\left(\Delta-\frac{d}{2}-s+h+1\right)},\tag{3.59}$$

which is derived from the reflection formula of the Gamma function. In the above calculation, we consider only the field of the principal series and $\Delta < d - \Delta - 1$. We can easily calculate other cases by applying the above result. If $d - \Delta - 1 < \Delta$, we just substitute $d - \Delta - 1$ into Δ . For a field of the complementary series, we extract a real part as

$$\langle \boldsymbol{\epsilon}_{1}^{S}.\hat{\Phi}(\tau,k)\,\boldsymbol{\epsilon}_{2}^{S}.\hat{\Phi}(\tau,k')\rangle = (2\pi)^{d-1}\delta^{d-1}(k+k')\operatorname{Re}\left[\tau^{2\Delta}\langle \boldsymbol{\epsilon}_{1}^{S}.\phi(\tau,k)\,\boldsymbol{\epsilon}_{2}^{S}.\phi(\tau,-k)\rangle'\right]. \tag{3.60}$$

3.3.2 Higuchi bound

To derive the Higuchi bound, let us decompose states in the helicity basis. In this section, we utilze properties of the spherical harmonics and the Gegenbauer polynomials. We recommend that those who are not familiar with these topics read Appendix. A. To begin with, it is convenient to choose the polarization vectors and the momentum as follows:

$$\mathbf{k} = (0, \dots 0, \mathbf{k}), \quad \boldsymbol{\epsilon}_1 = (\hat{x}, i), \quad \boldsymbol{\epsilon}_2 = (\hat{y}, -i),$$
 (3.61)

where \hat{x} and \hat{y} are unit vectors of d-2 dimensions. In this configuration, the following identities hold,

$$(\boldsymbol{\epsilon}_1 \cdot \boldsymbol{k})(\boldsymbol{\epsilon}_2 \cdot \boldsymbol{k}) = k^2, \quad \boldsymbol{\epsilon}_1 \cdot \boldsymbol{\epsilon}_2 = \hat{x} \cdot \hat{y} + 1.$$
 (3.62)

and

$$\langle \boldsymbol{\epsilon}_{1}^{S}.\phi(\boldsymbol{k})\boldsymbol{\epsilon}_{2}^{S}.\phi(-\boldsymbol{k})\rangle' = (-2)^{S} \frac{A_{S}}{\mathbf{k}^{d-1-2\Delta}} \frac{S!\Gamma(\Delta-1)}{\Gamma(\Delta+S-1)} P_{S}^{(\Delta-S-\frac{d}{2}-\frac{1}{2},\frac{d}{2}-\frac{5}{2})} \left(-\hat{x}\cdot\hat{y}\right). \tag{3.63}$$

The momentum is invariant under SO(d-2) rotation. Hence we factorize the states into irreducible elements under SO(d-2). This can be done by defining operators in the helicity basis as,

$$\phi_{lm}(\mathbf{k}) = \int d\Omega_{d-3} Y_{lm}(\hat{x}) \epsilon^{S}.\phi(\mathbf{k}), \qquad (3.64)$$

where Y_{lm} are spherical harmonics. Here, l represents an spin under SO(d-2) rotation. And, m denotes linearly independent elements, the number of which is N(d-2, l),

$$N(d-2,l) = \frac{2l+d-2}{l} \begin{pmatrix} l+d-3\\ l-1 \end{pmatrix}.$$
 (3.65)

Here, we use the combinatorial factorial,

$$\begin{pmatrix} \alpha \\ \beta \end{pmatrix} = \frac{\alpha!}{(\alpha - \beta)!\beta!}.$$
 (3.66)

Also, the integral is over a unit shpere. The spherical harmonics are normalized as

$$\int d\Omega_{d-3} Y_{lm}(\hat{x}) Y_{lm}(\hat{x}) = \delta_{ll'} \delta_{mm'}. \tag{3.67}$$

See Appendix. A.2 for details of the spherical harmonics. To derive two point functions in the helicity basis, let us reorganize Eq. (3.63). First, combining Eq. (A.13) and Eq. (A.14), we expand the Jacobi polynomial by the Gegenbauer polynomials as

$$P_{S}^{(\Delta - s - \frac{d}{2} - \frac{1}{2}, \frac{d}{2} - \frac{5}{2})}(-\hat{x} \cdot \hat{y}) = (-1)^{S} \sum_{l=0}^{S} \frac{d + 2l - 4}{(d + S + l - 4)!(S - l)!} \frac{\Gamma(\frac{d}{2} + S - \frac{3}{2})\Gamma(d - 4)}{\Gamma(\frac{d}{2} - \frac{3}{2})} \times \frac{\Gamma(d + S - \Delta - 2)}{\Gamma(\Delta - 1)} \frac{\Gamma(\Delta + l - 1)}{\Gamma(d + l - \Delta - 2)} C_{l}^{\frac{d}{2} - 2}(\hat{x} \cdot \hat{y}),$$
(3.68)

where the Gegenbauer polynomials are defiend as

$$C_n^{\alpha}(x) = \frac{\Gamma(n+2\alpha)}{\Gamma(2\alpha)\Gamma(n+1)} {}_2F_1 \left[\begin{array}{c} -n, n+2\alpha \\ \alpha + \frac{1}{2} \end{array}; \frac{1-x}{2} \right]. \tag{3.69}$$

We also used a symmetric property of the Gegenbauer polynomial,

$$C_l^{\frac{d}{2}-2}(-\hat{x}\cdot\hat{y}) = (-1)^l C_l^{\frac{d}{2}-2}(\hat{x}\cdot\hat{y})$$
(3.70)

See also Appendix. A.1 for details of the Gegenbauer polynomial. Further we apply the addition theorem of the spherical harmonics (See Appendix. A.2.1),

$$C_l^{\frac{d}{2}-2}(\hat{x}\cdot\hat{y}) = \frac{4\pi^{\frac{d-2}{2}}}{2l+d-4} \frac{1}{\Gamma(\frac{d}{2}-2)} \sum_{m=1}^{N(d-2,l)} Y_{lm}(\hat{x}) Y_{lm}(\hat{y}).$$
(3.71)

Then, Eq. (3.63) reads

$$\langle \boldsymbol{\epsilon}_{1}^{S}.\phi(\boldsymbol{k})\boldsymbol{\epsilon}_{2}^{S}.\phi(-\boldsymbol{k})\rangle' = 4\pi^{\frac{d-2}{2}}2^{S}S!\frac{A_{S}}{\mathbf{k}^{d-1-2\Delta}}\frac{\Gamma(d+S-\Delta-2)\Gamma(\frac{d}{2}+S-\frac{3}{2})\Gamma(d-4)}{\Gamma(\Delta+S-1)\Gamma(\frac{d}{2}-2)\Gamma(\frac{d}{2}-\frac{3}{2})}$$

$$\sum_{m=0}^{N(d-2,l)}\frac{1}{(d+S+l-4)!(S-l)!}\frac{\Gamma(\Delta+l-1)}{\Gamma(d+l-\Delta-2)}Y_{lm}(\hat{x})Y_{lm}(\hat{y}) \quad (3.72)$$

From the orthogonality of the spherical harmonics (3.67), we can derive the two point function in the helicity basis as,

$$\langle \phi_{lm}(\mathbf{k})\phi_{l'm'}(-\mathbf{k})\rangle' = 4\pi^{\frac{d-2}{2}} 2^{S} S! \frac{A_{S}}{\mathbf{k}^{d-1-2\Delta}} \frac{\Gamma(d+S-\Delta-2)\Gamma(\frac{d}{2}+S-\frac{3}{2})\Gamma(d-4)}{\Gamma(\Delta+S-1)\Gamma(\frac{d}{2}-2)\Gamma(\frac{d}{2}-\frac{3}{2})} \frac{1}{(d+S+l-4)!(S-l)!} \frac{\Gamma(\Delta+l-1)}{\Gamma(d+l-\Delta-2)} \delta_{ll'} \delta_{mm'}.$$
(3.73)

Let us examine the sign. First, we renormalize the coefficients as

$$\langle \phi_{lm}(\mathbf{k}) \phi_{lm}(-\mathbf{k}) \rangle' = \frac{B_l}{\mathbf{k}^{d-2\Delta-1}},$$
 (3.74)

where the coefficient of the maximum helicity is given by

$$B_S = A_S \frac{\Gamma(\frac{d}{2} + S - \frac{3}{2})\Gamma(d - 4)}{\Gamma(\frac{d}{2} - 2)\Gamma(\frac{d}{2} - \frac{3}{2})} \frac{4\pi^{\frac{d-2}{2}} 2^S S!}{(d + 2S - 4)!}.$$
(3.75)

The coefficients of lower helicity states are derived from the maximum helicity states as,

$$B_{l} = B_{S} \frac{(d+S-\Delta-2)\times\cdots\times(d+l-\Delta-2)}{(\Delta+S-2)\times\cdots\times(\Delta+l-1)} \frac{\Gamma(d+2S-3)\Gamma(S+1)}{\Gamma(d+S+l-3)\Gamma(S-l+1)}$$
(3.76)

Interestringly, if $\Delta < 1$, ⁴ the sign of B_0 becomes negative even when B_S is positive, which means that the lowest helicity state has a negative norm. Translating this into the condition of the mass by using the relation (3.33), we obtain the forbidden mass range,

$$0 < M^2 < H^2 S(S - d + 3). (3.77)$$

This is the Higuchi bound. We remark that $\Delta=1-\alpha$ ($\alpha=0\cdots S-1$) are exceptional. In these cases, the coefficient B_m diverges at $m=\alpha$. This means that B_S and consequently all coefficients vanish. Instead, the shadow operator of the dimension $\bar{\Delta}=\frac{d-1}{2}-\Delta$ becomes dominant. The contribution of the shadow operator is obtained by substituting $d-\Delta-1$ into Δ in Eq. (3.76). Then, we find that norms of lower helicity than $\alpha+1$ become zero. This implies that a gauge symmetry is emerged, and such states are gauged away. In particular, the field of $\alpha=S-1$ is a massless field. A field of $0 \le \alpha \le S-2$ are called partially massless fields due to a small gauge symmetry than a massless field. As a result, there appear no negative norm states for the massless and partially massless fields, and therefore they are not forbidden.

3.4 Implication for higher spin states in string theory

We conclude this section with discussing an implication of the Higuchi bound to the string spectrum. In general dimensional de Sitter space, a forbidden mass range of the Higuchi bound is

$$0 < M^2 < H^2 S(S - d + 3). (3.78)$$

This upper bound on the mass square grows quadrically as the spin increases. Recall the leading Regge trajectory in flat space, which is given by

$$M^2 = \frac{2}{\alpha'}(S-2). (3.79)$$

This Regge trajectory grows linearly as the spin increases. Therefore, there is a possibility that the string Regge trajectory is inconsistent with the Higuchi bound in de Sitter space (See Fig. 3.3). To

 $^{^4}B_0$ is also negative when $\Delta > d-2$. This case can be neglected since we assume that $\Delta < d-\Delta-1$, that is, $\Delta < \frac{d-1}{2}$.

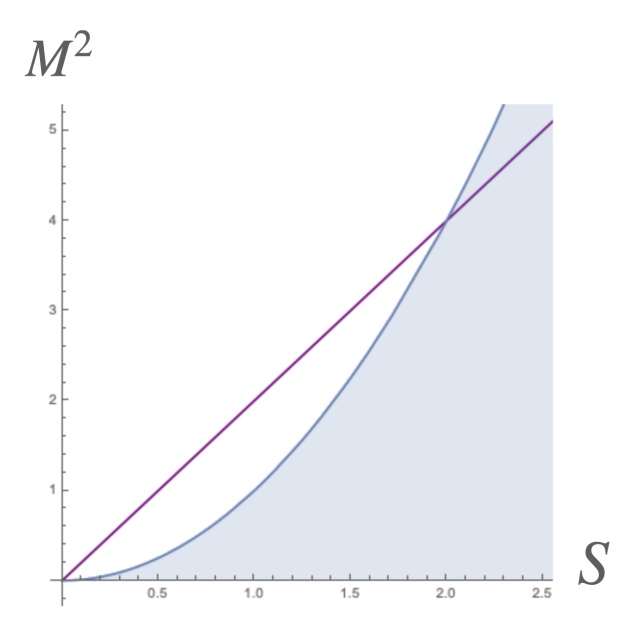


Figure 3.3: The Higuchi bound and the leading Regge trajectory(Red line): The blue region is prohibited by the Higuchi bound. The spin S and the energy E are plotted in the units of $1/(H^2\alpha')$ and R/α' , respectively

discuss more rigorously, let us consider what type of string states may violate the Higuchi bound. When they conflict, the spin and the mass become

$$S = \frac{2}{\alpha' H^2}, \quad M^2 = \frac{4}{\alpha'^2 H^2}.$$
 (3.80)

Hence a string length l becomes a comparable to the curvature scale of de Sitter space, which can be estimated as

$$l \simeq M \times \alpha' = \frac{2}{H} \,. \tag{3.81}$$

We note that α' is an inverse of the string tension. Such a long string should feel the curvature effect so that its spectrum may be modified. Otherwise we conclude that a worldsheet theory is inconsistent in de Sitter space. In the rest of this thesis, we study classical string spectra on de Sitter background and examine this potential inconsistency. A validity of a classical approximation is discussed at the beginning of the next chapter. First we study classical strings on dS_3 in Chap. 4 and generalize them to string on $dS_3 \times S_1$ in Chap. 5. We will see that string Regge trajectories are modified by curvature effects in a nontrivial way. One may wonder that the mild behavior of the Regge limit can be kept on under modified Regge trajectories. We will discuss this point as a concluding remark in Chap. 6.

Chapter 4

Classical strings on de Sitter space

The potential inconsistency between the flat space Regge trajectory and the Higuchi bound motivates us to study the string specturm in de Sitter space. For a rigorous discussion, first we have to quantize a worldsheet theory and then identify physical states which respect a worldsheet symmetry, as developed in Sec. 2.2. However, it is difficult to carry out the quantization straightforwardly because the worldsheet action is nonlinear on de Sitter background. To avoid this difficulty, we study a classical string spectrum. The violation of the Higuchi bound might occur when a string length approaches the cosmological horizon. A classical approximation must be good for such a long string regime because strings should be larger than its Compton length.

In this section, we study two classes of classical strings, a folded string and a spiky string. Results in flat space and in AdS space [38,50] indicate that spectra of these strings approximate the leading Regge trajectory and the sub-leading Regge trajectory respectively. The organization of this chapter is as follows. First we summarize a setup of our study in Sec. 4.1. Then, we study a fold string solution and a spiky string solution in order.

4.1 Setup

In this section we summarize basics of the worldsheet theory in de Sitter space necessary for our semiclassical analysis. See also Ref. [39] for a nice review on semiclassical strings in AdS. Our argument is analogous to the one there except for the fact that de Sitter space has an acceleration and a cosmological horizon accordingly, which turns out to bring about qualitative differences from the flat space and AdS cases.

4.1.1 Target space

In this chapter we study string Regge trajectories on dS_3 (which may also be identified with an appropriate subspace of a larger target space). We generalize to strings on $dS_3 \times S_1$ in the next chapter. For our purpose, it is convenient to analyse in the static coordinates of dS_3 . This coordinate system is obtained by setting d=3 in Eq. (3.16):

$$Y_3 + Y_0 = R\sqrt{1 - r^2}e^t$$
, $Y_3 - Y_0 = R\sqrt{1 - r^2}e^{-t}$, $Y_1 = R r \cos \phi$, $Y_2 = R r \cos \phi$, (4.1)

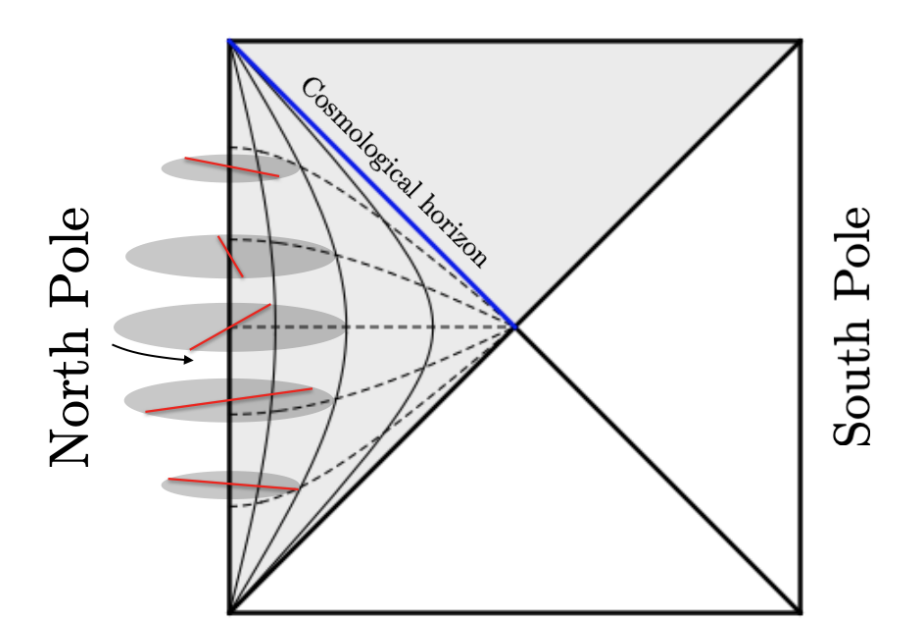


Figure 4.1: Penrose diagram of dS_3 : Each point represents an S^1 subspace and the edges correspond to the north and south poles of S^2 . For example, the planar coordinates cover a half of the whole space (the shaded region) and the cosmological horizon for an observer sitting at the north pole is the blue line. The static coordinates cover a half of the planar coordinates $Y_3 \pm Y_0 \ge 0$, that is inside the cosmological horizon. The dotted and rigid curves are sections of constant t and $r(=\sin \rho)$, respectively. We study strings rotating around the center r = 0 ($\rho = 0$) of the static coordinate.

where $-\infty < t < \infty$, $0 \le r \le 1$, and ϕ has a periodicity 2π . Also, we used a de Sitter radius R instead of the Hubble scale H as

$$R = \frac{1}{H} \,. \tag{4.2}$$

The corresponding metric is

$$ds^{2} = R^{2} \left[-(1 - r^{2})dt^{2} + \frac{dr^{2}}{1 - r^{2}} + r^{2}d\phi^{2} \right].$$
 (4.3)

To utilize results in AdS, it is convenient to introduce a coordinate ρ defined by $\sin \rho = r$ $(0 \le \rho \le \pi/2)$, in terms of which the metric reads

$$ds^{2} = R^{2} \left(-\cos^{2} \rho \, dt^{2} + d\rho^{2} + \sin^{2} \rho \, d\phi^{2} \right) \,. \tag{4.4}$$

Note that in these coordinates, the observer sitting at the origin and the cosmological horizon are located at $\rho = 0$ and $\rho = \pi/2$, respectively. Since global coordinates of AdS are obtained by a Wick rotation,

$$\rho \to -i\rho$$
, $t \to it$, $R^2 \to -R^2$, (4.5)

we may generalize semiclassical solutions in AdS to de Sitter space in a straightforward manner. Together with an internal S^1 parameterized by the coordinate φ , our target space metric is given 4.1. SETUP 43

by

$$ds^{2} = R^{2} \left(-\cos^{2} \rho \, dt^{2} + d\rho^{2} + \sin^{2} \rho \, d\phi^{2} + d\varphi^{2} \right) , \tag{4.6}$$

where for generality we leave the periodicity of φ a free parameter. In other words, we absorb the radius of the circle S^1 into the definition of φ .

4.1.2 Worldsheet theory

Let us consider the Nambu-Goto string on the target space (4.6):

$$S_{NG} = -\frac{1}{2\pi\alpha'} \int d\tau d\sigma \sqrt{-\dot{X}^2 X'^2 + (\dot{X} \cdot X')^2}, \qquad (4.7)$$

where $(2\pi\alpha')^{-1}$ is the string tension and we defined

$$\dot{X}^2 = G_{AB}\dot{X}^A\dot{X}^B \,, \quad X'^2 = G_{AB}X'^AX'^B \,, \quad \dot{X} \cdot X' = G_{AB}\dot{X}^AX'^B \,, \tag{4.8}$$

with $X^A = (t, \rho, \phi, \varphi)$ and a target space metric.

$$G_{AB} = R^2 \cdot \text{diag}\left(-\cos^2\rho, 1, \sin^2\rho, 1\right)$$
 (4.9)

Also the dot and prime stand for derivatives in the worldsheet time coordinate τ and the worldsheet spatial coordinate σ , respectively. The equation of motion for X^A reads

$$0 = \partial_{\tau} \left[\frac{G_{AB} \left(\dot{X}^{B} X'^{2} - X'^{B} \left(\dot{X} \cdot X' \right) \right)}{\sqrt{-\dot{X}^{2} X'^{2} + \left(\dot{X} \cdot X' \right)^{2}}} \right] + \partial_{\sigma} \left[\frac{G_{AB} \left(X'^{B} \dot{X}^{2} - \dot{X}^{B} \left(\dot{X} \cdot X' \right) \right)}{\sqrt{-\dot{X}^{2} X'^{2} + \left(\dot{X} \cdot X' \right)^{2}}} \right] - \frac{\partial_{A} G_{BC} \left[\dot{X}^{B} \dot{X}^{C} X'^{2} + X'^{B} X'^{C} \dot{X}^{2} - 2 \dot{X}^{B} X'^{C} \left(\dot{X} \cdot X' \right) \right]}{2\sqrt{-\dot{X}^{2} X'^{2} + \left(\dot{X} \cdot X' \right)^{2}}} . \tag{4.10}$$

Rigid string ansatz. Classical string solutions discussed in this thesis are captured by the following ansatz for closed string configurations:

$$t = \tau$$
, $\rho = \rho(\sigma)$, $\phi = \omega \tau + N\sigma$, $\varphi = \nu \tau + \psi(\sigma)$, (4.11)

where σ has a periodicity 2π and we require $\rho(\sigma+2\pi)=\rho(\sigma)$ and $\psi(\sigma+2\pi)=\psi(\sigma)$, assuming that the string has no winding along the circle S^1 . Also, ω and ν are constant angular velocities, and N is an integer characterizing the "winding" number along the angle ϕ . Note that the case without internal space is covered simply by setting $\nu=\psi=0$. As depicted, e.g., in Fig. 5.1, the string at a fixed time $t=\tau$ is spreading on the two-dimensional (ρ,ϕ) plane. It then rotates along ϕ and φ with angular velocities ω and ν .

With the ansatz (4.11), the equations of motion (4.10) reduce to the following (generally) independent three equations:

$$0 = -\partial_{\sigma} \left[\frac{\rho'(\cos^{2}\rho - \omega^{2}\sin^{2}\rho - \nu^{2})}{\sqrt{\mathcal{D}}} \right] + \frac{1}{2} \frac{\sin 2\rho \left[-(1+\omega^{2})(\rho'^{2} + \psi'^{2}) + 2N\nu\omega\psi' + N^{2}\cos 2\rho - N^{2}\nu^{2} \right]}{\sqrt{\mathcal{D}}},$$
(4.12)

$$0 = \partial_{\sigma} \left[\frac{\cos^2 \rho (N\omega \sin^2 \rho + \nu \psi')}{\sqrt{\mathcal{D}}} \right] , \qquad (4.13)$$

$$0 = \partial_{\sigma} \left[\frac{\nu \omega \sin^2 \rho \, \psi' + N(\cos^2 \rho - \nu^2) \sin^2 \rho}{\sqrt{\mathcal{D}}} \right] \,, \tag{4.14}$$

where we introduced

$$\mathcal{D} = \frac{-\dot{X}^2 X'^2 + (\dot{X} \cdot X')^2}{R^4}$$

$$= (\cos^2 \rho - \omega^2 \sin^2 \rho - \nu^2) \rho'^2 + (\cos^2 \rho - \omega^2 \sin^2 \rho) \psi'^2$$

$$+ 2N\nu\omega \sin^2 \rho \, \psi' + N^2 (\cos^2 \rho - \nu^2) \sin^2 \rho \,. \tag{4.15}$$

Note that reality conditions require $\mathcal{D} \geq 0$, otherwise the corresponding Nambu-Goto action becomes imaginary. Also one may show that when both $\mathcal{D} \neq 0$ and $\rho' \neq 0$ are satisfied, Eq. (4.12) follows from Eqs. (4.13) and (4.14).

Energy, spin and internal U(1) charge. To close the section, let us write down the energy E, spin S, and internal U(1) charge J, which are of interest in the discussion of the Regge trajectory. Defining them as conjugates of Rt, $-\phi$, and $-\varphi$, respectively, we have

$$E = \frac{R}{2\pi\alpha'} \int_0^{2\pi} d\sigma \frac{\cos^2 \rho (\rho'^2 + N^2 \sin^2 \rho + \psi'^2)}{\sqrt{D}},$$
 (4.16)

$$S = \frac{R^2}{2\pi\alpha'} \int_0^{2\pi} d\sigma \frac{\sin^2 \rho(\omega \rho'^2 + \omega \psi'^2 - N\nu\psi')}{\sqrt{\mathcal{D}}},$$
(4.17)

$$J = \frac{R^2}{2\pi\alpha'} \int_0^{2\pi} d\sigma \frac{\nu \rho'^2 + N^2 \nu \sin^2 \rho - N\omega \sin^2 \rho \psi'}{\sqrt{\mathcal{D}}}, \qquad (4.18)$$

which satisfies the following relation:

$$\frac{R^2}{2\pi\alpha'} \int_0^{2\pi} d\sigma \sqrt{\mathcal{D}} = RE - \omega S - \nu J. \tag{4.19}$$

4.2 Folded strings

Let us begin with studying folded strings (See Ref. [38] for folded strings in AdS). The folded string configuration is captured by the ansatz (4.11) with $\nu = N = \psi = 0$, under which Eqs. (4.13)-(4.14) become trivial, whereas Eq. (4.12) gives

$$\partial_{\sigma} \left(\frac{\rho'}{|\rho'|} \right) \sqrt{\cos^2 \rho - \omega^2 \sin^2 \rho} = 0 \iff \delta(\sigma - \sigma_f) \sqrt{\cos^2 \rho - \omega^2 \sin^2 \rho} = 0. \tag{4.20}$$

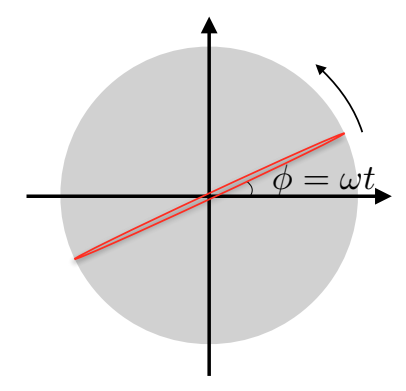


Figure 4.2: A folded closed string rotating around the origin $\rho = 0$ along an equator of S^2 with angular velocity ω .

Notice that the equation of motion is localized at the folding point $\sigma = \sigma_f$ where ρ' flips the sign, simply because changes in the bulk profile $\rho(\sigma)$ ($\sigma \neq \sigma_f$) are gauge degrees of freedom associated to string reparameterization. Also the folding point satisfies

$$\cos^2 \rho - \omega^2 \sin^2 \rho = 0, \tag{4.21}$$

and so it propagates with the speed of light, which is essentially the same as the familiar statement that open string end points propagate with the speed of light. Then, for given ω , the radius ρ_f of the folding point is determined by

$$\cot^2 \rho_f = \omega^2 \,, \tag{4.22}$$

which is the maximum distance dictated by causality prohibiting superluminal propagation of the string. In general, closed strings may have multiple foldings, so that the solutions are parameterized by the angular velocity ω , and the folding number N_f .

Conserved charges. For these folded strings, the conserved charges (4.16)-(4.17) read

$$E = \frac{4N_f R}{2\pi\alpha'} \int_0^{\rho_f} d\rho \frac{\cos^2 \rho}{\sqrt{1 - (\sin^2 \rho / \sin^2 \rho_f)}} , \qquad (4.23)$$

$$S = \omega \times \frac{4N_f R^2}{2\pi\alpha'} \int_0^{\rho_f} d\rho \frac{\sin^2 \rho}{\sqrt{1 - (\sin^2 \rho / \sin^2 \rho_f)}}$$
(4.24)

One may also rewrite them in terms of incomplete elliptic integrals,

$$\mathcal{E}\left(\zeta|k^2\right) = \int_0^{\zeta} d\theta \sqrt{1 - k^2 \sin^2 \theta} \ , \quad \mathcal{F}\left(\zeta|k^2\right) = \int_0^{\zeta} d\theta \frac{1}{\sqrt{1 - k^2 \sin^2 \theta}} \ , \tag{4.25}$$

as follows:

$$E = \frac{4N_f R}{2\pi \alpha'} \left[\sin^2 \rho_f \mathcal{E} \left(\rho_f | \csc^2 \rho_f \right) + \cos^2 \rho_f \mathcal{F} \left(\rho_f | \csc^2 \rho_f \right) \right] , \qquad (4.26)$$

$$S = \omega \times \frac{4N_f R^2}{2\pi\alpha'} \sin^2 \rho_f \left[-\mathcal{E} \left(\rho_f | \csc^2 \rho_f \right) + \mathcal{F} \left(\rho_f | \csc^2 \rho_f \right) \right]$$
(4.27)

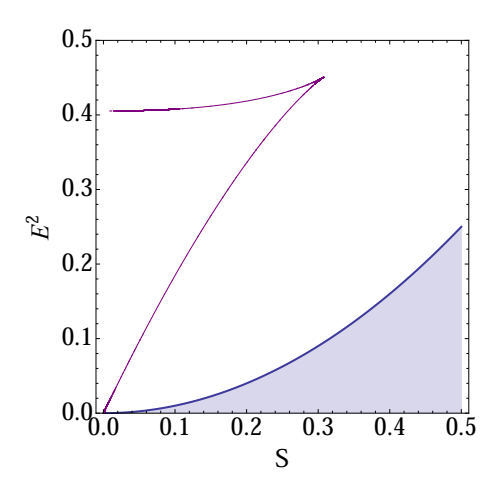


Figure 4.3: Leading Regge trajectory vs. Higuchi bound: The leading Regge trajectory (the spiky curve) turns back to lower spins at a maximum spin before hitting the shaded region prohibited by the Higuchi bound. The spin S and the energy E are plotted in the units of R^2/α' and R/α' , respectively. The same units are used in Fig. 4.4.

These expressions can be used to derive energy-spin relations and draw Regge trajectories.

This provides the energy-spin relation through the parameter ρ_f characterizing the length of the string. In Fig. 4.3 we plot the energy squared E^2 as a function of the spin S. See also Fig. 4.4 for S and E^2 as functions of ρ_0 . As we explain below, there exists a maximum spin at the intermediate scale [36]¹. The leading Regge trajectory then turns out to be consistent with the Higuchi bound.

4.2.1 Short strings

Let us first look at the spectrum of short strings. When the angular velocity ω is large, strings cannot be so long because of causality. In this regime, we have $\rho_f \simeq \omega^{-1}$ and the string does not feel the spacetime curvature. The energy and spin are then the same as the flat space ones,

$$E \simeq \frac{R}{\alpha'} \rho_f \,, \quad S \simeq \frac{R^2}{2\alpha'} \rho_f^2 \,,$$
 (4.28)

which enjoy the linear Regge trajectory:

$$E^2 \simeq \frac{2}{\alpha'} S. \tag{4.29}$$

4.2.2 Long strings

Another extremal case is the small ω limit, under which we have $\rho_f \simeq \pi/2 - \omega$. In this regime, the string end points approach to the cosmological horizon $\rho = \pi/2$, so that the spacetime curvature is not negligible. It is easy to evaluate the energy and spin as

$$E \simeq \frac{2R}{\pi \alpha'}, \quad S \simeq -\frac{2R^2}{\pi \alpha'} \omega \ln \omega.$$
 (4.30)

¹Existence of a similar maximum spin was also observed in the context of the AdS/dS correspondence [86].

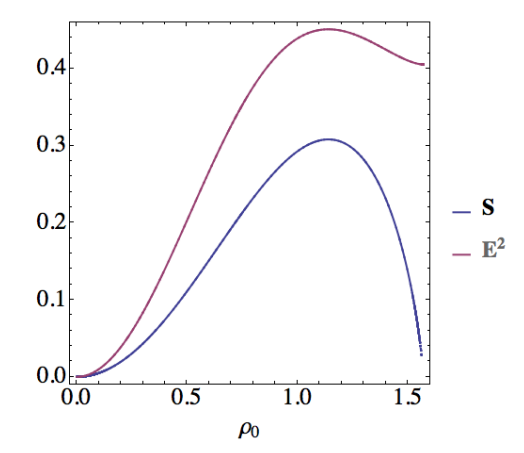


Figure 4.4: The spin S and energy squared E^2 as functions of ρ_f : We find that both have a peak at $\rho_f \simeq 1.14$. Recall that there are two sources of the energy: one proportional to the string length and the other from the string rotation. Then, the maximum energy appears when the spin takes the maximum value. As a result, Fig. 4.3 has a spiky shape.

Interestingly, the spin vanishes in this limit, whereas the mass approaches to a fixed value. This is in a sharp contrast to the AdS case [36,38].

It will be instructive to elaborate on the qualitative difference of Regge trajectories on flat space, AdS, and dS. As we mentioned, the length of rotating strings characterized by ρ_f is determined by causality of the Nambu-Goto string. On flat space, the velocity of the string end points is given by $\rho_f \omega$, so that causality tells us that $\rho_f = \omega^{-1}$. In particular, ω and ρ_f can take an arbitrary positive value. On the other hand, on AdS, there is a lower-bound $\omega > 1$ on ω , which is saturated by rotating strings touching the AdS boundary, essentially because AdS is compact. In both cases, the spin increases as we decrease the angular velocity ω (or equivalently as the string length ρ_0 increases).

Finally, let us consider the de Sitter case, where the accelerated expansion of the universe plays a crucial role. First, the Hubble law implies that velocity exceeds the speed of light beyond the Hubble horizon. Therefore, the end points of a folded closed string cannot stretch beyond the horizon. Note that when the end points touch the cosmological horizon, their velocity coincides with the speed of light for $\omega = 0$, so that any nonzero ω leads to a causality violation. Therefore, there exists a maximum value of the string length ρ_f , for which the angular velocity ω and then the spin S have to vanish.

In this way, the spectrum of long strings on de Sitter is qualitatively different from the flat space and AdS ones. In particular, the longest string has a vanishing spin and a finite mass due to the accelerated expansion.

4.2.3 Maximum spin

We have argued that both the shortest string $\rho_f = 0$ and the longest one $\rho_f = \pi/2$ have a vanishing spin S = 0. It suggests that there exists a maximum spin S_* on the Regge trajectory. From the

expression (4.27), we find that the maximum spin appears at $\rho_f \simeq 1.14$, for which the mass E_* and the spin S_* are

$$E_* \simeq 0.67 \times R/\alpha', \quad S_* \simeq 0.31 \times R^2/\alpha',$$
 (4.31)

which is above the Higuchi bound. The full trajectory for $0 \le \rho_f \le \pi/2$ is give in Fig. 4.3, which shows that the semiclassical rotating strings have a spectrum consistent with the Higuchi bound. Even though our analysis focused on a rotating folded closed string, any more internal structures will increase the mass, hence the spectrum shown in Fig. 4.3 will provide the leading Regge trajectory. We therefore conclude that the semiclassical string spectrum on de Sitter space is consistent with the Higuchi bound. Note that our conclusion is independent of the ratio M_s/H as long as $M_s \gg H$ (i.e., within the validity of the semiclassical approximation).

4.3 Spiky strings

Next, we study spiky strings (see Ref. [50] for spiky strings in AdS). In this section we focus on the case without internal motion, so that our ansatz here is Eq. (4.11) with $\nu = \psi = 0$, under which the equations of motion (4.12)-(4.14) reduce to

$$0 = -\partial_{\sigma} \left[\frac{\rho'(\cos^{2}\rho - \omega^{2}\sin^{2}\rho)}{\sqrt{(\cos^{2}\rho - \omega^{2}\sin^{2}\rho)\rho'^{2} + N^{2}\cos^{2}\rho\sin^{2}\rho}} \right]$$

$$+ \frac{1}{2} \frac{\sin 2\rho[-(1+\omega^{2})\rho'^{2} + N^{2}\cos 2\rho]}{\sqrt{(\cos^{2}\rho - \omega^{2}\sin^{2}\rho)\rho'^{2} + N^{2}\cos^{2}\rho\sin^{2}\rho}},$$
(4.32)

$$0 = \partial_{\sigma} \left[\frac{\cos^2 \rho \sin^2 \rho}{\sqrt{(\cos^2 \rho - \omega^2 \sin^2 \rho)\rho'^2 + N^2 \cos^2 \rho \sin^2 \rho}} \right]. \tag{4.33}$$

To follow the string dynamics, it is convenient to integrate Eq. (4.33) as

$$|\rho'| = \frac{N}{2} \frac{\sin 2\rho}{\sin 2\rho_0} \sqrt{\frac{\sin^2 2\rho - \sin^2 2\rho_0}{\cos^2 \rho - \omega^2 \sin^2 \rho}},$$
 (4.34)

where the integration constant ρ_0 is chosen such that $\rho'=0$ for $\rho=\rho_0$. For later use, we also define ρ_1 such that $\cot^2\rho_1=\omega^2$ and $0<\rho_1<\frac{\pi}{2}$. In this language, we have

$$|\rho'| = \frac{N\sin\rho_1\sin2\rho}{\sqrt{2}\sin2\rho_0} \sqrt{\frac{\cos^22\rho_0 - \cos^22\rho}{\cos2\rho - \cos2\rho_1}}.$$
 (4.35)

Three shapes. Notice that ρ' has to flip a sign somewhere in order for a closed string to form a loop, otherwise the string stretches forever. Such a sign flip may appear when $\rho' = 0$ or $\rho' = \infty$. Eq. (4.35) shows that $\rho' = 0$ is satisfied at $\rho = \rho_0$, $\frac{\pi}{2} - \rho_0$. At these points, the string smoothly turns back from inside to outside or vice versa. Without loss of generality, we assume $0 < \rho_0 < \frac{\pi}{4}$ in the following. On the other hand, $\rho' = \infty$ is satisfied at $\rho = \rho_1$, where the string turns back forming a spike. Based on the value of ρ_1 relative to ρ_0 and $\frac{\pi}{2} - \rho_0$, we may classify shapes of the string into the following three classes:

4.3. SPIKY STRINGS 49

1. Outward spikes $(\rho_0 < \rho_1 < \frac{\pi}{2} - \rho_0)$

Recall that the inside of the square root in Eq. (4.35) has to be positive for ρ to be real. Therefore, the reality condition implies that for this parameter set, the string may stretch only inside the region $\rho_0 \leq \rho \leq \rho_1$. This means that the outer turning points are spiky, and the inner ones are smooth. We call such strings outward spike solutions. See Fig. 4.6.

2. Rounded spikes $(\rho_0 < \frac{\pi}{2} - \rho_0 < \rho_1)$

Similarly, for $\frac{\pi}{2} - \rho_0 < \rho_1 < \frac{\pi}{2}$, the reality condition implies that the string may stretch only inside the region $\rho_0 \le \rho \le \frac{\pi}{2} - \rho_0$. In contrast to the case of outward spikes, strings in this class have no spikes and all the turning points are smooth. We call such strings rounded spike solutions. See Fig. 4.10. Note that these strings are specific to de Sitter space and there are no counterpart in flat space and AdS.

3. Inward spikes $(\rho_1 < \rho_0 < \frac{\pi}{2} - \rho_0)$

Finally, for $\rho_1 < \rho_0$, the string may stretch only inside the region $\rho_1 \le \rho \le \rho_0$. This means that the outer turning points are smooth, and the inner ones are spiky. We call such strings inward spike solutions. See Fig. 4.11.

Periodicity conditions. The above argument is useful enough to classify local shapes of the string. On the other hand, the full string is made of multiple segments between the spikes. In order for a closed string to form a loop, the angle $\Delta \phi$ of each segment has to be quantized appropriately. For our ansatz, an explicit form of $\Delta \phi$ is given by

$$\Delta \phi = 2N \int_{\rho_{\min}}^{\rho_{\max}} \frac{d\rho}{\rho'}$$

$$= 2 \int_{\rho_{\min}}^{\rho_{\max}} d\rho \frac{\sqrt{2} \sin 2\rho_0}{\sin \rho_1 \sin 2\rho} \sqrt{\frac{\cos 2\rho - \cos 2\rho_1}{\cos^2 2\rho_0 - \cos^2 2\rho}},$$
(4.36)

where ρ_{\min} and ρ_{\max} are the minimum and the maximum values of ρ . More explicitly, $(\rho_{\min}, \rho_{\max}) = (\rho_0, \rho_1), (\rho_0, \frac{\pi}{2} - \rho_0), (\rho_1, \rho_0)$ for outward spikes, rounded spikes, and inward spikes, respectively. Then, the global consistency requires that

$$\Delta \phi = \frac{2\pi N}{n} \,, \tag{4.37}$$

where n is a positive integer characterizing the number of spikes. This determines the value of ρ_1 for given ρ_0 , n, and N. See also Fig. 4.5 for a plot of $2\pi/\Delta\phi$ as a function of ρ_0 and ρ_1 , which shows a smooth transition from outward spikes to rounded spikes for fixed n and N.

Energy and spin. For later convenience, we provide the energy and the spin (4.16)-(4.17) for the present class of solutions by using Eq. (4.35) as

$$E = \frac{\omega S}{R} + \frac{R}{2\pi\alpha'}(2n) \int_{\rho_{\min}}^{\rho_{\max}} d\rho \sin 2\rho \frac{\sqrt{\cos^2 \rho - \omega^2 \sin^2 \rho}}{\sqrt{\sin^2 2\rho - \sin^2 2\rho_0}},$$
 (4.38)

$$S = \frac{R^2}{2\pi\alpha'} \times \frac{1}{2} (2n) \int_{\rho_{\min}}^{\rho_{\max}} d\rho \frac{\omega \sin \rho}{\cos \rho} \frac{\sqrt{\sin^2 2\rho - \sin^2 2\rho_0}}{\sqrt{\cos^2 \rho - \omega^2 \sin^2 \rho}}, \tag{4.39}$$

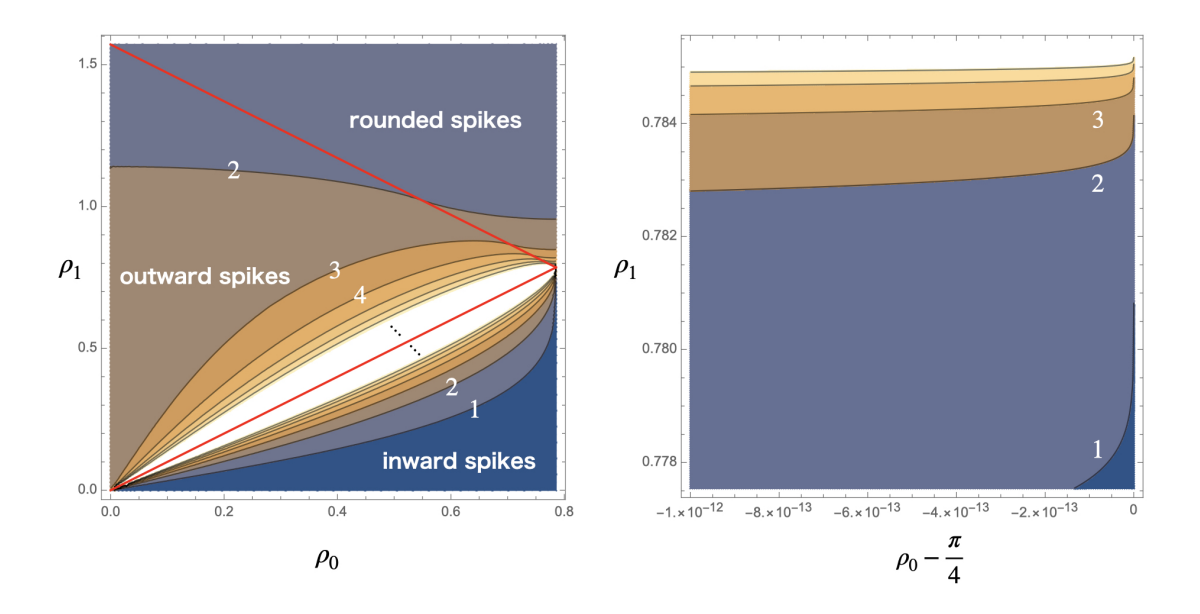


Figure 4.5: Contour plot of $2\pi/\Delta\phi$ as a function of ρ_0 and ρ_1 : An integer on each contour represents the value of $2\pi/\Delta\phi$ for given ρ_0 and ρ_1 , which has to be n/N for n-spike strings with the winding number N. The two red lines, $\rho_1 = \rho_0$ and $\rho_1 = \frac{\pi}{2} - \rho_0$, separate the $\rho_0 - \rho_1$ plane into three regions which accommodate outward spikes, rounded spikes, and inward spikes, respectively. We find in particular that the string shape has a smooth transition from outward spikes to rounded spikes, as ρ_0 increases from 0 to $\pi/4$ for fixed n and N. Another important observation is that for inward spikes, $\rho_1 < \frac{\pi}{4}$ at $\rho_0 = \frac{\pi}{4}$ for a finite $2\pi/\Delta\phi$ (see the right zoom-in figure around $(\rho_0, \rho_1) = (\frac{\pi}{4}, \frac{\pi}{4})$).

where we used Eq. (4.19) to derive Eq. (4.38). In the rest of the section, we study the three types of string solutions in more details.

4.3.1 Outward spike solutions

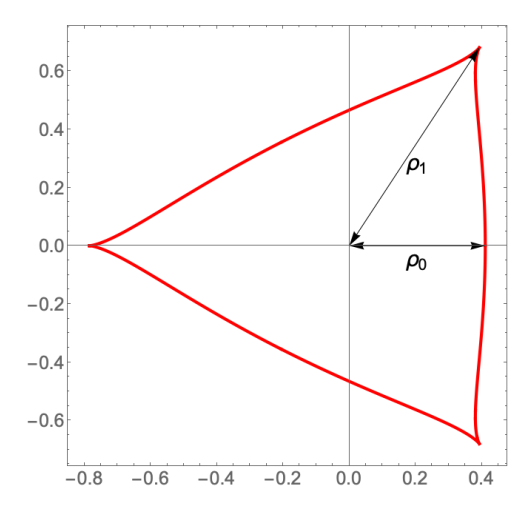
We begin with outward spike solutions ($\rho_0 < \rho_1 < \frac{\pi}{2} - \rho_0$), whose typical shapes are given in Fig. 4.6. See also the left panel of Fig. 4.9 for strings with more windings. To identify the shapes, first we derive a relation between ρ_0 and ρ_1 . If the number of spikes n and the winding number N are specified, we may derive the relation from the periodicity condition (4.36)-(4.37) as

$$\frac{2\pi N}{n} = 2 \int_{\rho_0}^{\rho_1} d\rho \frac{\sqrt{2}\sin 2\rho_0}{\sin \rho_1 \sin 2\rho} \sqrt{\frac{\cos 2\rho - \cos 2\rho_1}{\cos^2 2\rho_0 - \cos^2 2\rho}}.$$
 (4.40)

Now, we are left with one parameter ρ_0 , which characterizes the size of the string. If we further specify ρ_0 , we may identify the shape of the string simply by integrating

$$\frac{d\phi}{d\rho} = \pm \frac{\sqrt{2}\sin 2\rho_0}{\sin \rho_1 \sin 2\rho} \sqrt{\frac{\cos 2\rho - \cos 2\rho_1}{\cos^2 2\rho_0 - \cos^2 2\rho}}.$$
(4.41)

For example, the plots in Fig. 4.6 are obtained in this way. It is also instructive to compare the shapes there with those in flat space and AdS. See Fig. 4.7. We find that in de Sitter space, the



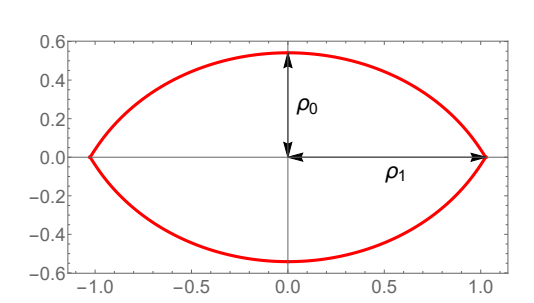


Figure 4.6: Typical shapes of outward spike solutions. The left panel shows the solution with three outward spikes and one winding for $\rho_0 \simeq 0.41$ and $\rho_1 = \frac{\pi}{4}$. The right panel shows the solution with two outward spikes and one winding for $\rho_0 \simeq 0.54$ and $\rho_1 \simeq 1.03$. The latter type of solutions are specific to de Sitter space.

inner turning points shift outward compared to the flat space case due to de Sitter acceleration whereas in AdS, the inner turning points shift inward due to AdS deceleration. In particular, the n=2N case reflects this effect most clearly: As depicted in the right figure of Fig. 4.6, de Sitter space accommodates spiky strings which can be thought of as a fatter version of the folded strings. Both in flat space and AdS, such a spiky string is not stable because the string tension always overcomes the centrifugal force, so that it collapses to the folded string. In sharp contrast, de Sitter acceleration helps the spiky string to maintain the shape without collapsing into a folded string.

Regge trajectories. Using the $\rho_0 - \rho_1$ relation (4.40), we can calculate the energy E and the spin S as a function of ρ_0 , which defines Regge trajectories. See Fig. 4.8 for those of winding number N=1 solutions. First, we find that each trajectory has an approximately linear form up to the maximum spin point and then it turns back, similarly to the folded string case. In particular, the spin at the turning point is smaller than that of the folded string. As a result, the spectrum satisfies the Higuchi bound. We also find that the tilt in the linear region is steeper for strings with a larger number of spikes. Second, the upper endpoint of the Regge trajectory does not touch the vertical axis S=0 in contrast to the folded string case. In the next subsection, we show that the trajectory is smoothly connected to that of rounded spike solutions, which touches the vertical axis S=0. Third, spiky strings with a fixed winding number N scan a finite region of the energy-spin plane. Therefore, to obtain solutions with a larger spin, we need to increase the winding number N. See Fig. 4.9.

Besides, another remark is needed on the Regge trajectory of n = 2N solutions. See the red curve in the upper panel of Fig. 4.8 for n = 2 and N = 1. As we mentioned, the n = 2N solutions can be thought of as a fatter version of folded strings, which are supported by de Sitter acceleration. Then, one may expect that such solutions collapse into folded strings when the string is small and

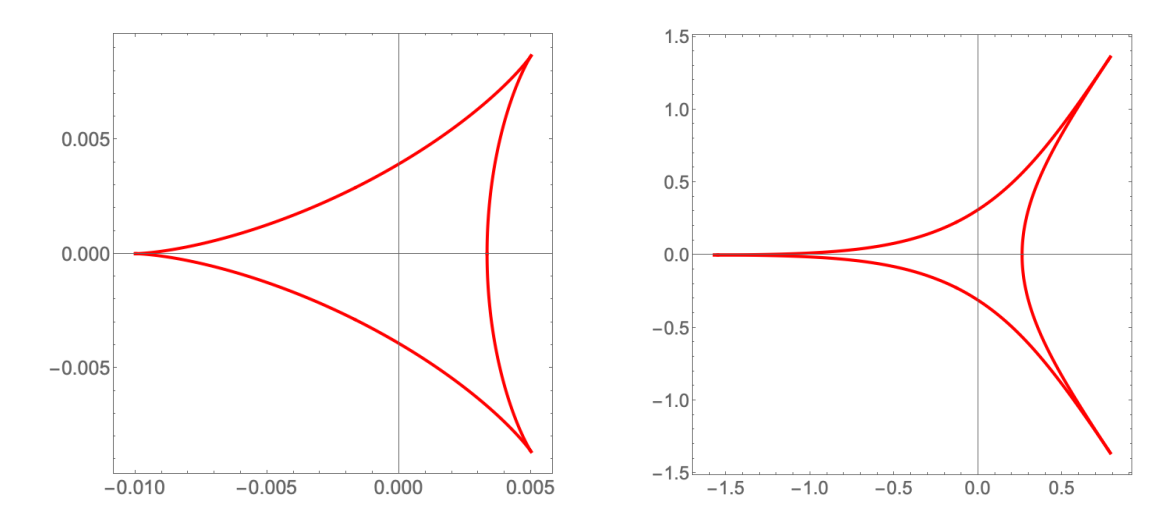


Figure 4.7: Typical shapes of spiky strings with three outward spikes in flat space (the left panel) and AdS (the right panel).

so the support of de Sitter acceleration is not enough. Indeed, we find that the Regge trajectory of n = 2N outward spikes branches from the turning point of the folded string trajectory.

Short strings. To provide more quantitative discussion, let us study the short string regime of outward spike solutions:

$$\rho_0, \ \rho_1 \ll \frac{\pi}{2}.$$
(4.42)

For such short strings, the $\rho_0 - \rho_1$ relation (4.40) is approximated as

$$\frac{2\pi N}{n} \simeq 2 \frac{\rho_0}{\rho_1} \int_{\rho_0}^{\rho_1} \frac{d\rho}{\rho} \frac{\sqrt{\rho_1^2 - \rho^2}}{\sqrt{\rho^2 - \rho_0^2}} = \frac{\rho_1 - \rho_0}{\rho_1} \pi \quad \leftrightarrow \quad \left(1 - \frac{2N}{n}\right) \rho_1 \simeq \rho_0. \tag{4.43}$$

This shows that $\rho_0 = 0$ for n = 2N at least under the short string approximation, which is consistent with the fact that the n = 2N solutions are extrapolated to folded strings as they become smaller. Also, the energy and spin are approximated as

$$E \simeq \frac{R}{2\pi\alpha'} \times 2n \int_{\rho_0}^{\rho_1} d\rho \frac{\rho(\rho_1^2 - \rho_0^2)}{\rho_1\sqrt{\rho^2 - \rho_0^2}\sqrt{\rho_1^2 - \rho^2}} = \frac{nR}{2\alpha'} \frac{\rho_1^2 - \rho_0^2}{\rho_1} = 2N \left(1 - \frac{N}{n}\right) \frac{R}{\alpha'} \rho_1, \tag{4.44}$$

$$S \simeq \frac{R^2}{2\pi\alpha'} \times 2n \int_{\rho_0}^{\rho_1} d\rho \ \rho \frac{\sqrt{\rho^2 - \rho_0^2}}{\sqrt{\rho_1^2 - \rho^2}} = \frac{nR^2}{4\alpha'} (\rho_1^2 - \rho_0^2) = N \left(1 - \frac{N}{n}\right) \frac{R^2}{\alpha'} \rho_1^2, \tag{4.45}$$

from which the energy-spin relation reads

$$E^2 \simeq \frac{4}{\alpha'} N \left(1 - \frac{N}{n} \right) S. \tag{4.46}$$

This correctly reproduces the linear Regge trajectory in flat space. We find that the tilt of the Regge trajectory is steeper for a larger number of spikes. In particular, in the limit of infinitely many spikes (for N fixed), the tilt approaches to $\frac{4}{\alpha'}N$. We will find in Sec. 4.3.3 that steeper Regge trajectories are realized by inward spike solutions.

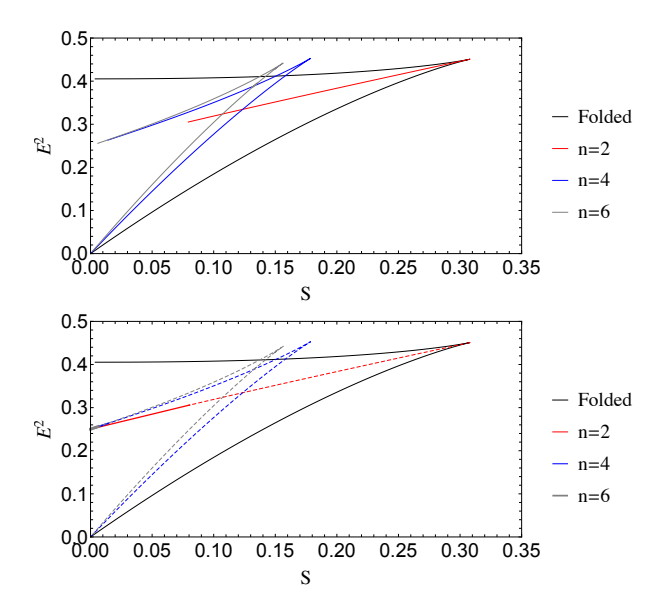


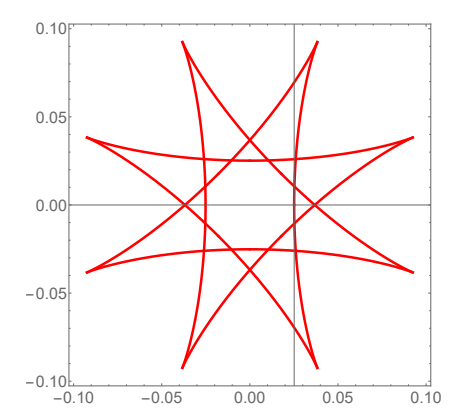
Figure 4.8: Regge trajectories of outward spike solutions (the upper panel) and rounded spike solutions (the lower panel) for the winding number N=1. The spin S and the energy E are plotted in units of R^2/α' and R/α' , respectively, as before. For comparison, we also illustrate the Regge trajectory of one-folded strings. The dotted curves in the lower panel are the Regge trajectories for outward spikes, which are smoothly connected with those for rounded spikes.

Long strings. Finally, let us take a closer look at the long string regime. First, the condition $\rho_0 < \rho_1 < \frac{\pi}{2} - \rho_0$ of outward spikes implies that ρ_0 cannot be larger than $\pi/4$. Also, as ρ_0 approaches to $\pi/4$, ρ_1 approaches to $\pi/4$ and so the spin decreases essentially because the closed string becomes nearly circular and the change of the worldsheet profile by rotation becomes smaller. To interpolate the short string regime, where the spin increases, and the long string regime, where the spin decreases, the Regge trajectory needs to have the maximum spin.

More quantitatively, the maximum value of ρ_0 depends on the number of spikes n and the winding number N. As we mentioned earlier, we obtain the $\rho_0 - \rho_1$ relation (4.40) depicted in Fig. 4.5, once n and N are specified. As we increase ρ_0 for given n and N, each curve on the $\rho_0 - \rho_1$ plane enters the rounded spike regime at some critical value and so there exists a smooth transition from outward spikes to rounded spikes. For example, the critical value for n=4 and N=1 reads $\rho_0 \simeq 0.75$, which corresponds to the upper endpoint of the Regge trajectory (see Fig. 4.8). Beyond the critical value, the Regge trajectory describes rounded spike solutions, which we study in the next subsection.

4.3.2 Rounded spike solutions

Next, we discuss rounded spike solutions ($\rho_0 < \frac{\pi}{2} - \rho_0 < \rho_1$). See Fig. 4.10 for a typical shape of the string, which is regular everywhere. As we have just mentioned, this class of solutions are smooth continuation of outward spike solutions. Then, we may interpret that outward spikes for $\rho_1 < \frac{\pi}{2} - \rho_0$ are rounded when ρ_0 crosses the critical value defined by $\rho_1 = \frac{\pi}{2} - \rho_0$ (for given n and



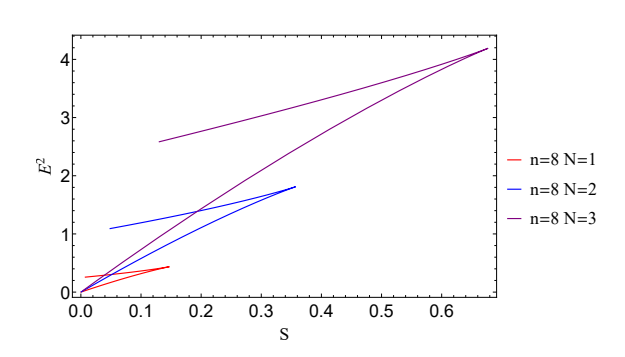


Figure 4.9: The left panel shows the shape of spiky string with 8 outward spikes and 3 windings for $\rho_0 \simeq 0.025$ and $\rho_1 = 0.1$. The right panel shows the Regge trajectories of different windings. The spin S and the energy E are plotted in the units of R^2/α' and R/α' , respectively.

N). Based on this interpretation, we call solutions with $\rho_1 > \frac{\pi}{2} - \rho_0$ rounded spike solutions.

The procedure to identify the shape is parallel to the case of outward spikes. First, we specify the number of spikes n and the winding number N, and derive a relation between ρ_0 and ρ_1 from the periodicity condition,

$$\frac{2\pi N}{n} = 2 \int_{\rho_0}^{\pi/2 - \rho_0} d\rho \, \frac{\sqrt{2} \sin 2\rho_0}{\sin \rho_1 \sin 2\rho} \sqrt{\frac{\cos 2\rho - \cos 2\rho_1}{\cos^2 2\rho_0 - \cos^2 2\rho}} \,. \tag{4.47}$$

Then, integrating Eq. (4.41), we may identify the shape of the string for each ρ_0 . Notice that this type of solutions do not exist for small ρ_0 . See Fig. 4.5. For example, the allowed parameter range of ρ_0 for n=4 and N=1 reads $0.75 \lesssim \rho_0 < \frac{\pi}{4}$.

Regge trajectories. Varying the value of ρ_0 , we may draw the Regge trajectories as depicted in the right panel of Fig. 4.8. There, for comparison, we also illustrate the Regge trajectories of outward spike solutions by the dotted lines. Since rounded spikes exhibit a smooth transition to outward spikes, the Regge trajectories are connected with those of outward spikes. We also find that each Regge trajectory touches the vertical axis S = 0, similarly to the folded string. However, as we discuss in the next paragraph, the mechanism how the spin vanishes is different from the folded string.

Circular string limit. To see how the spin vanishes, let us consider the limit $\rho_0 \to \frac{\pi}{4}$. Recalling that $\rho_0 \le \rho(\sigma) \le \frac{\pi}{2} - \rho_0$, we find that in this limit, the solution is reduced to

$$\rho(\sigma) = \rho_0 = \frac{\pi}{4} \text{ (constant)}, \qquad (4.48)$$

which is nothing but the static circular string studied in Ref. [87]. As discussed there, such a static circular string solution exists in de Sitter space because the string tension and the de Sitter acceleration balance and cancel each other out. Note that the equations of motion (4.32)-(4.33) are

4.3. SPIKY STRINGS 55

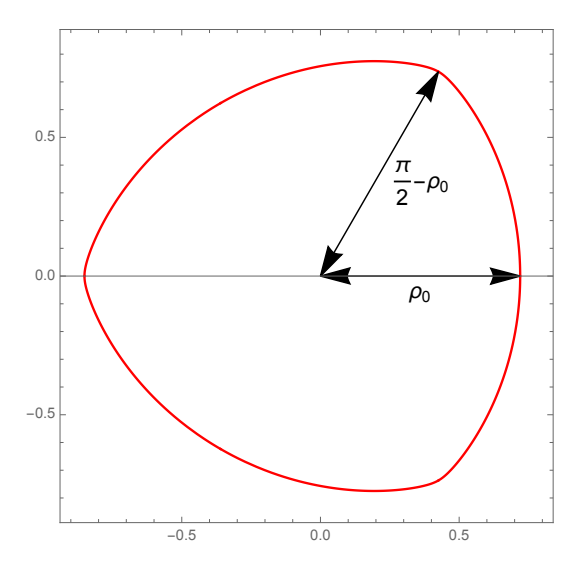


Figure 4.10: Rounded spike solution for $\rho_0 = 0.72$ and $\rho_1 \simeq 0.86$. We call the turning points defined by $\rho = \pi/2 - \rho_0$ rounded spikes.

satisfied for an arbitrary value of ω , since rotations do not change the worldsheet profile and so they are gauge degrees of freedom. The conserved charges (4.16)-(4.17) for these circular strings read

$$E = \frac{NR}{2\alpha'}, \quad S = 0. \tag{4.49}$$

In particular, the string has no spin for an arbitrary ω because the circular string has no structures generating nonzero angular momenta.

4.3.3 Inward spike solutions

Finally, we discuss inward spike solutions ($\rho_1 < \rho_0 < \frac{\pi}{2} - \rho_0$), whose typical shape is illustrated in Fig. 4.11. The procedure to identify the shape is parallel to the case of outward and rounded spikes. First, we specify the number of spikes n and the winding number N and derive a relation between ρ_0 and ρ_1 from the periodicity condition,

$$\frac{2\pi N}{n} = 2 \int_{\rho_1}^{\rho_0} d\rho \, \frac{\sqrt{2}\sin 2\rho_0}{\sin \rho_1 \sin 2\rho} \sqrt{\frac{\cos 2\rho - \cos 2\rho_1}{\cos^2 2\rho_0 - \cos^2 2\rho}} \,. \tag{4.50}$$

Then, by integrating Eq. (4.41) for a specific value of ρ_0 , we may identify the shape.

Regge trajectories. The Regge trajectories are illustrated in Fig. 4.12. Similarly to the previous cases, each Regge trajectory has the maximum energy and spin, which is helpful for the spectrum to satisfy the Higuchi bound. In contrast to outward spikes, the tilt in the short string regime decreases as the number of spikes increases. However, the tilt is always steeper than those of outward spike solutions and folded strings, as we discuss in the next paragraph in more details. Note that the Regge trajectory does not touch the vertical axis S = 0. As far as we know, there are no solutions at least within our ansatz that extrapolate the trajectory to S = 0, in contrast to the outward spike case.

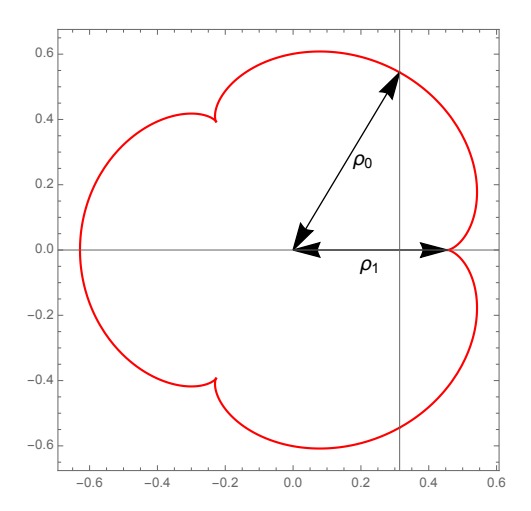


Figure 4.11: Solution with three inward spikes and one winding for $\rho_0 = \pi/5$ and $\rho_1 \simeq 0.46$.

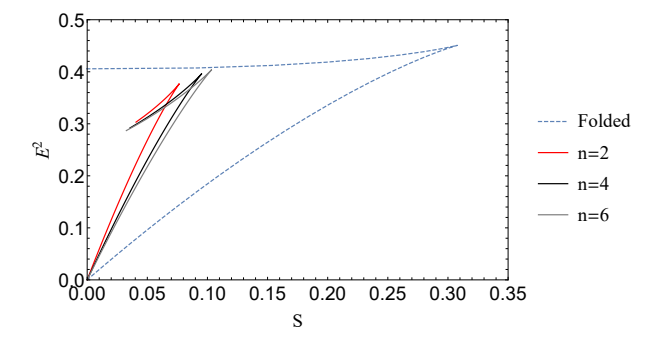


Figure 4.12: Regge trajectories of inward spike solutions for N=1. The spin S and the energy E are plotted in the units of R^2/α' and R/α' , respectively. For comparison, we illustrate the Regge trajectory of the one-folded string by the dotted blue curve.

Short strings. Then, let us take a closer look at the short string regime:

$$\rho_0, \ \rho_1 \ll \frac{\pi}{2}.$$
(4.51)

For such strings, the $\rho_0 - \rho_1$ relation (4.50) is approximated as

$$\frac{2\pi N}{n} \simeq 2 \frac{\rho_0}{\rho_1} \int_{\rho_1}^{\rho_0} \frac{d\rho}{\rho} \frac{\sqrt{\rho_1^2 - \rho^2}}{\sqrt{\rho^2 - \rho_0^2}} = \frac{\rho_0 - \rho_1}{\rho_1} \pi \quad \leftrightarrow \quad \left(1 + \frac{2N}{n}\right) \rho_1 \simeq \rho_0 \,, \tag{4.52}$$

which implies that spiky strings can have an arbitrary number of inward spikes n and an arbitrary winding number N (recall that inward spike solutions in the short string regime have a condition n > 2N). Also, the energy and the spin are approximated as

$$E \simeq \frac{R}{2\pi\alpha'} \times 2n \int_{\rho_1}^{\rho_0} d\rho \frac{\rho(\rho_1^2 - \rho_0^2)}{\rho_1 \sqrt{\rho^2 - \rho_0^2} \sqrt{\rho_1^2 - \rho^2}} = \frac{nR}{2\alpha'} \frac{\rho_0^2 - \rho_1^2}{\rho_1} = 2N \left(1 + \frac{N}{n} \right) \frac{R}{\alpha'} \rho_1, \tag{4.53}$$

$$S \simeq \frac{R^2}{2\pi\alpha'} \times 2n \int_{\rho_1}^{\rho_0} d\rho \ \rho \frac{\sqrt{\rho^2 - \rho_0^2}}{\sqrt{\rho_1^2 - \rho^2}} = \frac{nR^2}{4\alpha'} (\rho_0^2 - \rho_1^2) = N \left(1 + \frac{N}{n} \right) \frac{R^2}{\alpha'} \rho_1^2, \tag{4.54}$$

4.3. SPIKY STRINGS 57

which reproduce the linear Regge trajectories in flat space,

$$E^2 \simeq \frac{4}{\alpha'} N \left(1 + \frac{N}{n} \right) S. \tag{4.55}$$

We find that the tilt of the Regge trajectory decreases as the number of inward spikes increase. In particular, in the limit of infinitely many spikes, the tilt approaches to $\frac{4}{\alpha'}N$.

Long strings. Finally, let us consider the long string regime. As depicted in Fig. 4.5, we always have $\rho_1 < \rho_0$ even in the limit $\rho_0 \to \frac{\pi}{4}$ for a finite n. For example, for inward spike solutions with n=2 and N=1, ρ_1 is bounded as $\rho_1 \lesssim 0.784 (<\frac{\pi}{4})$, which is saturated when $\rho_0 = \frac{\pi}{4}$. Therefore, the string shape does not approach to a circular form as long as we consider a finite n. This is why the upper endpoint of the Regge trajectory does not touch the vertical axis S=0. This is analogous to the outward spike case, but there are no analogue of rounded spike solutions that extrapolate the Regge trajectory of inward spike solutions to S=0, at least within our ansatz.

We conclude this section by summarizing implications of our results. First, in the short string regime, Regge trajectories of spiky strings have a steeper tilt than that of folded strings. This means that Regge trajectories of spiky strings are subleading Regge trajectories (whose contributions to the Regge limit amplitudes are subleading). Second, similarly to the folded string case, each Regge trajectory has the maximum spin and energy. In particular, this property is helpful for the spectra to be consistent with the Higuchi bound. This also implies that a single Regge trajectory has a finite number of higher-spin states, in contrast to flat space and AdS. Third, we found that spiky string solutions for a fixed winding number N scan a finite region on the energy-spin plane. Therefore, in order to have an infinite number of higher-spin states, we need to take into account an infinite number of Regge trajectories with an increasing winding number N. It would be important to further study implications of this result for high-energy scattering in de Sitter space.

Chapter 5

Classical strings with internal motion

Superstring theory is defined in ten dimensional spacetime. Hence we have to involve a compactified internal space. In this chapter, we study classical string solutions in $dS_3 \times S_1$. The internal S_1 can be regarded as a subspace of six dimensional internal space. If there exists a translation symmetry in internal space, a conserved charge are introduced in a four dimensional theory corresponding to a momentum in internal space. We examine how Regge trajectories are changed when having the internal charge.

5.1 Folded strings with internal motion

We begin by generalizing folded string solutions in the previous chapter to include motion along the internal circle S^1 . The folded string configuration is captured by the ansatz (4.11) with $N = \psi = 0$, under which Eqs. (4.13)-(4.14) become trivial, whereas Eq. (4.12) gives

$$\partial_{\sigma} \left(\frac{\rho'}{|\rho'|} \right) \sqrt{\cos^2 \rho - \omega^2 \sin^2 \rho - \nu^2} = 0 \iff \delta(\sigma - \sigma_f) \sqrt{\cos^2 \rho - \omega^2 \sin^2 \rho - \nu^2} = 0. \tag{5.1}$$

Similarly to the case of no internal motion, the equation of motion is localized at the folding point $\sigma = \sigma_f$, where the following equation should be satisfied,

$$\cos^2 \rho - \omega^2 \sin^2 \rho - \nu^2 = 0. \tag{5.2}$$

Therefore, similarly to the solution of no internal motion, the folding point propagates with the speed of light. Then, for given ω and ν , the radius ρ_f of the folding point is determined by

$$\cot^2 \rho_f = \frac{\omega^2 + \nu^2}{1 - \nu^2} \,, \tag{5.3}$$

which is the maximum distance dictated by causality prohibiting superluminal propagation of the string. In general, closed strings may have multiple foldings, so that the solutions are parameterized by the angular velocities ω and ν , and the folding number N_f . See Fig. 5.1.

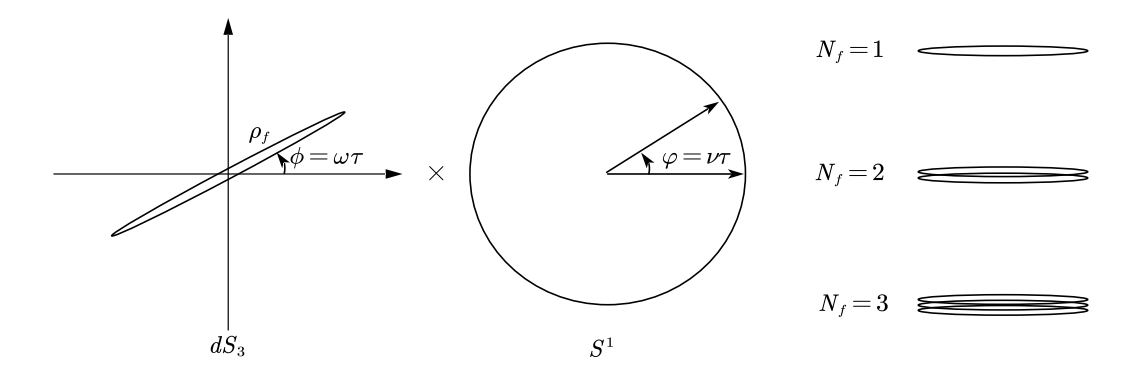


Figure 5.1: Illustration of ω , ν and N_f : ω is the angular velocity in the ϕ direction. ν is the angular velocity in the φ direction. N_f is the folding number.

Conserved charges. For these folded strings, the conserved charges (4.16)-(4.18) read

$$E = \frac{1}{\sqrt{1 - \nu^2}} \times \frac{4N_f R}{2\pi\alpha'} \int_0^{\rho_f} d\rho \frac{\cos^2 \rho}{\sqrt{1 - (\sin^2 \rho / \sin^2 \rho_f)}} , \qquad (5.4)$$

$$S = \frac{\omega}{\sqrt{1 - \nu^2}} \times \frac{4N_f R^2}{2\pi\alpha'} \int_0^{\rho_f} d\rho \frac{\sin^2 \rho}{\sqrt{1 - (\sin^2 \rho / \sin^2 \rho_f)}} , \qquad (5.5)$$

$$J = \frac{\nu}{\sqrt{1 - \nu^2}} \times \frac{4N_f R^2}{2\pi\alpha'} \int_0^{\rho_f} d\rho \frac{1}{\sqrt{1 - (\sin^2 \rho / \sin^2 \rho_f)}} . \tag{5.6}$$

One may also rewrite them in terms of incomplete elliptic integrals,

$$\mathcal{E}\left(\zeta|k^2\right) = \int_0^{\zeta} d\theta \sqrt{1 - k^2 \sin^2 \theta} \ , \quad \mathcal{F}\left(\zeta|k^2\right) = \int_0^{\zeta} d\theta \frac{1}{\sqrt{1 - k^2 \sin^2 \theta}} \ , \tag{5.7}$$

as follows:

$$E = \frac{1}{\sqrt{1 - \nu^2}} \times \frac{4N_f R}{2\pi\alpha'} \left[\sin^2 \rho_f \mathcal{E} \left(\rho_f | \csc^2 \rho_f \right) + \cos^2 \rho_f \mathcal{F} \left(\rho_f | \csc^2 \rho_f \right) \right] , \qquad (5.8)$$

$$S = \frac{\omega}{\sqrt{1 - \nu^2}} \times \frac{4N_f R^2}{2\pi\alpha'} \sin^2 \rho_f \left[-\mathcal{E}\left(\rho_f | \csc^2 \rho_f\right) + \mathcal{F}\left(\rho_f | \csc^2 \rho_f\right) \right] , \qquad (5.9)$$

$$J = \frac{\nu}{\sqrt{1 - \nu^2}} \times \frac{4N_f R^2}{2\pi\alpha'} \mathcal{F}\left(\rho_f | \csc^2 \rho_f\right) . \tag{5.10}$$

These expressions can be used to derive energy-spin relations and draw Regge trajectories.

Regge trajectories. The left panel of Fig. 5.2 shows Regge trajectories of one-folded strings $(N_f = 1)$ with a fixed internal charge J. First, the trajectory for J = 0 matches with the trajectory of no internal motion (Fig. 4.3). Next, if one increases the internal charge J, the trajectory shifts upwards simply because the internal motion increases the energy. Also the maximum spin decreases, so that the maximum spin of one-folded strings is the one for the J = 0 string. Then, one-folded

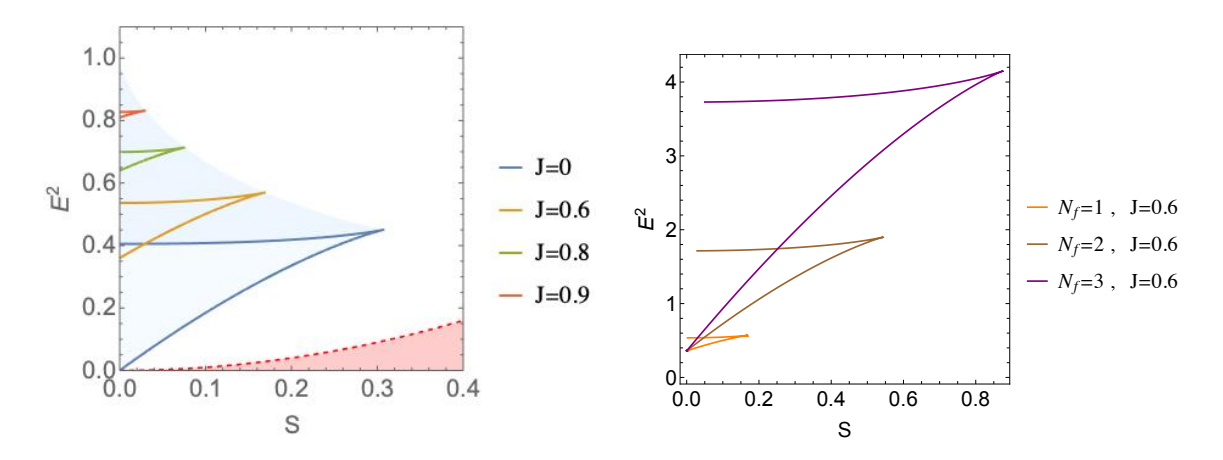


Figure 5.2: The left panel shows Regge trajectories for $N_f=1$ with different internal charge J. The right panel shows Regge trajectories for different N_f with $J=0.6R^2/\alpha'$. The energy E, spin S and internal charge J are in the units of R/α' , R^2/α' and R^2/α' , respectively. We find that the Regge trajectories always satisfy the Higuchi bound $(E^2 \geq \frac{S(S-1)}{R^2})$, which prohibits the red region.

strings scan a finite region in the energy-spin plane represented by the blue shaded region. In particular, one needs to consider multiple folded strings ($N_f = 2, 3, ...$) to have infinitely many higher spins (see the right panel of Fig. 5.2). Note that the Higuchi bound is satisfied in the entire region. In the rest of the section, we study several limits and provide more quantitative arguments.

5.1.1 Bound on internal charge J

Fig. 5.2 implies that for a fixed folding number N_f , there exists a maximum value of the internal charge J. To see this more quantitatively, let us recall

$$\frac{\nu}{\sqrt{1-\nu^2}} \le \sqrt{\frac{\nu^2 + \omega^2}{1-\nu^2}} = \cot \rho_f \,, \tag{5.11}$$

where the inequality is saturated for $\omega = 0$ (for which we have $\nu = \cos \rho_f$). Then, we find

$$J \le \frac{N_f R^2}{\alpha'} \frac{2}{\pi} \int_0^{\rho_f} d\rho \frac{\cos \rho_f}{\sqrt{\sin^2 \rho_f - \sin^2 \rho}}.$$
 (5.12)

This simply says that the folding point has the speed of light and so for a fixed string length ρ_f , the internal motion is maximized when the string does not rotate inside dS_3 . As depicted in Fig. 5.3, the right hand side is maximized in the short string limit $\rho_f \to 0$:

$$J \le \frac{N_f R^2}{\alpha'} \frac{2}{\pi} \int_0^{\rho_f} d\rho \frac{\cos \rho_f}{\sqrt{\sin^2 \rho_f - \sin^2 \rho}} \le \frac{N_f R^2}{\alpha'}. \tag{5.13}$$

Therefore, the N_f -folded string has the maximum internal charge $J = N_f R^2/\alpha'$ when $\omega = 0$ and $\nu = \cos \rho_f \to 1$. Note that the energy E and the spin S in this limit are

$$E = \frac{N_f R}{\alpha'}, \quad S = 0,$$
 (5.14)

which correspond to the upper boundary point of the shaded region in Fig. 5.2.

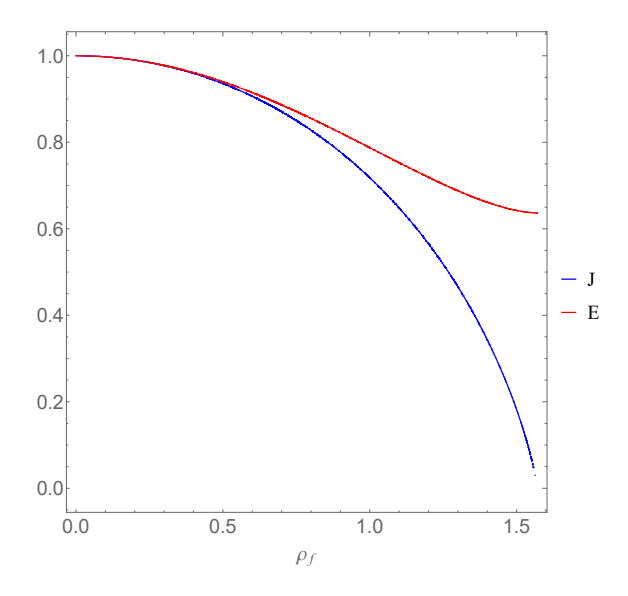


Figure 5.3: The energy E and the internal U(1) charge J as a function of ρ_f . They are plotted in the units of $N_f R/\alpha'$ and $N_f R^2/\alpha'$, respectively.

5.1.2 Regge trajectories for fixed J

Short strings. Next, let us take a closer look at the Regge trajectory profile for a fixed J. For this, we first consider the short string limit $\rho_f \ll 1$. In this regime, we have

$$\rho_f \simeq \sqrt{\frac{1-\nu^2}{\omega^2 + \nu^2}} \ll 1,$$
(5.15)

so that the short string limit is realized for $\omega \gg 1$, $\nu \simeq 1$, or both (recall that causality requires $0 \le \nu^2 \le 1$). At the leading order in ρ_f , the charges (5.8)-(5.10) are approximated as

$$E \simeq \frac{1}{\sqrt{1-\nu^2}} \times \frac{4N_f R}{2\pi\alpha'} \int_0^{\rho_f} d\rho \frac{1}{\sqrt{1-(\rho/\rho_f)^2}} = \frac{1}{\sqrt{1-\nu^2}} \times \frac{N_f R}{\alpha'} \rho_f , \qquad (5.16)$$

$$S \simeq \frac{\omega}{\sqrt{1 - \nu^2}} \times \frac{4N_f R^2}{2\pi\alpha'} \int_0^{\rho_f} d\rho \frac{\rho^2}{\sqrt{1 - (\rho/\rho_f)^2}} = \frac{1}{2} \sqrt{\frac{\omega^2}{\omega^2 + \nu^2}} \times \frac{N_f R^2}{\alpha'} \rho_f^2 , \qquad (5.17)$$

$$J \simeq \frac{\nu}{\sqrt{1 - \nu^2}} \times \frac{4N_f R^2}{2\pi\alpha'} \int_0^{\rho_f} d\rho \frac{1}{\sqrt{1 - (\rho/\rho_f)^2}} = \frac{\nu}{\sqrt{1 - \nu^2}} \times \frac{N_f R^2}{\alpha'} \rho_f . \tag{5.18}$$

Then, in the regime $\omega \gg 1$, which implies $J \ll 1$ in particular, we find the relation,

$$E^2 \simeq \frac{J^2}{R^2} + \frac{2N_f}{\alpha'} S$$
. (5.19)

Recall that the short string limit is also achieved when $\omega = O(1)$ and $\nu \simeq 1$. In this regime, the internal charge (5.18) is not necessarily small because the prefactor $\frac{\nu}{\sqrt{1-\nu^2}}$ cancels out the suppression by the small ρ_f . Taking into account the next-to-leading order terms in Eqs. (5.16), (5.18) carefully, we find a more general energy-spin relation,

$$E^2 \simeq \frac{J^2}{R^2} + \sqrt{1 - \left(\frac{\alpha'}{N_f R^2} J\right)^2 \frac{2N_f}{\alpha'} S},$$
 (5.20)

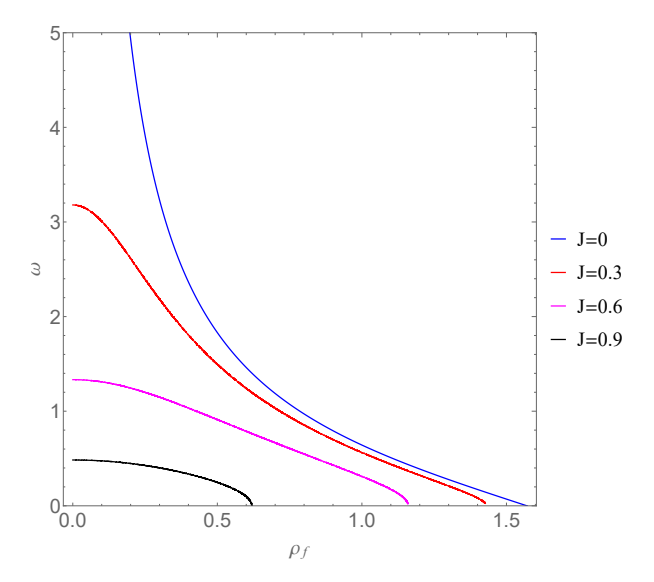


Figure 5.4: The angular velocity ω as a function of ρ_f (*J* is in the unit of $N_f R^2/\alpha'$).

which is applicable for an arbitrary value of J as long as the string is short $\rho_f \ll 1$. Note that the first term is the Kaluza-Klein mass associated to the internal motion, which explains how the Regge trajectory shifts upwards as J increases.

Long strings. To discuss longer strings, it is convenient to rewrite Eq. (5.10) as

$$\omega^{2} = \frac{\cot^{2} \rho_{f} \cdot \left[\frac{4N_{f}R^{2}}{2\pi\alpha'} \mathcal{F} \left(\rho_{f} | \csc^{2} \rho_{f} \right) \right]^{2} - J^{2}}{\left[\frac{4N_{f}R^{2}}{2\pi\alpha'} \mathcal{F} \left(\rho_{f} | \csc^{2} \rho_{f} \right) \right]^{2} + J^{2}},$$
(5.21)

where the right hand side monotonically decreases as ρ_f increases (see Fig. 5.4). It implies that for a fixed J, there exists an upper bound on the angular velocity ω :

$$0 \le \omega^2 \le \frac{\frac{N_f^2 R^4}{\alpha'^2} - J^2}{J^2} \,, \tag{5.22}$$

where the upper bound is saturated in the short string limit $\rho_f \to 0$. Also, for a fixed J, the string has a maximum length when $\omega = 0$, for which the conserved charges read

$$E = \frac{1}{\sin \rho_f} \times \frac{4N_f R}{2\pi\alpha'} \left[\sin^2 \rho_f \mathcal{E} \left(\rho_f | \csc^2 \rho_f \right) + \cos^2 \rho_f \mathcal{F} \left(\rho_f | \csc^2 \rho_f \right) \right] , \qquad (5.23)$$

$$S = 0 (5.24)$$

$$J = \cot \rho_f \times \frac{4N_f R^2}{2\pi\alpha'} \mathcal{F}\left(\rho_f | \csc^2 \rho_f\right). \tag{5.25}$$

For a given J, the maximum length is determined by solving Eq. (5.25). Then, substituting it into Eq. (5.23) gives the energy of the longest string. See also Fig. 5.3. This gives the upper endpoint of each Regge trajectory with a fixed J depicted in Fig. 5.2.

5.2 Spiky strings with internal motion

Finally, we study spiky strings with internal motion (see Ref. [75] for the corresponding solutions in $AdS_3 \times S^1$). We employ the full ansatz (4.11), under which the equations of motion are Eqs. (4.12)-(4.14). For later convenience, we introduce a new variable r by

$$r = \sin^2 \rho \,, \tag{5.26}$$

which will be used mainly in the rest of the section instead of ρ . To follow the string dynamics, we first integrate the equations of motion (4.13)-(4.14) as

$$C = \frac{\omega Nr + \nu \psi'}{\sqrt{D}} (1 - r), \qquad (5.27)$$

$$\lambda = \frac{\omega N r + \nu \psi'}{\nu \omega \psi' + N(1 - \nu^2 - r)} \frac{1 - r}{r}, \qquad (5.28)$$

where C and λ are real integration constants. Notice here that nontrivial solutions with $\nu \neq 0$ exist only when ψ' is σ -dependent, otherwise r has to be a constant. Also note that we have four parameters $(\omega, \nu, C, \lambda)$ characterizing the solutions.

Then, we reformulate Eqs. (5.27)-(5.28) such that ψ' and ρ' are expressed in terms of variables without derivatives. First, Eq. (5.28) implies

$$\psi' = Nr \frac{\lambda \left(1 - r - \nu^2\right) - \omega (1 - r)}{\nu (1 - r - \lambda \omega r)}.$$
(5.29)

Second, as discussed in Appendix D.1, we can reorganize Eq. (5.27) together with Eq. (5.29) into the form,

$$r^{2} = 4r(1-r)\rho^{2} = Tr^{2}(1-r)^{2} \frac{(r-r_{A})(r-r_{B})(r-r_{C})}{(r-r_{S})^{2}}.$$
(5.30)

This shows that for generic values of $(\omega, \nu, C, \lambda)$, r'^2 has a double pole and three zeros, in addition to the two double zeros located at r = 0, 1. The location of the double pole is determined by ω and λ alone as

$$r_S = \frac{1}{1 + \lambda \omega} \,. \tag{5.31}$$

On the other hand, the locations of the three zeros depend on the four parameters $(\omega, \nu, C, \lambda)$ in a more complicated manner, which we denote by r_A , r_B , and r_C (see Appendix D.1 for details). Note that $r_{A,B,C}$ are complex in general. Besides, the overall constant T reads

$$T = \frac{4N^2\lambda^2(1+\omega^2)}{C^2(1+\lambda\omega)^2},$$
(5.32)

which is non-negative since N is a positive integer and ω , λ , and C are real numbers. Integrating Eqs. (5.29)-(5.30) gives string solutions for given $(\omega, \nu, C, \lambda)$.

5.2.1 Outward and inward spike solutions

Now we are ready to study shapes and Regge trajectories of the solutions described by our ansatz (4.11). Our task is basically parallel to the one in Sec. 4.3, but it is more complicated simply because there are more parameters of the solution. In the present thesis, for illustration, we focus on two classes of solutions that reduce to those of the previous section in the limit $J \to 0$, which simplifies the analysis considerably. We call them outward spike solutions and inward spike solutions by analogy with the solutions in Sec. 4.3. In the following, we present properties of these solutions.

Ansatz on r_A , r_B , r_C , and r_S . In Sec. 4.3, we demonstrated that shapes of the string depend on the location of zeros and poles of ρ'^2 . Similarly, the outward and inward spike solutions can be classified based on the values of r_A , r_B , r_C , and r_S . First, for both classes of solutions, r_A , r_B , and r_C are all real and positive. Without loss of generality, we assume that $r_A < r_B < r_C$. These values relative to r_S are also relevant for us, based on which we perform the following classification:

Outward spike solutions:
$$r_A < r_B < r_S < r_C$$
, (5.33)

Inward spike solutions:
$$r_S < r_A < r_B < r_C$$
. (5.34)

In Appendix D.2, we show that in the limit $J \to 0$, these solutions indeed reduce to their counterparts in Sec. 4.3.

Reality conditions. Next let us take care of reality conditions. First, Eq. (5.30) shows that reality of $r(\sigma)$ requires $r_A \leq r(\sigma) \leq r_B$ or $r(\sigma) \geq r_C$ (recall that the overall coefficient T is positive). Also, in order for the closed string to form a loop, r' has to flip the sign somewhere on the worldsheet, otherwise the string stretches forever. Then, for the outward and inward spike solutions, the string has to be inside the regime $r_A \leq r(\sigma) \leq r_B$.

Periodicity conditions. Finally, we take into account global structures of the string. As before, the angle $\Delta \phi$ (on the r- ϕ plane) between the two spikes¹ has to be quantized appropriately. More explicitly, for n-spike solutions, we require

$$\Delta \phi = \frac{2\pi N}{n} \,. \tag{5.35}$$

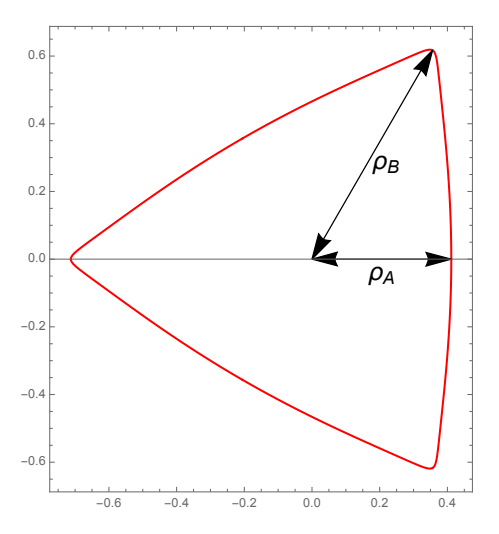
Within the ansatz (5.33)-(5.34), an explicit form of $\Delta \phi$ reads

$$\Delta \phi = 2N \int_{r_A}^{r_B} \frac{dr}{r'} = \frac{2N}{\sqrt{T}} \int_{r_A}^{r_B} \frac{dr}{r(1-r)} \frac{|r-r_S|}{\sqrt{(r-r_A)(r-r_B)(r-r_C)}}.$$
 (5.36)

In the present setup, we also need to take care of periodicity along the internal S^1 . For simplicity, we assume that the string has no winding along the S^1 , which implies

$$0 = \int_0^{2\pi} d\sigma \psi' = 2n \int_{r_A}^{r_B} \frac{dr}{r'} \psi' = \pm \frac{2nNr_S}{\nu\sqrt{T}} \int_{r_A}^{r_B} \frac{dr}{1-r} \frac{\lambda (1-\nu^2-r) - \omega(1-r)}{\sqrt{(r-r_A)(r-r_B)(r-r_C)}}.$$
 (5.37)

¹As we see shortly, the string is smooth everywhere for $\nu \neq 0$, but we can interpret that spikes are rounded, similarly to the rounded spikes in Sec. 4.3. Therefore, we use the terminology "spikes" as before.



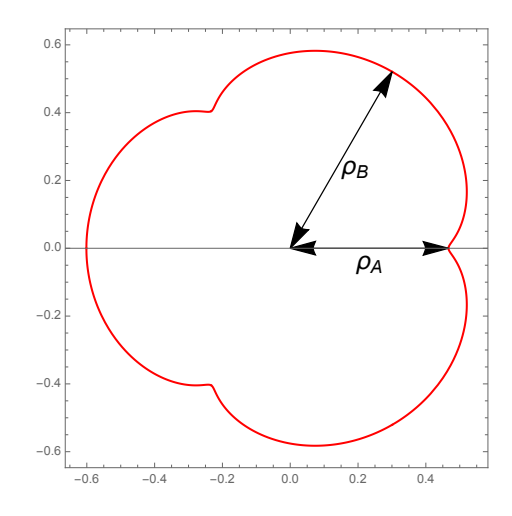


Figure 5.5: Shapes of outward spike solutions and inward spike solutions: ρ_A and ρ_B are defined by $r_A = \sin^2 \rho_A$ ($0 \le \rho_A \le \frac{\pi}{2}$) and similarly for ρ_B . For outward spike solutions, we chose $(\omega, \nu, C, \lambda) \simeq (0.89, 0.47, 0.41, 1.31)$, which corresponds to $(\rho_A, \rho_B) \simeq (0.41, 0.71)$. For inward spike solutions, we chose $(\omega, \nu, C, \lambda) \simeq (1.65, 0.51, 0.94, 2.57)$, which corresponds to $(\rho_A, \rho_B) \simeq (0.47, 0.60)$.

Here the plus and minus signs are for outward and inward spike solutions, respectively. As we mentioned, there are four parameters of the solutions. If we specify the number of spikes n and the winding number N, there are two constraints originating from the periodicity conditions. Then, we are left with two degrees of freedom characterizing the size of the string and the internal motion.

Shapes. In Fig. 5.5, we illustrate outward and inward spike solutions for n=3 and N=1. The four parameters $(\omega, \nu, C, \lambda)$ are chosen such that the two periodicity conditions are satisfied. In contrast to the case without internal motion, the spikes are indeed rounded.

Regge trajectories. Finally, we study Regge trajectories. First, substituting Eqs. (5.27)-(5.28) into Eqs. (4.16)-(4.18), we find a simplified expression for conserved charges²:

$$E = \frac{NR}{2\pi\alpha'} \frac{\lambda}{C} \int_0^{2\pi} d\sigma \, r \, \frac{(1-r)^2 - C^2}{1 - r - \lambda\omega r}$$
 (5.38)

$$= \pm \frac{NR}{2\pi\alpha'} \frac{2n\lambda r_S}{C\sqrt{T}} \int_{r_A}^{r_B} \frac{dr}{1-r} \frac{(1-r)^2 - C^2}{\sqrt{(r-r_A)(r-r_B)(r-r_C)}},$$
 (5.39)

$$S = \frac{NR^2}{2\pi\alpha'} \frac{1}{C} \int_0^{2\pi} d\sigma \, r \, \frac{(1-r)r\lambda\omega - C^2}{1-r-\lambda\omega r} \,, \tag{5.40}$$

$$=\pm \frac{NR^2}{2\pi\alpha'} \frac{2nr_S}{C\sqrt{T}} \int_{r_A}^{r_B} \frac{dr}{1-r} \frac{(1-r)r\lambda\omega - C^2}{\sqrt{(r-r_A)(r-r_B)(r-r_C)}},$$
 (5.41)

²To derive them, it is convenient to use Eq. (D.1) and Eq. (D.3) provided in Appendix.

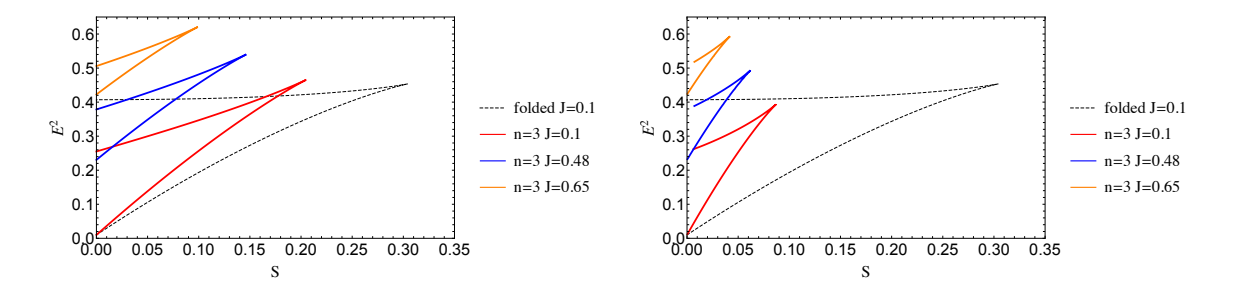


Figure 5.6: Regge trajectories of spiky strings with internal charges. The left and right figures are for outward and inward spike solutions, respectively. For comparison, we also illustrate the Regge trajectory of the folded string in the dotted lines. The energy, spin and internal charge are in the units of R/α' , R^2/α' and R^2/α' , respectively.

$$J = \frac{NR^2}{2\pi\alpha'} \frac{1}{\nu C} \int_0^{2\pi} d\sigma \, r \, \frac{(1-r)\lambda\nu^2 - C^2(\lambda-\omega)}{1-r-\lambda\omega r}$$
 (5.42)

$$= \pm \frac{NR^2}{2\pi\alpha'} \frac{2nr_S}{\nu C\sqrt{T}} \int_{r_A}^{r_B} \frac{dr}{1-r} \frac{(1-r)\lambda\nu^2 - C^2(\lambda-\omega)}{\sqrt{(r-r_A)(r-r_B)(r-r_C)}},$$
 (5.43)

where the plus and minus signs are again for outward and inward spikes, respectively.

As we mentioned, once we specify the number of spikes n and the winding number N, we are left with two degrees of freedom associated with the size of the string and the internal motion. If we further specify the internal charge through Eq. (5.43), we are left with one degree of freedom characterizing the size of the string. Then, by varying the size of the string, we can draw Regge trajectories for fixed n, N and J. See Fig. 5.6 for Regge trajectories of outward and inward spike solutions with n=3, N=1, and different values of J. We find that as the internal charge increases, the Regge trajectory shifts upwards. Also, the maximum spin decreases and the maximum energy increases. In particular, Regge trajectories for fixed n and N scan a finite region of the energy-spin plane. These properties are qualitatively the same as folded strings with internal charges and spiky strings without internal charges, respectively. Besides, we find that Regge trajectories for outward spike stouch the vertical axis S=0 twice. This explains that in the limit $J\to 0$, outward spike solutions reduce to both the outward and rounded spike solutions presented in the previous section. See Appendix D.2 for more details.

Chapter 6

Conclusion

In this thesis, we studied Regge trajectories of folded strings and spiky strings in de Sitter space and examined their consistency with the Higuchi bound. Regge trajectories of folded strings have a maximum spin and energy in contrast to flat space and AdS space. For each spin below the maximum value, the energy is larger than the Higuchi bound. Simililarly, Regge trajectories of spiky strings have a maximum spin and energy. Spiky strings have a larger energy than folded strings for each spin. Intuitively, this is because an extra energy is needed to spread strings. Hence the Higuchi bound is not violated also for spiky strings. Besides, as we increase internal charge, strings get an energy and a maximum value of spin becomes smaller. Therefore internal motion may not cause a confliction with the Higuchi bound. Thus string theory seems to be consistent in de Sitter space from the view point of string spectra.

While the boundedness of spin is helpful to string spectra to be consistent with the Higuchi bound, this implies that a single Regge trajectory has only a finite number of higher spin states. Even if including internal charges, Regge trajectories scan a finite region of the energy-spin plane, and therefore higher spin states remain finite. To have an infinite number of higher spin states, we need infinitely many Regge trajectories with an increasing winding numbers.

More intuitively, the above mentioned properties are natural consequences of de Sitter acceleration. First, the string can have a large spin if it is long and rotates with a large angular velocity. On the other hand, causality requires that the string worldsheet cannot propagate faster than the speed of light, which gives an upper bound on the string length in terms of the angular velocity. In flat space and AdS, the string stretches with an infinite length if the angular velocity approaches to zero. In particular, the large string length competes against the smallness of the angular velocity, so that strings have larger spins as they stretch more. In sharp contrast, de Sitter space has an acceleration, so that there exists a natural cutoff dictated by causality: the string cannot rotate anymore when touching the horizon. Therefore, the only way for a string to have a large spin is to shrink inside the horizon, fold as much as possible, and rotate quickly. This is why string Regge trajectories in de Sitter space are qualitatively different from the flat space and AdS ones. Besides, de Sitter acceleration makes spiky strings fatter, leading to several new classes of solutions which do not exist in flat space and AdS.

We conclude this thesis with discussions on several future directions. The first direction is to investigate high energy scattering in de Sitter space. UV behavior of string theory would be affected by higher spin spectra as indicated by the Regge behavior. The results of this thesis imply that UV behavior in de Sitter space may be qualitatively different from flat space above the scale $M_{\star} \simeq 0.6 M_S^2/H$ (a maximum energy of one-folded Regge trajectories). M_S is the string scale and H is the Hubble scale. Our question is whether string theory can have a mild UV behavior in de Sitter space or not. Scattering amplitudes should be mild below the scale M_{\star} since the string spectrum is almost the same as flat space. On the other hand, the mild behavior may not be maintained above M_{\star} . In this case, string theory would experience a phase transition to a strong coupling regime in order to UV complete gravity; that is, we lose the perturbative control of string theory. Notice that this is not a problem if M_{\star} is higher than the Planck scale $M_{\rm pl}$. In other words, the Hubble scale H is bounded from above by $0.6 M_S^2/M_{\rm pl}$. Interestringly, when we apply the typical string scale ($M_S \simeq 10^{16}~{\rm GeV}$) and the 4d Planck scale ($M_{\rm pl} \simeq 10^{18}~{\rm GeV}$), the bound saturates the target sensitivity of the near future observations of CMB B-modes such as the LiteBIRD experiment [88]. If the primordial gravitational waves were not detected in the near future, such a theoretical bound could reduce the possibility of high-scale inflation. Otherwise, can string theory UV complete gravity beyond M_{\star} with a weak coupling?

It would be important to study this issue further by generalizing developments in holographic correlation functions in AdS [89–95], which would provide cosmological Veneziano amplitudes. A related important question is to formulate a framework to study consistency of high-energy scattering in de Sitter space. For example, in the case of AdS, we know what are the AdS analogues of the Regge limit amplitudes and the hard scattering amplitudes (see, e.g., [96–105]). For de Sitter space, there is a known flat space limit of late-time correlators corresponding to the hard scattering limit (see, e.g., [99, 106, 107]). However, to our knowledge, its understanding is still limited compared to the AdS case, even at the quantum field theory level before taking into account stringy effects. It would be important to clarify which kinematics of which quantities is useful to define consistency of high-energy scattering in de Sitter space. We hope that this direction would open up a new road toward understanding of de Sitter space in string theory.

Appendix A

Special functions

In this appendix, we summarize several properties of special functions used in this thesis. First we introduce the Gegenbauer polynomials and summarize their useful properties in Sec. A.1. Also, we introduce the Jacobi polynomials as an extension of the Gegenbauer polynomials. Second we summarize spherical harmonics in general dimensions in Sec. A.2. In particular, we study their relation with the Gegenbauer polynomials.

A.1 Orthogonal polynomials

We introduce Gegenbauer polynomials and Jacobi polynomials, and summarize their useful properties. These polynomials are kinds of orthogonal polynomials. Let us consider a set of orthogonal polynomials ϕ_n of degree n, which satisfy

$$\int_{-1}^{1} dx \,\phi_n(x)\phi_m(x)w(x) = 0 \qquad \text{for} \quad n \neq m.$$
(A.1)

 $\omega(x)$ is called a weight function. Once specifying a weight function, we can have a set of orthogonal polynomials by using the Rodrigues' formula,

$$\phi_n(x) = \frac{C}{w(x)} \frac{d^n}{dx^n} w(x) (1 - x^2)^n,$$
(A.2)

where C is a constant. Gegenbauer polynomials are orthogonal polynomials for $w(x) = (1-x^2)^{\alpha-\frac{1}{2}}$,

$$C_n^{\alpha}(x) = \frac{(-1)^n}{2^n n!} \frac{\Gamma(\alpha + \frac{1}{2})\Gamma(n + 2\alpha)}{\Gamma(2\alpha)\Gamma(\alpha + n + \frac{1}{2})} (1 - x^2)^{\frac{1}{2} - \alpha} \frac{d^n}{dx^n} w(x) (1 - x^2)^{n + \alpha - \frac{1}{2}}.$$
 (A.3)

The Gegenbauer polynomials can be also written as

$$C_n^{\alpha}(x) = \frac{\Gamma(n+2\alpha)}{\Gamma(2\alpha)\Gamma(n+1)} {}_2F_1 \left[\begin{array}{c} -n, n+2\alpha \\ \alpha + \frac{1}{2} \end{array}; \frac{1-x}{2} \right], \tag{A.4}$$

where ${}_{2}F_{1}\left[\begin{array}{c} \alpha, \beta \\ \gamma \end{array}; x\right]$ is the hypergeometric function,

$${}_{2}F_{1}\left[\begin{array}{c}\alpha,\beta\\\gamma\end{array};x\right] = \sum_{n=0}^{\infty} \frac{1}{n!} \frac{(\alpha)_{n}(\beta)_{n}}{(\gamma)_{n}} x^{n}.$$
(A.5)

Here $(a)_n$ is a shifted factorial,

$$(a)_n = a \cdot (a+1) \cdot \cdots \cdot (a+n-1). \tag{A.6}$$

The inner products are given by

$$\int_{-1}^{1} dx \ C_m^{\alpha}(x) C_n^{\alpha}(x) (1 - x^2)^{\alpha - \frac{1}{2}} = \delta_{m,n} \frac{\pi 2^{1 - 2\alpha} \Gamma(n + 2\alpha)}{n! (n + \alpha) \Gamma(\alpha)^2}.$$
(A.7)

If $\alpha = \frac{1}{2}$, the Gegenbauer polynomials reduce to the Legendre polynomials. Also, if $\alpha = \frac{d}{2} - 1$, these are d-dimensional extensions of the Legendre polynomials. Besides, let us introduce d-dimensional extensions of the Legendre functions of the second kind. First we define

$$D_n^{\alpha}(z) = \sqrt{\pi} \frac{\Gamma(\alpha + \frac{1}{2})\Gamma(n + 2\alpha)}{\Gamma(1 + n + \alpha)\Gamma(2\alpha)} (2z)^{-n-1} {}_{2}F_{1} \begin{bmatrix} \frac{n+1}{2}, \frac{n+2}{2} \\ 1 + n + \alpha \end{bmatrix}; \frac{1}{z^{2}}$$
(A.8)

If $\alpha = \frac{1}{2}$, these functions reduce to the Legendre functions of the second kind. Also, if $\alpha = \frac{d}{2} - 1$, these are d-dimensional extensions of the Legendre functions of the second kind. $C_n^{\alpha}(z)$ and $D_n^{\alpha}(z)$ satisfies the same differential equation,

$$(1 - z^2)\frac{d^2}{dz^2}f(z) - (2\alpha + 1)z\frac{d}{dz}f(z) + n(n + 2\alpha)f(z) = 0.$$
(A.9)

 $C_n^{\alpha}(z)$ has a branch cut along $(-\infty, -1)$ unless $n \in \mathbb{N}$. Also, $D_n^{\alpha}(z)$ has a branch cut along (-1, 1). In particular, its discontinuity is given by

$$D_n^{\alpha}(z+i\epsilon) - D_n^{\alpha}(z-i\epsilon) = -i\pi(1-z^2)^{\alpha-\frac{1}{2}}C_n^{\alpha}(z).$$
 (A.10)

Finally let us introduce Jacobi polynomials, which are for $w(x) = (1-x)^{\alpha}(1+x)^{\beta}$,

$$P_n^{(\alpha,\beta)}(x) = \frac{(-1)^n}{2^n n!} (1-x)^{-\alpha} (1+x)^{-\beta} \frac{d^n}{dx^n} (1-x)^{\alpha} (1+x)^{\beta} (1-x^2)^n.$$
 (A.11)

In terms of the hypergeometric functions, the Jacobi polynomials are written as

$$P_n^{(\alpha,\beta)}(x) = \frac{\Gamma(\alpha+n+1)}{\Gamma(n+1)\Gamma(\alpha+1)} {}_2F_1 \left[\begin{array}{c} -n, 1+\alpha+\beta+n \\ \alpha+1 \end{array}; \frac{1-x}{2} \right]. \tag{A.12}$$

The Jacobi polynomials can be expanded by a set of the Jacobi polynomials as

$$P_{n}^{(a,b)}(x) = \sum_{k=0}^{n} \frac{(b+2k+\delta+1)(a-\delta)_{n-k}}{(n-k)!} \frac{\Gamma(b+n+1)\Gamma(a+b+k+n+1)\Gamma(b+k+\delta+1)}{\Gamma(b+k+1)\Gamma(a+b+n+1)\Gamma(b+k+n+\delta+2)} P_{k}^{(\delta,b)}(x)$$
(A.13)

If the upper parameters have the same value, the Jacobi polynomials reduce to the Gegenbauer polynomials,

$$C_n^{\alpha}(x) = \frac{\Gamma(\alpha + \frac{1}{2})\Gamma(n + 2\alpha)}{\Gamma(2\alpha)\Gamma(\alpha + n + \frac{1}{2})} P_n^{(\alpha - \frac{1}{2}, \alpha - \frac{1}{2})}(x)$$
(A.14)

A.2 Spherical Harmonics

In this section, we summarize several properties of spherical harmonics (See also a nice review [108]). Spherical harmonics are introduced as homogeneous harmonic functions restricted on a unit sphere. Homogeneous harmonic functions $H_{lm}(x)$ of degree l are defined as follows:

$$\Delta_d H_{lm}(x) = 0, \quad H_{lm}(\lambda x) = \lambda^l H_{lm}(x), \tag{A.15}$$

where Δ_d is the d-dimensional Laplacian,

$$\Delta_d = \frac{\partial^2}{\partial x_1^2} + \dots + \frac{\partial^2}{\partial x_d^2} \tag{A.16}$$

The second argument m denotes linearly independent elements, the number of which is N(d, l),

$$N(d,l) = \frac{2l+d-2}{l} \begin{pmatrix} l+d-3\\ l-1 \end{pmatrix}.$$
 (A.17)

which we will prove in the end of this section. Here we introduced a combinatorial factorial as,

$$\begin{pmatrix} \alpha \\ \beta \end{pmatrix} = \frac{\alpha!}{(\alpha - \beta)!\beta!}.$$
 (A.18)

Spherical harmonics are defined as a homogeneous harmonic function restricted on an unit sphere,

$$Y_{lm}(\hat{x}) = H_{lm}(x)|_{x_1^2 + \dots + x_n^2 = 1},$$
 (A.19)

where \hat{x} represents coordinates of an unit sphere. One can find from the former of Eqs. (A.15) that the spherical harmonics satisfy the Casimir equation for a spin l representation of SO(d), ¹

$$\frac{1}{2}M_{ij}M_{ji}Y_{lm}(\hat{x}) = l(l+d-2)Y_{nm}(\hat{x}), \qquad (A.20)$$

where M_{ij} are generators of d dimensional rotation,

$$M_{ij} = x_i \frac{\partial}{\partial x_j} - x_j \frac{\partial}{\partial x_i}. \tag{A.21}$$

Spherical harmonics of different degree l are orthonormal each other. In particular, we use the following normalization,

$$\int d\Omega_{d-1} Y_{lm}(\hat{x}) Y_{l'm'}(\hat{x}) = \delta_{l,l'} \delta_{m,m'}, \qquad (A.22)$$

where $d\Omega_{d-1}$ is an element of the solid angle in d dimension. The integration is done for \hat{x} . We will prove this orthogonality in Sec. A.2.2.

$$\frac{1}{2r^2}M_{ij}M_{ji} = (d-1)r\frac{\partial}{\partial r} + \frac{\partial^2}{\partial r^2} - \Delta.$$

¹To derive Eq. (A.20), it is convenient to use

A.2.1 Addition theorem

A relation with the Gegenbauer polynomials is an important issue of the spherical harmonics. To see this, let us consider the following function,

$$F_l(\hat{x}, \hat{y}) = \sum_{m=1}^{m=N(d,l)} Y_{lm}(\hat{x}) Y_{lm}(\hat{y}). \tag{A.23}$$

This function is invariant under rotation,

$$F_l(R\hat{x}, R\hat{y}) = F_l(\hat{x}, \hat{y}). \tag{A.24}$$

See the end of this section for this proof. This means that this function depends only on an inner product. The reason as follows: Without loss of generality, we set the vectors as

$$\hat{x} = (1, 0, \dots), \quad \hat{y} = (t, \sqrt{1 - t^2}, \dots).$$
 (A.25)

When we rotate the vectors by π , these can be also written as,

$$\hat{x} = (1, 0, \cdots), \quad \hat{y} = (t, -\sqrt{1 - t^2}, \cdots).$$
 (A.26)

For the function to be invariant under the rotation, the function should include only even powers of $\sqrt{1-t^2}$. Therefore,

$$F_l(\hat{x}, \hat{y}) = F_l(t) = F_l(\hat{x} \cdot \hat{y}). \tag{A.27}$$

Also, recalling that $Y_{lm}(\hat{y})$ is made from a homogeneous function of degree l, one can find that $F_l(t)$ is a polynomial of order l. Another important property is an orthogonality

$$\int d\Omega_{d-1} F_l(\hat{x} \cdot \hat{y}) F_{l'}(\hat{x} \cdot \hat{y}) = \Omega_{d-2} \int_{-1}^1 dt \, (1 - t^2)^{\frac{d-3}{2}} F_l(t) F_{l'}(t) = F_l(1) \delta_{l,l'} \,, \tag{A.28}$$

where

$$F_l(1) = \frac{1}{\Omega_{d-1}} \int d\Omega_{d-1} \sum_{m=1}^{m=N(d,l)} Y_{lm}(\hat{x}) Y_{lm}(\hat{x}) = \frac{N(d,l)}{\Omega_{d-1}}.$$
 (A.29)

And also, Ω_d is the area of S_d , which is given by

$$\Omega_d = \int d\Omega_d = \frac{2\pi^{\frac{d+1}{2}}}{\Gamma(\frac{d+1}{2})}.$$
(A.30)

Hence $F_l(t)$ consists of a set of orthonormal polynomials with a weight function $(1-t^2)^{\frac{d-3}{2}}$. From the Rodrigues' formula, $F_l(t)$ is identified with the Gegenbauer polynomials. Eq. (A.28) determines overall factors. Then, $F_l(\hat{x} \cdot \hat{y})$ can be written as

$$F_l(\hat{x}\cdot\hat{y}) = \sum_{m=0}^{N(d,l)} Y_{lm}(\hat{x}) Y_{lm}(\hat{y}) = \frac{2l+d-2}{4\pi^{\frac{d}{2}}} \Gamma(\frac{d}{2}-1) C_l^{\frac{d}{2}-1} (\hat{x}\cdot\hat{y}).$$
 (A.31)

A.2.2 Detailed calculation

In this subsection, we carry out calculation postponed in Subsec. A.2.

Calculation of N(d, l) Here we show that the number of linearly independent elements of Y_{lm} is N(d, l). As a first step, let us count the number of linearly independent elements for homogenous functions of degree l, S_l , which we denote K(d, l) below. These functions are defined as

$$S_l(\lambda x_1, \dots, \lambda x_d) = \lambda^l S_l(x_1, \dots, x_d). \tag{A.32}$$

First we expand S_l as

$$S_l(\lambda x_1, \dots, \lambda x_d) = \sum_{n=0}^l (x_d)^n S_{l-n}(x_1, \dots, x_{d-1}),$$
(A.33)

where S_{l-n} are homogeneous functions of degree l-n. Hence K(d,l) is represented as

$$K(d,l) = \sum_{n=0}^{l} K(d-1,l-n).$$
(A.34)

Second let us introduce a generating function,

$$G(d) = \sum_{l=0}^{\infty} r^{l} K(d, l).$$
 (A.35)

When we apply the relation Eq. (A.34), the generating function is organized as,

$$G(d) = \sum_{l=0}^{\infty} r^{l} \sum_{n=0}^{l} K(d-1, l-n)$$

$$= \sum_{k=0}^{\infty} K(d-1, k) r^{k} \left(\sum_{n=0}^{\infty} r^{n} \right) ,$$

$$= \frac{G(d-1)}{1-r} . \tag{A.36}$$

Repeating this transformation and using G(0) = 1, we obtain

$$G(d) = \frac{1}{(1-r)^d} \,. \tag{A.37}$$

Finally, we use the following identity,

$$\frac{1}{(1-r)^d} = \sum_{l=0}^{\infty} \binom{l+d-1}{l} r^l.$$
 (A.38)

Substituting this into Eq. (A.37) and comparing with Eq. (A.35), we find

$$K(d,l) = \frac{(p+l-1)!}{l!(p-1)!}.$$
(A.39)

As a second step, we calculate N(d, l). First, we expand a homogeneous function as

$$H_{lm}(x_1, \dots, x_d) = \sum_{n=0}^{l} (x_d)^n S_{l-n}(x_1, \dots, x_{d-1}).$$
(A.40)

The harmonic property of the homogenous function is rephrased as recursion relations,

$$\Delta_{d-1}S_0 = 0$$

$$\Delta_{d-1}S_1 = 0$$

$$\Delta_{d-1}S_n = -(l-n+2)(l-n+1)S_{n-2} \text{ for } n \ge 2.$$
(A.41)

First we observe that S_0 and S_1 satisfy the harmonic equation automatically. Second, if we specify S_l and S_{l-1} , we can fix the remaining homogenous functions. Hence,

$$N(d,l) = K(d-1,l) + K(d-1,l-1) = \frac{2l+d-2}{l} \begin{pmatrix} l+d-3\\l-1 \end{pmatrix}$$
(A.42)

Orthogonality of Y_{lm} Here we show the orthogonality of spherical harmonics stated in (A.22). It is convenient to consider the following integration,

$$I = \int_{B_d} d^d x \frac{\partial}{\partial x^i} \left[H_{lm}(x) \frac{\partial}{\partial x^i} H_{l'm'}(x) - H_{l'm'}(x) \frac{\partial}{\partial x^i} H_{lm}(x) \right], \tag{A.43}$$

where the integration region is an unit ball in d dimensions. On one hand, this integration is always vanish due to the harmonic property of H_{lm} ,

$$I = 0. (A.44)$$

On the other hand, this integral can be rephrased as

$$I = \int_{S_{d-1}} d\Omega_{d-1} \hat{x}^i \left[H_{lm}(\hat{x}) \frac{\partial}{\partial x^i} H_{l'm'}(\hat{x}) - H_{l'm'}(\hat{x}) \frac{\partial}{\partial x^i} H_{lm}(\hat{x}) \right], \tag{A.45}$$

where the integration region is an unit sphere. Note that we used the Stokes' theorem. Further, we use the homogenous property and replace H_{lm} with Y_{lm} . Then, Eq. (A.46) reads

$$I = \int_{S_{d-1}} d\Omega_{d-1}(l - l') \left[H_{lm}(\hat{x}) H_{l'm'}(\hat{x}) \right], \qquad (A.46)$$

Hence the following are derived,

$$\int_{S_{d-1}} d\Omega_{d-1} Y_{lm}(\hat{x}) Y_{l'm'}(\hat{x}) = 0 \quad \text{unless } l = l'.$$
(A.47)

Rotation invariance of $F_l(\hat{x}, \hat{y})$ Finally we show that $F_l(\hat{x}, \hat{y})$ is invariant under rotation. First we expand the rotated spherical harmonics as

$$Y_{lm}(R\hat{x}) = \sum_{m'=1}^{N(d,l)} C_{mm'} Y_{lm'}(\hat{x}), \qquad (A.48)$$

where the coefficients are determined by

$$C_{mm'} = \int d\Omega_{d-1} Y_{lm}(R\hat{x}) Y_{lm'}(\hat{x}). \tag{A.49}$$

These coefficients should satisfy

$$\sum_{p=1}^{N(d,l)} C_{mp} C_{sp} = \delta_{ms} \,, \tag{A.50}$$

which is derived straightforwardly from the identity,

$$\int d\Omega_{d-1} Y_{lm}(\hat{x}) Y_{ls}(\hat{x}) = \int d\Omega_{d-1} Y_{lm}(R\hat{x}) Y_{ls}(R\hat{x}) = \delta_{ms}.$$
 (A.51)

Applying the above, one can find that

$$F_{l}(R\hat{x}, R\hat{y}) = \sum_{m=1}^{N(d,l)} \left(\sum_{s=1}^{N(d,l)} C_{ms} Y_{ls}(\hat{x}) \right) \left(\sum_{p=1}^{N(d,l)} C_{mp} Y_{lp}(\hat{x}) \right)$$

$$= \sum_{s=1}^{N(d,l)} \sum_{p=1}^{N(d,l)} \delta_{ps} Y_{ls}(\hat{x}) Y_{lp}(\hat{x})$$

$$= \sum_{s=1}^{N(d,l)} Y_{ls}(\hat{x}) Y_{ls}(\hat{x}). \tag{A.52}$$

Appendix B

More on scattering amplitudes

In this appendix, we derive several properties of scattering amplitudes used in this thesis. In Sec. B.1 we derive an unitarity bound and apply this bound to scattering amplitudes in a plane wave basis. In particular, we show that the Einstein gravity violates the unitarity bound around the Planck scale in four dimensions. In Sec. B.2, we introduce angular momentum eigenstates. We show that partial wave amplitudes are scattering amplitudes for angular momentum eigenstates. Also, we apply the unitarity bound in this basis. One can find that the Einstein gravity violates the unitarity bound around the Planck scale also in dimensions higher that or equal to six. In Sec. B.2.3, we discuss complex angular momentum necessary to develop the Regge theory. In Sec. B.3, we calculate four point amplitudes mediated by gravity for a minimally coupled scalar field.

B.1 Unitarity bounds

In this section, we derive bounds on scattering amplitudes as consequences of S-matrix unitarity. Let us begin with summarizing notations for scattering amplitudes and their related concepts. A transition amplitude from an initial state $|A\rangle$ to a final state $|B\rangle$ is described by the S matrix as,

$$\langle B|S|A\rangle$$
, (B.1)

where the S-matrix is introduced as

$$S = \lim_{t \to \infty} e^{-iHt} \,. \tag{B.2}$$

Here H is the Hamiltonian. To study scattering processes, it is convenient to define T-matrix as

$$S = 1 + iT. (B.3)$$

The identity operator does not change the initial state. Hence information on interactions is encoded in the T-matrix. As long as the Hamiltonian is Hermitian, the S matrix must be unitary,

$$SS^{\dagger} = 1. \tag{B.4}$$

In the language of the T-matrix, the S-matrix unitary reads

$$-i\left(T - T^{\dagger}\right) = TT^{\dagger}. \tag{B.5}$$

One can find that Eq. (B.5) gives bounds on the matrix elements. First let us sandwiches both sides of Eq. (B.5) by a state $|\alpha\rangle$. Second, Insert a set of orthogonal states $\sum_{\gamma} |\gamma\rangle\langle\gamma|$ in the right hand side. Then Eq. (B.5) reads

$$2\operatorname{Im}T_{\alpha\alpha} = \sum_{\gamma} |T_{\alpha\gamma}|^2, \tag{B.6}$$

where $T_{\alpha\beta}$ is a matrix element, $T_{\alpha\beta} = \langle \alpha | T | \beta \rangle$. Notice that each element of the summation is positive. Hence the following inequality is derived,

$$2\operatorname{Im}T_{\alpha\alpha} \ge |T_{\alpha\alpha}|^2. \tag{B.7}$$

Also, taking the absolute values on both sides, we obtain

$$2 \ge |T_{\alpha\alpha}| \tag{B.8}$$

Below we study consequences of the inequalities for scattering amplitudes.

Bounds in place wave basis Scattering amplitudes are defined by subtracting a delta function from *T*-matrix elements,

$$\langle B|T|A\rangle = (2\pi)^d \delta^d(p_B - p_A)M(A \to B),$$
 (B.9)

where p_A and p_B are momentums of the initial state and the final state. Along the derivation of Eq. (B.7), let us sandwiches Eq. (B.5) with states $\langle B|$ and $|A\rangle$, and insert a complete set in the plane wave basis,

$$\sum_{C} \prod_{i=1}^{N_C} \int \frac{d^{d-1}p_i}{(2\pi)^{d-1}} \frac{1}{2E(p_i)} |p_1, \dots, p_{N_C}\rangle \langle p_1, \dots, p_{N_C}|,$$
 (B.10)

where C runs all states in the complete set, and N_C counts the number of particles. Each state in the complete set is a product of one particle states, which are normalized as

$$\langle \boldsymbol{p}|\boldsymbol{q}\rangle = (2\pi)^{d-1}\delta^{d-1}(\boldsymbol{p}-\boldsymbol{q})E(\boldsymbol{p}).$$
 (B.11)

Here $E(\mathbf{p})$ is an energy,

$$E(\mathbf{p}) = \sqrt{m^2 + \mathbf{p}^2}. \tag{B.12}$$

Then, Eq. (B.5) reads

$$-i(2\pi)^{D}\delta^{d}(p_{A}-p_{B}) (M_{AB}-M_{BA}^{\star})$$

$$=\sum_{C} \prod_{i=1}^{N_{C}} \int \frac{d^{d-1}\mathbf{p}}{(2\pi)^{D-1}} \frac{1}{2E_{i}(\mathbf{p}_{i})} (2\pi)^{d}\delta^{d}(p_{A}-p_{B})(2\pi)^{d}\delta^{d}(p_{A}-p_{C})M_{CB}M_{CA}^{\star}. \tag{B.13}$$

To derive a bound, we assume that the in and out states are two particle states, and they experience a forward scattering, $|A\rangle = |B\rangle$. With this assumption, Eq. (B.15) becomes

$$-i (M_{AA} - M_{AA}^{\star}) = \sum_{C} \prod_{i=1}^{N_C} \int \frac{d^{d-1} \mathbf{p}_i}{(2\pi)^{d-1}} \frac{1}{2E_i(\mathbf{p}_i)} (2\pi)^d \delta(\sqrt{s} - p_C^0) \delta^{d-1}(\mathbf{p}_C) |M_{CA}|^2 , \qquad (B.14)$$

Here we set $p_A = (\sqrt{s}, 0, \dots, 0)$ without loss of generally. Since the right hand side of Eq. (B.15) is positive for each intermediate state, one can find the following bound,

$$-i \left(M_{AA} - M_{AA}^{\star} \right)$$

$$\geq \prod_{i=1}^{N_{C'}} \int \frac{d^{d-1} \boldsymbol{p}_{i}}{(2\pi)^{d-1}} \frac{1}{2E_{i}(\boldsymbol{p}_{i})} (2\pi)^{d} \delta(\sqrt{s} - p_{C'}^{0}) \delta^{d-1}(\boldsymbol{p}_{C'}) \left| M_{C'A} \right|^{2},$$
(B.15)

where C' is one instance picked up from the complete set. For example, let us consider that A and C are two particle states with mass m. In this case, Eq. (B.15) reads

$$2\operatorname{Im} M(s, \cos \theta = 1) \ge \int \frac{d^{d-1} \mathbf{P}}{(2\pi)^{d-2}} \frac{1}{4E(\mathbf{P})^2} \delta(\sqrt{s} - 2\sqrt{m^2 + \mathbf{P}^2}) |M_{CA}|^2$$

$$= 2 \times \frac{1}{(2\pi)^{d-2}} \frac{1}{\sqrt{s}} \left(\frac{s}{4} - m^2\right)^{\frac{d-3}{2}} \int d\Omega_{d-2} |M(s, \cos \theta)|^2, \qquad (B.16)$$

where we introduced

$$\boldsymbol{P} = \frac{\boldsymbol{p}_1 - \boldsymbol{p}_2}{2} \,, \tag{B.17}$$

Also, we introduce a scattering angle θ , which can be written as ¹

$$\cos \theta = 1 + \frac{t}{s - 4m^2} \,. \tag{B.18}$$

Further, taking an absolute value for the left hand side of the inequality (B.16), we obtain

$$|M(s,\cos\theta = 1)| \ge \frac{1}{(2\pi)^{d-2}} \frac{1}{\sqrt{s}} \left(\frac{s}{4} - m^2\right)^{\frac{d-3}{2}} \int d\Omega_{d-2} |M(s,\cos\theta)|^2 , \qquad (B.19)$$

By the power counting of both sides, one can find that

$$M(s, \cos \theta) \le C \cdot s^{\frac{4-d}{2}} \quad \text{for } s \to \infty, \theta : \text{fixed},$$
 (B.20)

where C is a constant. This bound is satisfied by known renormalizable theories, for e.g. $\lambda \phi^4$ theory. On the other hand, the Einstein gravity, which is non-renormalizable, does not respect this bound.

$$s = -(p_1 + p_2)^2, t = -(p_1 - p_3)^2, u = -(p_1 - p_4)^2,$$

where p_1 and p_2 are momentums of an in state, and p_3 and p_4 are momentums if a final state.

¹We use the following convention for the Mandelstam variable:

Application to Einstein gravity Finally we examine the constant C of this bound more carefully for the Einstein gravity in four dimensions. As an illustrative example, we consider the Einstein gravity with a minimally coupled scalar field. A four point amplitude of scalar fields at tree level is given by

$$M(s,t) = \frac{1}{M_{\rm pl}^2} \left[\left(\frac{tu}{s} + \frac{us}{t} + \frac{st}{u} \right) + 6m^2 - 2m^4 \left(\frac{1}{s} + \frac{1}{t} + \frac{1}{u} \right) \right], \tag{B.21}$$

where m is the mass of the scalar field. See Appendix. B.3 for the derivation of Eq. (B.21). We note that the inequality (B.19) becomes ill-defined caused by IR divergences of the massless graviton. To resolve this difficulty, let us introduce a tiny mass Λ for the graviton as an IR cutoff, which shifts the massless poles by Λ^2 . In the hard scattering limit ($s \gg m^2$, θ : fixed), the amplitude (B.21) reads

$$M(s,t) \simeq \frac{(3+z^2)^2}{4} \frac{s^3}{(s(1-\cos\theta)+2\Lambda^2)(s(1+\cos\theta)+2\Lambda^2)}$$
 (B.22)

We substitute this into the inequality (B.19). In the small Λ limit, the integral of the right hand side is localized at $\cos \theta = \pm 1$. Hence, the right hand side is approximated as,

$$\frac{1}{\pi^2} \int_{-1}^1 dz \left(\frac{s^4}{s(1-z) + 2\Lambda^2} \right)^2 + \left(\frac{s^4}{s(1+z) + 2\Lambda^2} \right)^2 \simeq \frac{1}{M_{\rm pl}^4} \frac{1}{4\pi^2} \frac{s^3}{\Lambda^2}$$
 (B.23)

Then, the inequality (B.19) reads

$$\frac{1}{M_{\rm pl}^2} \frac{s^2}{\Lambda^2} \ge \frac{1}{4\pi^2 M_{\rm pl}^4} \frac{s^3}{\Lambda^2} \,. \tag{B.24}$$

This means that the unitarity bound are respected only for

$$s \le 2\pi M_{\rm pl}^2 \,. \tag{B.25}$$

Notice that the above prescription does not make sense for dimensions other than four. This is because the left and right hand side of the inequality (B.19) have a different power of Λ . For $d \geq 6$, an angular momentum basis is suitable to know a bound for the Einstein Gravity instead of the plane wave basis. In the next appendix, we develop an angular momentum basis.

B.2 Partial wave expansion

In this section, we study scattering amplitudes in an angular momentum basis. First we define this basis in Subsec. B.2.1. Also we show that scattering amplitudes in this basis is equivalent to the partial wave expansion of scattering amplitudes. In Subsec. B.2.2, we illustrate unitarity bounds in an angular momentum basis. We also apply this bound to gravitational theories in dimensions higher than or equal to six. Finally, we discuss a complex angular momentum in Subsec. B.2.3. In particular, we illustrate a nice analytic continuation of partial wave amplitudes necessary to develop the Regge theory.

B.2.1 Definition

First let us move on to the center-of-mass frame, where a momentum sum has a form $(E_{\text{CM}}, 0, \dots, 0)$. This momentum is invariant under SO(d-1) rotation. Hence, we can classify a state by two label (l, m) in addition to a momentum sum. More explicitly, for two particle states, angular momentum eigenstates are defined as,

$$|(E_{\rm cm}, 0); l, m\rangle = \int d\Omega_{d-2} Y_{lm}(\hat{p}) |\boldsymbol{p}, -\boldsymbol{p}\rangle,$$
 (B.26)

where \hat{p} is a unit vector defined as $\hat{p} = p/|p|$. The first argument denotes the sum of the four vectors. And, l represents the angular momentum. Below, we consider two particle states with an identical mass m. While we used the center-of-mass frame, we can also define such states for general frames by acting the Lorentz transformation. From the orthogonality of the spherical harmonics, the plane wave state is expanded as,

$$|\boldsymbol{p}, -\boldsymbol{p}\rangle = \sum_{l=0}^{\infty} \sum_{m=0}^{N(l, d-1)} Y_{l, m}(\hat{p}) |l, m\rangle.$$
(B.27)

Also, recalling the normalization of the plane wave basis Eq. B.11, we can calculate the inner product of the angular momentum eigenstates as

$$\langle P; l, m | P'; l, m \rangle = (2\pi)^d \delta^d (P - P') \frac{(2\pi)^{d-2} \sqrt{s}}{2\left(\frac{s}{4} - m^2\right)^{\frac{d-3}{2}}} \delta_{ll'} \delta_{mm'}.$$
 (B.28)

Scattering amplitudes for the angular momentum basis can be written as,

$$M(\{P; l, m\} \to \{P'; l', m'\}) = f_l(s)\delta_{l,l'}\delta_{m,m'},$$
 (B.29)

where the Kronecker deltas come from the angular momentum conservation. $f_l(s)$ is called a partial wave amplitude. Since this amplitude only depends on the center-of-mass momentum and the angular momentum, the partial wave amplitude is a function of the Mandelstam s and the angular momentum. Using the expansion rule B.27, one can find a relation between scattering amplitudes,

$$M(s,t) = \sum_{l=0}^{\infty} \sum_{m=0}^{N(l,d-1)} \sum_{l'=0}^{\infty} \sum_{m'=0}^{N(l',d-1)} Y_{l',m'}(\hat{q}) Y_{l,m}(\hat{p}) \langle l',m'|T|l,m \rangle.$$

$$= \frac{\Gamma(\frac{d}{2} - \frac{3}{2})}{4\pi^{\frac{d-1}{2}}} \sum_{l=0}^{\infty} (2l + d - 3) f_l(s) C_l^{\frac{d}{2} - \frac{3}{2}} (1 + \frac{2t}{s - 4m^2}), \qquad (B.30)$$

where we used the addition theorem as

$$\sum_{m'=0}^{N(l',d-1)} Y_{l,m}(\hat{q}) Y_{l,m}(\hat{p}) = \frac{\Gamma(\frac{d}{2} - \frac{3}{2})}{4\pi^{\frac{d-1}{2}}} C_l^{\frac{d}{2} - 1}(\hat{p} \cdot \hat{q}) = \frac{\Gamma(\frac{d}{2} - \frac{3}{2})}{4\pi^{\frac{d-1}{2}}} C_l^{\frac{d}{2} - \frac{3}{2}} (1 + \frac{2t}{s - 4m^2}).$$
 (B.31)

Oppositely, the partial wave amplitude can be written as

$$f_l(s) = \frac{(4\pi)^{\frac{d-3}{2}}\Gamma(l+1)\Gamma(\frac{d-3}{2})}{\Gamma(l+d-3)} \int_1^1 dz (1-z)^{\frac{d-3}{2}} M(s,z) C_l^{\frac{d}{2}-\frac{3}{2}}(z).$$
 (B.32)

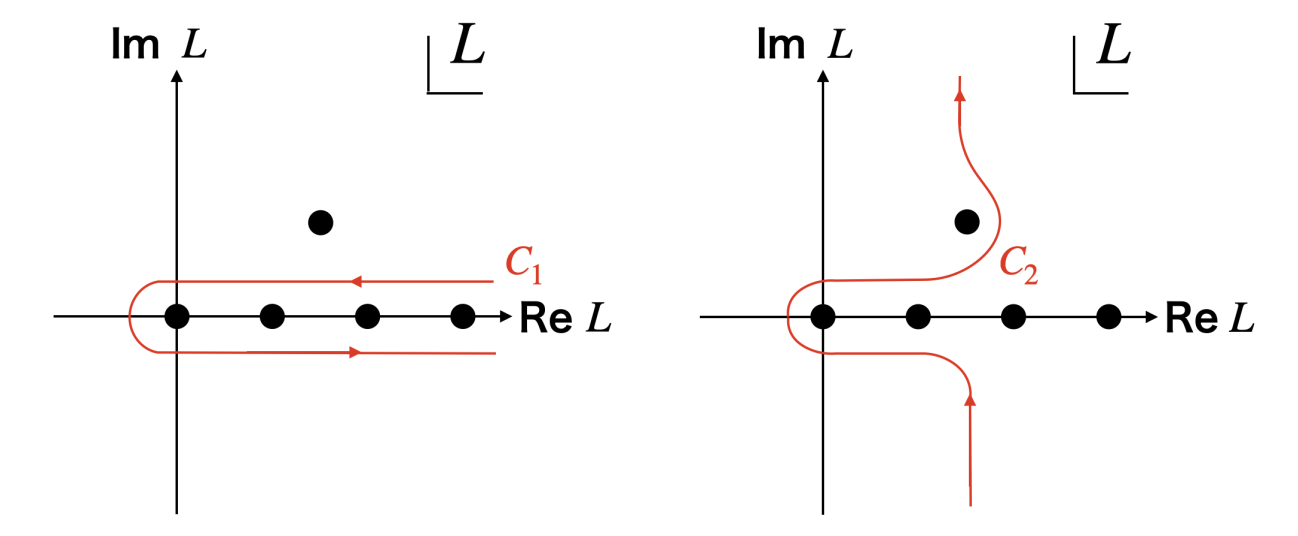


Figure B.1: The left figure shows the integration contour of Eq. (B.38). The left contour is equivalent to the right contour if an integration of the infinity is negligible.

B.2.2 Partial wave unitarity

Let us examine the unitarity bounds for angular momentum eigenstate basis. We set $|\alpha\rangle = |P; l, m\rangle$ in the bound. Notice that this state appears in a complete set as,

$$\int \frac{d^d P}{(2\pi)^d} \frac{2\left(\frac{s}{4} - m^2\right)^{\frac{d-3}{2}}}{\sqrt{s}} |P; l, m\rangle\langle P; l, m| \tag{B.33}$$

Then, this bound is rephrased as

$$\operatorname{Im} f_l(s) \ge \frac{1}{(2\pi)^{d-2}} \frac{\left(\frac{s}{4} - m^2\right)^{\frac{d-3}{2}}}{\sqrt{s}} f_l(s)^2.$$
 (B.34)

Taking the absolute values, we obtain

$$f_l(s) \le \frac{(2\pi)^{d-2}\sqrt{s}}{\left(\frac{s}{4} - m^2\right)^{\frac{d-3}{2}}}.$$
 (B.35)

Let us examine this bound for the Einstein gravity. Notice that the partial wave expansion does not converge in dimensions smaller than six due to the massless pole. For example, when d=10, l=0, the partial wave amplitude in the hard scattering limit $(s \gg m, \theta : \text{fixed})$ is calculated as

$$f_0(s) \simeq \frac{1}{M_{\rm pl}^3} \frac{832\pi^4}{635} s$$
. (B.36)

Hence, comparing this with the inequality (B.35), one can find that the partial wave amplitude violates the unitarity bound around the Planck scale.

B.2.3 Gribov-Froissart projection

To develop the Regge theory in Sec. 2.4, it was necessary to find an analytic continuation of $f_L(t)$, which does not grow exponentially for large |L|. In this appendix, we illustrate this method called the Gribov-Froissart projection. First, to recall the notation, let us look back the Regge theory. To study t-channel physics, we carried out a partial wave expansion as follows:

$$M(s,t) = \frac{\Gamma(\frac{d}{2} - \frac{3}{2})}{4\pi^{\frac{d-1}{2}}} \sum_{l=0}^{\infty} (2L + d - 3) f_L(t) C_L^{\frac{d}{2} - 1} (1 + \frac{2s}{t - 4m^2}).$$
 (B.37)

This series diverges in the region $s \gg 1, t < 0$ which we are interested in. To make an analytic continuation to this region, we introduced complex angular momentum and expressed Eq. (B.37) as,

$$M(s,t) = \frac{\Gamma(\frac{d}{2} - \frac{3}{2})}{4\pi^{\frac{d-1}{2}}} \frac{i}{2} \int_{C_1} \frac{dL}{\sin \pi L} (2L + d - 3) f_L(t) C_L^{\frac{d}{2} - \frac{3}{2}}(-z),$$
 (B.38)

where

$$z = 1 + \frac{2s}{t - 4m^2} \,. ag{B.39}$$

Further, we deform the integration contour to C_2 of Fig. B.1. For large |L|, the Gegenbauer polynomials behave as

$$C_L^{\frac{d}{2} - \frac{3}{2}}(-\cos\theta) \sim e^{i(\pi - \theta)L} + e^{-i(\pi - \theta)L} \quad \text{for } 0 < \theta < \frac{\pi}{2}.$$
 (B.40)

Hence, if $f_L(t)$ should not grow exponentially for large |L|, we can carry out this deformation. Below, we show that one can find such an expression. Let us begin with the following expression for -1 < z < 1,

$$f_L(t) = \frac{\pi^{\frac{d-3}{2}}}{2^{2-d}\Gamma(\frac{d}{2} - \frac{3}{2})} \frac{\Gamma(L+1)}{\Gamma(L+d-3)} \int_{-1}^1 dz (1-z^2)^{\frac{d}{2}-2} C_L^{\frac{d}{2}-\frac{3}{2}}(z) M(t,z).$$
 (B.41)

First we rewrite Eq. (B.41) in terms of the Legendre function of the second kind or its extension as,

$$f_L(t) = \frac{\pi^{\frac{d-3}{2}}}{2^{2-d}\Gamma(\frac{d}{2} - \frac{3}{2})} \frac{\Gamma(L+1)}{\Gamma(L+d-3)} \int_{C_3} dz D_L^{\frac{d}{2} - \frac{3}{2}}(z) M(t,z),$$
(B.42)

where we used the following identity on the branch cut (-1 < z < 1),

$$D_L^{\frac{d}{2} - \frac{3}{2}}(z + i\epsilon) - D_L^{\frac{d}{2} - \frac{3}{2}}(z - i\epsilon) = -i\pi(1 - z^2)^{\frac{d}{2} - 2}C_L^{\frac{d}{2} - \frac{3}{2}}(z).$$
(B.43)

See Appendix. A.1 for details of $D_l^{\alpha}(z)$. To go further, we need three observations. First, M(t,z) has branch cuts, $(-\infty, -z_1)$ and (z_2, ∞) ,

$$z_1 = -1 + 2\frac{t - 4m^2 + M^2}{t - 4m^2} > 1, \quad z_2 = 1 + 2\frac{M^2}{t - 4m^2} > 1,$$
 (B.44)

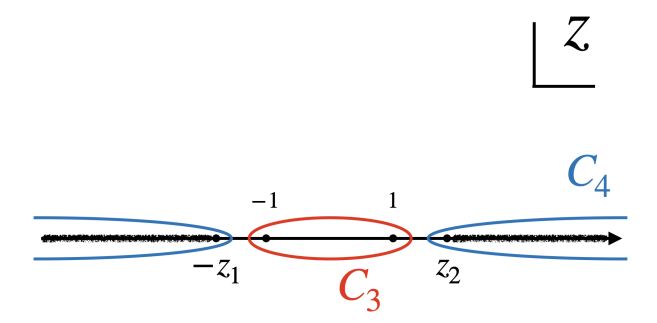


Figure B.2: Contours for the integrals of Eq. (B.42) and Eq. (B.47)

where M is a mass of the lightest particle. z_1 and z_2 correspond to the u-channel pole and the s-channel pole respectively. Second, the scattering amplitude is bounded as,

$$M(t,z) < z^{L_0}. (B.45)$$

This boundedness is guaranteed by locality. Third, $D_L^{\frac{d}{2}-\frac{3}{2}}(z)$ behaves as

$$D_L^{\frac{d}{2} - \frac{3}{2}}(z) \sim z^{-L - 1}$$
 (B.46)

Hence, for $L > L_0$, we can deform the contour integral C_4 as depicted in Fig. B.2,

 $f_L(t)$

$$= \frac{\pi^{\frac{d-3}{2}}}{2^{2-d}\Gamma(\frac{d}{2} - \frac{3}{2})} \frac{\Gamma(L+1)}{\Gamma(L+d-3)} \left[\int_{-z_1}^{-\infty} dz D_L^{\frac{d}{2} - \frac{3}{2}}(z) \operatorname{Disc}_z M(t,z) + \int_{z_2}^{\infty} dz D_L^{\frac{d}{2} - \frac{3}{2}}(z) \operatorname{Disc}_z M(t,z) \right],$$

$$= \frac{\pi^{\frac{d-3}{2}}}{2^{2-d}\Gamma(\frac{d}{2} - \frac{3}{2})} \frac{\Gamma(L+1)}{\Gamma(L+d-3)} \left[(-1)^L \int_{z_1}^{\infty} dz D_L^{\frac{d}{2} - \frac{3}{2}}(z) \operatorname{Disc}_z M(t,z) + \int_{z_2}^{\infty} dz D_L^{\frac{d}{2} - \frac{3}{2}}(z) \operatorname{Disc}_z M(t,z) \right],$$
(B.47)

where Disc means the discontinuity on the branch cuts,

$$\operatorname{Disc}_{z} M(t, z) = M(t, z + i\epsilon) - M(t, z - i\epsilon). \tag{B.48}$$

We note that one has to deal with odd and even L separately. Otherwise, $(-1)^L = e^{i\pi L}$ leads an exponentially growing for imaginary L. Therefore we decompose scattering amplitudes into an odd L part and an even L part, and analyze separately. For each L, the integrals fall off exponentially because

$$D_L^{\frac{d}{2} - \frac{3}{2}}(\cosh \chi) \sim e^{-L\chi}, \quad \text{(for } \chi > 0).$$
 (B.49)

Also, the coefficient does not grow for d = 4 and falls off for d > 4,

$$\frac{\Gamma(L+1)}{\Gamma(L+d-3)} \sim L^{4-d} \,. \tag{B.50}$$

Hence $f_L(t)$ falls off exponentially. Thus we have found the desirable expression of $f_L(t)$. Notice that this expression is only applicable for $\text{Re}L \geq L_0$.

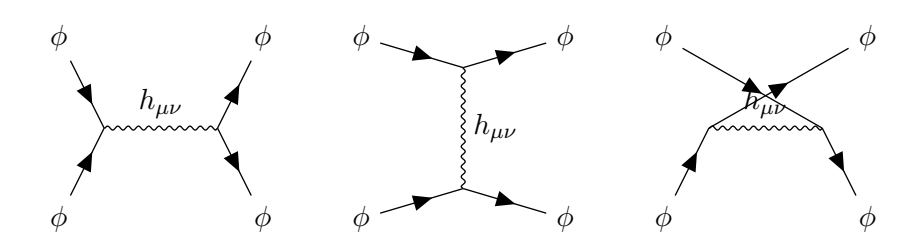


Figure B.3: $\phi\phi \to \phi\phi$ scattering processes at tree level.

B.3 Gravity mediated amplitudes

In this appendix, we calculate scattering amplitudes mediated by gravity. As an illustrative example, we consider the Einstein Gravity with a minimally coupled scalar field,

$$S = \frac{M_{\rm pl}^{d-2}}{2} \int d^d x \sqrt{-g} R - \int d^d x \sqrt{-g} \left(\frac{1}{2} g^{\mu\nu} \partial_\mu \phi \partial_\nu \phi + \frac{m^2}{2} \phi^2 \right) . \tag{B.51}$$

In particular, we analyse $\phi\phi \to \phi\phi$ scattering at tree level. Corresponding Feynman diagrams are depicted in Fig. B.3. Relevant terms are

$$S = \frac{M_{\rm pl}^{d-2}}{2} \int d^d x \left(-\frac{1}{4} \partial^{\lambda} h^{\mu\nu} \partial_{\lambda} h_{\mu\nu} + \frac{1}{2} \partial_{\mu} h^{\mu\rho} \partial^{\nu} h_{\nu\rho} + \frac{1}{2} h \partial_{\mu} \partial_{\nu} h^{\mu\nu} + \frac{1}{4} \partial^{\rho} h \partial_{\rho} h \right)$$
$$- \int d^d x \left(\frac{1}{2} \partial^{\mu} \phi \partial_{\mu} \phi + \frac{m^2}{2} \phi^2 - \frac{1}{2} h^{\mu\nu} \partial_{\mu} \phi \partial_{\nu} \phi + \frac{1}{4} h \partial^{\mu} \phi \partial_{\mu} \phi + \frac{m^2}{4} h \phi^2 \right) + \cdots, \tag{B.52}$$

where $h_{\mu\nu}$ is a perturbation around the flat metric,

$$h_{\mu\nu} = g_{\mu\nu} - \eta_{\mu\nu} . \tag{B.53}$$

This system has the gauge symmetry under

$$h_{\mu\nu} \to h_{\mu\nu} + \partial_{\mu}\Lambda_{\nu} + \partial_{\nu}\Lambda_{\mu}$$
 (B.54)

To fix this redundancy, we add the gauge fixing term,

$$S_{\rm GF} = \frac{M_{\rm pl}^{d-2}}{2} \int d^d x Q_B \left[\bar{C}^{\mu} (\partial^{\nu} h_{\mu\nu} - \frac{1}{2} \partial_{\mu} h + \frac{1}{2} \xi B_{\mu}) \right] , \qquad (B.55)$$

where Q_B is BRST charge, and BRST transformations are given by,

$$Q_B h_{\mu\nu} = \partial_{\mu} C_{\nu} + \partial_{\nu} C_{\mu} ,$$

$$Q_B C_{\mu} = 0 ,$$

$$Q_B \bar{C}_{\mu} = B_{\mu} ,$$

$$Q_B B_{\mu} = 0 .$$
(B.56)

After integrating B_{μ} , the action reads

$$S + S_{GF} = \frac{M_{\rm pl}^{d-2}}{2} \int d^dx \left[-\frac{1}{4} \partial^{\lambda} h^{\mu\nu} \partial_{\lambda} h_{\mu\nu} + \frac{1}{2} \left(1 - \frac{1}{\xi} \right) \partial_{\mu} h^{\mu\rho} \partial^{\nu} h_{\nu\rho} + \frac{1}{2} \left(1 - \frac{1}{\xi} \right) h \partial_{\mu} \partial_{\nu} h^{\mu\nu} \right.$$

$$\left. + \frac{1}{4} \left(1 - \frac{1}{2\xi} \right) \partial^{\rho} h \partial_{\rho} h + \bar{C}^{\mu} \partial^2 C_{\mu} \right]$$

$$\left. - \int d^dx \left[\frac{1}{2} \partial^{\mu} \phi \partial_{\mu} \phi + \frac{m^2}{2} \phi^2 - \frac{1}{2} h^{\mu\nu} \partial_{\mu} \phi \partial_{\nu} \phi + \frac{1}{4} h \partial^{\mu} \phi \partial_{\mu} \phi + \frac{m^2}{4} h \phi^2 \right] + \cdots \right]$$
(B.57)

Next let us make Feynman rules to calculate the diagrams. First we calculate the time-ordered propagator of the graviton. This satisfies the differential equation,

$$\left[\delta^{\alpha}_{\mu} \delta^{\beta}_{\nu} \partial^{2} - \frac{1}{2} \eta_{\mu\nu} \eta^{\alpha\beta} \partial^{2} - \left(1 - \frac{1}{\xi} \right) \left(\delta^{\alpha}_{\mu} \partial_{\nu} \partial^{\beta} + \delta^{\alpha}_{\nu} \partial_{\mu} \partial^{\beta} - \eta_{\mu\nu} \partial^{\alpha} \partial^{\beta} + \partial_{\mu} \partial_{\nu} \eta^{\alpha\beta} + \frac{1}{2} \eta_{\mu\nu} \eta^{\alpha\beta} \partial^{2} \right) \right] \times \langle T \left[h_{\alpha\beta}(x) h_{\rho\sigma}(y) \right] \rangle_{|0} = i \frac{2}{M_{\rm pl}^{d-2}} \left(\delta_{\mu\rho} \delta_{\nu\sigma} + \delta_{\mu\sigma} \delta_{\nu\rho} \right) \delta^{d}(x - y) , \quad (B.58)$$

where $_{|0}$ means that we turn off the couplings. The derivatives are in terms of x. In the momentum space, this differential equation is solved as

$$\langle T \left[h_{\mu\nu}(x) h_{\rho\sigma}(y) \right] \rangle_{|0} = \frac{2}{M_{\rm pl}^{d-2}} \int \frac{d^d p}{(2\pi)^d} e^{ipx} \frac{-i}{p^2} \left[-\frac{2}{d-2} \eta_{\mu\nu} \eta_{\rho\sigma} + \eta_{\mu\rho} \eta_{\nu\sigma} + \eta_{\mu\sigma} \eta_{\nu\rho} - 4 \left(1 - \frac{1}{\xi} \right) \frac{p_{(\mu} \eta_{\nu)(\rho} p_{\sigma)}}{p^2} \right]$$
(B.59)

Therefore, the Feynman rule for the graviton propagator reads as,

$$h_{\mu\nu} \sim h_{\rho\sigma}$$

$$= \frac{-2i}{M_{\rm pl}^{d-2} p^2} \left[-\frac{2}{d-2} \eta_{\mu\nu} \eta_{\rho\sigma} + \eta_{\mu\rho} \eta_{\nu\sigma} + \eta_{\mu\sigma} \eta_{\nu\rho} - 4 \left(1 - \frac{1}{\xi} \right) \frac{p_{(\mu} \eta_{\nu)(\rho} p_{\sigma)}}{p^2} \right]$$
(B.60)

The Feynman rule for the $\phi\phi h$ vertex reads from the action (B.57) straightforwardly as,

Then we calculate the scattering amplitudes. The s-channel amplitude is calculated as,

$$M(s,t)_s = \frac{1}{M_{\rm pl}^{d-2}} \left[\frac{tu}{s} + 2m^2 - 4\frac{d-3}{d-2} \frac{m^4}{s} \right].$$
 (B.62)

This amplitude has no ξ dependence, which guarantees the gauge invariance. t and u channels are calculated by permutation of the Mandelstam valuables. Finally, we add all channels and obtain

$$M(s,t) = \frac{1}{M_{\rm pl}^{d-2}} \left[\left(\frac{tu}{s} + \frac{us}{t} + \frac{st}{u} \right) + 6m^2 - 4m^4 \frac{d-3}{d-2} \left(\frac{1}{s} + \frac{1}{t} + \frac{1}{u} \right) \right].$$
 (B.63)

Appendix C

Massless higher spin theory

In this chapter, we derive the field equation of higher spin fields (3.32). We begin with massless higher spin fields. These actions are uniquely determined by a higher spin gauge symmetry. Notice that in curved spacetime, mass terms appear due to a coupling with curvature tensors even in massless cases. An action of massive higher spin fields are determined by adding a mass term to the massless action. Massive higher spin fields should satisfy the Fierz-Pauli condition. Imposing this condition, the field equations reduce to Eq. (3.32).

In Sec. C.1, first we study an example of massless spin two fields. One can find that the gauge symmetry is realized as a divergence free condition of an equation of motion. Second, we produce a system of massive spin two fields by adding the Fierz-Pauli mass term. We show that massive spin 2 fields are constrained by the Fietz-Pauli condition. By imposing these constraint, the field equation reduces to Eq. (3.32). Besides, one can find that there appears a gauge symmetry for a specific mass, for which fields are called a partially massless field. In Sec. C.2, first we determine an action of massless spin S fields by utilizing a higher spin gauge symmetry in flat space. Next, we extend it to (A)dS space. The main difference is the mass term coming from the curvature. Finally, adding a mass term, we obtain massive higher spin theories.

C.1 Spin two example

By illustrating massless spin two fields in de Sitter space, we show how a gauge symmetry can be seen in their field equation. Besides, we also study massive cases. One can find that there appears a gauge symmetry for a specific mass.

Massless field One can obtain a field equation of a massless spin two field by considering a second order perturbation of Einstein gravity, which is given by

$$X_{\mu\nu} = D_{\rho}D^{\rho}\phi_{\mu\nu} - D_{\mu}D^{\rho}\phi_{\rho\nu} - D_{\nu}D^{\rho}\phi_{\rho\mu} + D_{\mu}D_{\nu}\phi + g_{\mu\nu}\left(D_{\rho}D_{\sigma}\phi^{\rho\sigma} - D_{\rho}D^{\rho}\phi\right) - 2H^{2}\left(\phi_{\mu\nu} + \frac{1}{2}\phi g_{\mu\nu}\right) = 0, \quad (C.1)$$

where

$$\phi = g^{\mu\nu}\phi_{\mu\nu} \,. \tag{C.2}$$

We note that $\mu = 0$ or $\nu = 0$ components of Eq. (C.6) have no second time derivative. Hence these are constraint equations. The divergence of these constraint does not yield a new constraint. Instead, it becomes an identity,

$$D^{\mu}X_{\mu\nu} = 0$$
. (C.3)

Notice that this equality holds without using equations of motion. This implies an existence of a gauge symmetry. Let us consider the following transformation,

$$\delta\phi_{\mu\nu} = D_{\mu}\Lambda_{\nu} + D_{\nu}\Lambda_{\mu}\,,\tag{C.4}$$

where Λ_{μ} is an arbitrary vector function. A variation of an action reads

$$\delta S = \int d^d x \sqrt{-g} X_{\mu\nu} \, \delta \phi^{\mu\nu} \,, \tag{C.5}$$

which is a consequence of the variation principal. Substituting (C.4) and integrating by parts, we can check that the right hand side vanishes. Thus, the action is invariant under the transformation. Notice this gauge symmetry originates from the diffeomorphism invariance of the Einstein gravity.

Massive field An equation of motion of a massive spin two field is given by adding a Fierz-Pauli mass term to the massless field equation,

$$X_{\mu\nu} = D_{\rho}D^{\rho}\phi_{\mu\nu} - D_{\mu}D^{\rho}\phi_{\rho\nu} - D_{\nu}D^{\rho}\phi_{\rho\mu} + D_{\mu}D_{\nu}\phi + g_{\mu\nu}\left(D_{\rho}D_{\sigma}\phi^{\rho\sigma} - D_{\rho}D^{\rho}\phi\right)$$
$$-2H^{2}\left(\phi_{\mu\nu} + \frac{1}{2}\phi g_{\mu\nu}\right) - m^{2}(\phi_{\mu\nu} - \phi g_{\mu\nu}) = 0 \tag{C.6}$$

Similarly to the massless fields, $\mu=0$ or $\nu=0$ components of Eq. (C.6) have no second time derivative. Hence, these are constraint equations. The divergence of the constraints also requires a constraint,

$$D^{\nu}X_{\mu\nu} = m^2(D^{\nu}\phi_{\nu\mu} - D_{\mu}\phi) = 0, \qquad (C.7)$$

Furthermore, the divergence of the constraint (C.7) requires an additional constraint, ¹

$$D^{\mu}D^{\nu}X_{\nu\mu} - m^2g^{\mu\nu}X_{\mu\nu} = m^2(m^2 - 2H^2)\phi = 0.$$
 (C.8)

The constrains for $m^2 \neq 0, H^2$ are summarized as

$$\phi = 0 \,, \quad D^{\mu} \phi_{\mu\nu} = 0 \,.$$
 (C.9)

$$R_{\mu\nu\rho\sigma} = \frac{1}{H^2} (g_{\mu\rho}g_{\nu\sigma} - g_{\mu\sigma}g_{\nu\rho}) \,,$$

and the identities of the covariant derivatives, e.g.

$$[D_{\mu}, D_{\nu}]\phi_{\rho\sigma} = R_{\mu\nu\rho}{}^{\lambda}\phi_{\lambda\sigma} + R_{\mu\nu\sigma}{}^{\lambda}\phi_{\rho\lambda}.$$

¹To derive Eqs. (C.7)-(C.8), it is convenient to use the Riemann curvature,

C.2. GENERAL SPIN 89

The above constraints reduce ten degrees of freedom of a rank two symmetric tensor to five, which is the appropriate number for spin two fields. Under the transverse and traceless condition, Eq. (C.6) is simplified to

$$D_{\rho}D^{\rho}\phi_{\mu\nu} - (2H^2 + m^2)\phi_{\mu\nu} = 0. \tag{C.10}$$

We note that Eqs. (C.7) and (C.8) become trivial if $m^2 = 0$ or $m^2 = 2H^2$, which implies that the system has a gauge symmetry. The massless case was studied in the last paragraph. In the $m^2 = 2H^2$ case, an action is invariant under a gauge symmetry,

$$\delta\phi_{\mu\nu} = \left(D_{\mu}D_{\nu} + m^2 g_{\mu\nu}\right)\omega\,,\tag{C.11}$$

where ω is an arbitrary scalar. ² This gauge symmetry is small compared to the massless case. Hence, the spin two field with the mass squared $2H^2$ is called a partially massless field. For simplicity, we do not consider the massless and partially massless fields in the rest of this section.

C.2 General spin

Let us determine a field equation and an action for higher spin fields of general spin by utilizing a higher spin gauge symmetry. First, we study a flat space background. Because it is complicated to consider an entire gauge symmetry, we begin with a partially gauge-fixed situation, where fields are double traceless. Second, we extend it to maximally symmetric spacetime, which is de Sitter space for a positive curvature and is anti-de Sitter space for a negative curvature. The main difference is a mass term due to a coupling with curvature tensors. The coefficients are also fixed by the higher spin gauge symmetry. Finally, By addint a mass term and applying the Fierz-Pauli condition, we obtain the field equations of massive higher spin fields (3.32).

Flat space Let us start with a flat space background. A gauge transformation for spin S fields is given by

$$\delta\Phi_{\mu_1\cdots\mu_S} = \partial_{(\mu_1}\Lambda_{\mu_2\cdots\mu_S)}, \qquad (C.13)$$

where $\Lambda_{\mu_1\cdots\mu_{S-1}}$ is an arbitrary function. In general, $\Phi_{\mu_1\cdots\mu_S}$ is just symmetric, and hence possible terms of an action are considerable. To avoid this complexity, first we fix the gauge symmetry partially such that the field is double-traceless,

$$\eta^{\mu_1 \mu_2} \eta^{\mu_3 \mu_4} \Phi_{\mu_1 \cdots \mu_S} = \text{perm} = 0.$$
 (C.14)

The perm means a permutation for the indices. The residual gauge symmetry is given by

$$\eta^{\mu_1 \mu_2} \Lambda_{\mu_1 \cdots \mu_{S-1}} = \text{perm} = 0.$$
(C.15)

$$\delta S = \int \sqrt{-g} X^{\mu\nu} \cdot \left(D_{\mu} D_{\nu} + m^2 g_{\mu\nu} \right) \omega = -\int \sqrt{-g} \left(D_{\mu} D_{\nu} - m^2 g_{\mu\nu} \right) X^{\mu\nu} \cdot \omega . \tag{C.12}$$

In the partially massless case, $\delta S=0$ because $\left(D_{\mu}D_{\nu}-2H^{2}g_{\mu\nu}\right)X^{\mu\nu}=0$.

²Under the gauge transformation (C.11), the action varies as

A generic action for double-traceless fields can be written as

$$S = -\frac{1}{2} \int d^d x \sqrt{-g} \, \Phi^{\mu_1 \cdots \mu_S} \, X_{\mu_1 \cdots \mu_S} \,,$$

where $X_{\mu_1 \dots \mu_s}$ is

$$X_{\mu_{1} \dots \mu_{s}} = \partial^{2} \Phi_{\mu_{1} \dots \mu_{S}} + A \partial_{(\mu_{1}} \partial^{\nu} \Phi_{\mu_{2} \dots \mu_{S}) \nu} + B g_{(\mu_{1} \mu_{2}} \partial^{2} \Phi_{\mu_{3} \dots \mu_{S}) \nu}^{\nu} + C g_{(\mu_{1} \mu_{2}} \partial_{\mu_{3}} \partial^{\nu} \Phi_{\mu_{4} \dots \mu_{S}) \nu \rho}^{\rho} + D g_{(\mu_{1} \mu_{2}} \partial^{\rho} \partial^{\sigma} \Phi_{\mu_{3} \dots \mu_{S}) \rho \sigma} + D \partial_{(\mu_{1}} \partial_{\mu_{2}} \Phi_{\mu_{3} \dots \mu_{S}) \nu}^{\mu}.$$
 (C.16)

Notice that we can take the same coefficient for the last two terms because they are equivalent up to a total derivative. A field equation is given by

$$X_{\mu_1 \cdots \mu_S} = 0. \tag{C.17}$$

Let us fix the coefficients by demanding that the action is invariant under the gauge transformation. A variation of the action is given by

$$\delta S = -\int d^d x \,\,\partial^{(\mu_1} \Lambda^{\mu_2 \cdots \mu_S)} \,\, X_{\mu_1 \cdots \mu_S} = \int d^d x \,\,\Lambda^{\mu_2 \cdots \mu_S} \,\,\partial^{\mu_1} X_{\mu_1 \mu_2 \cdots \mu_S} \,. \tag{C.18}$$

Hence the gauge invariance is equivalent to the divergence free condition of $X_{\mu_1 \mu_2 \dots \mu_S}$. The divergent term is calculated as

$$\partial^{\mu_1} X_{\mu_1 \mu_2 \cdots \mu_S} = \left(1 + \frac{A}{S}\right) \partial^2 \partial^{\nu} \Phi_{\mu_2 \cdots \mu_S \nu} + \left(\frac{S - 1}{S} A + \frac{2}{S} D\right) \partial^{\nu} \partial^{\rho} \partial_{(\mu_2} \Phi_{\mu_3 \cdots \mu_S) \nu \rho}$$

$$+ \frac{2}{S} (B + D) \partial_{(\mu_2} \partial^2 \Phi_{\mu_3 \cdots \mu_S) \nu}^{\nu} + \left(\frac{2}{S} C + \frac{S - 2}{S} D\right) \partial_{(\mu_2} \partial_{\mu_3} \partial^{\rho} \Phi_{\mu_4 \cdots \mu_S) \rho \nu}^{\nu} + \cdots, \qquad (C.19)$$

where we neglected terms which have indices of the metric, e.g.,

$$g_{(\mu_1 \,\mu_2} \partial^{\rho} \partial^{\sigma} \Phi_{\mu_3 \,\cdots \,\mu_S) \rho \sigma} \,. \tag{C.20}$$

These terms do not contribute to the variation (C.18) since the gauge parameter $\Lambda_{\mu_1 \dots \mu_S}$ is traceless. For the action to be gauge invariant, the coefficients should be

$$A = -S, \quad B = -\frac{S(S-1)}{2}, \quad C = -\frac{S(S-1)(S-2)}{4}, \quad D = \frac{S(S-1)}{2}.$$
 (C.21)

Curved background In the curved background, we have to include a coupling with curvature tensors even in the massless case. Here, we consider a maximally symmetric space for simplicity, where the Riemann tensor becomes

$$R_{\mu\nu\rho\sigma} = \frac{R}{d-2} \left(g_{\mu\rho} g_{\nu\sigma} - g_{\mu\sigma} g_{\nu\rho} \right) . \tag{C.22}$$

In particular, for de Sitter space,

$$R = H^2 d(d-1). (C.23)$$

C.2. GENERAL SPIN 91

Similarly to the flat space case, we study the double-traceless field,

$$g^{\mu_1 \mu_2} g^{\mu_3 \mu_4} \Phi_{\mu_1 \dots \mu_S} = \text{perm} = 0.$$
 (C.24)

The gauge transformation is given by

$$\delta\Phi_{\mu_1\cdots\mu_S} = D_{(\mu_1}\Lambda_{\mu_2\cdots\mu_S)}, \tag{C.25}$$

where $\Lambda_{\mu_1 \dots \mu_{S-1}}$ is traceless,

$$g^{\mu_1\mu_2}\Lambda_{\mu_1\cdots\mu_{S-1}} = \text{perm} = 0.$$
 (C.26)

A meaning of perm is the same as the flat space case. A generic action of the double-traceless field is given by

$$S = -\frac{1}{2} \int d^d x \sqrt{-g} \, \Phi^{\mu_1 \cdots \mu_S} \, X_{\mu_1 \cdots \mu_S} \,,$$

where $X_{\mu_1 \cdots \mu_s}$ is

$$X_{\mu_{1} \dots \mu_{s}} = D^{2} \Phi_{\mu_{1} \dots \mu_{S}} - SD_{(\mu_{1}} D^{\nu} \Phi_{\mu_{2} \dots \mu_{S}) \nu} - \frac{S(S-1)}{2} g_{(\mu_{1} \mu_{2}} D^{2} \Phi_{\mu_{3} \dots \mu_{S}) \nu}^{\nu}$$

$$- \frac{S(S-1)(S-2)}{4} g_{(\mu_{1} \mu_{2}} D_{\mu_{3}} D^{\nu} \Phi_{\mu_{4} \dots \mu_{S}) \nu \rho}^{\rho} + \frac{S(S-1)}{2} g_{(\mu_{1} \mu_{2}} D^{\rho} D^{\sigma} \Phi_{\mu_{3} \dots \mu_{S}) \rho \sigma}$$

$$+ \frac{S(S-1)}{2} D_{(\mu_{1}} D_{\mu_{2}} \Phi_{\mu_{3} \dots \mu_{S}) \nu}^{\mu} + Z_{1} R \Phi_{\mu_{1} \dots \mu_{S}} + Z_{2} R g_{(\mu_{1} \mu_{2}} \Phi_{\mu_{3} \dots \mu_{S}) \nu}^{\nu}. \tag{C.27}$$

We chose the parameters as this action reduces to Eq. (C.16) in the flat space limit. The two terms proportional to the curvature cannot be fixed, which are determined by the gauge invariance. A variation of the action becomes

$$\delta S = \int d^d x \, \Lambda^{\mu_2 \cdots \mu_S} \, D^{\mu_1} X_{\mu_1 \, \mu_2 \cdots \mu_S} \,. \tag{C.28}$$

Hence the gauge invariance is equivalent to the divergent free condition of $X_{\mu_1 \mu_2 \cdots \mu_S}$. The divergent is calculated as,

$$D^{\mu_1} X_{\mu_1 \mu_2 \dots \mu_S} = \left(Z_1 + \frac{S^2 + S(d-6) - 2d + 6}{d(d-1)} \right) D^{\mu_1} \Phi_{\mu_1 \mu_2 \dots \mu_S} + \left(Z_2 + \frac{S(S-1)}{d(d-1)} \right) R D_{(\mu_2} \Phi_{\mu_3 \dots \mu_S)\nu}^{\nu}$$
 (C.29)

For the action to be invariant under the transformation (C.25), the coefficients should be

$$Z_1 = -\frac{S^2 + S(d-6) - 2d + 6}{d(d-1)}, \quad Z_2 = -\frac{S(S-1)}{d(d-1)}.$$
 (C.30)

A field equation of massless higher spin fields is $X_{\mu_1...\mu_S}$. By fixing the gauge as the field is symmetric, traceless and transverse, and adding a mass term, we can yield a field equation of massive higher spin fields (3.30),

$$[D_{\mu}D^{\mu} + H^{2}(S^{2} + (d-6)S - 2d + 6) - m^{2}] \Phi_{\mu_{1} \cdots \mu_{S}} = 0.$$
 (C.31)

Appendix D

Details of spiky strings with internal motion

In this appendix, we summarize details of spiky strings with internal motion.

D.1 Derivation of Eq. (5.30)

We begin by providing a derivation of Eq. (5.30). For this, it is convenient to note the following relation which follows from Eq. (5.29):

$$\omega Nr + \nu \psi' = N \lambda r_S r \frac{(1 - \nu^2) - (1 + \omega^2)r}{r_S - r},$$
(D.1)

where we defined

$$r_S = \frac{1}{1 + \lambda \omega} \,. \tag{D.2}$$

Substituting this into Eq. (5.27) gives

$$\mathcal{D} = \frac{(\omega N r + \nu \psi')^2 (1 - r)^2}{C^2} = \frac{N^2 \lambda^2 r_S^2}{C^2} \cdot \frac{r^2 (1 - r)^2}{(r_S - r)^2} \cdot \left((1 - \nu^2) - (1 + \omega^2) r \right)^2. \tag{D.3}$$

On the other hand, we can reformulate Eq. (4.15) using Eq. (5.29) as

$$\mathcal{D} = ((1 - \nu^2) - (1 + \omega^2)r) \left(\rho'^2 - \frac{N^2 r_S^2}{\nu^2} \cdot \frac{r(1 - r)}{(r_S - r)^2} \cdot F(r)\right), \tag{D.4}$$

where F(r) is a quadratic polynomial defined by

$$F(r) = (\lambda - \omega)^2 r^2 + ((1 + \lambda^2)\nu^2 - (\lambda - \omega)^2) r - \nu^2.$$
 (D.5)

Comparing Eq. (D.3) and Eq. (D.4) gives

$$\rho'^{2} = \frac{N^{2} \lambda^{2} r_{S}^{2}}{C^{2}} \cdot \frac{r(1-r)}{(r_{S}-r)^{2}} \cdot \left[r(r-1) \left((1+\omega^{2})r - (1-\nu^{2}) \right) + \frac{C^{2}}{\lambda^{2} \nu^{2}} F(r) \right]. \tag{D.6}$$

 $D.2. \quad J = 0 \text{ LIMIT}$

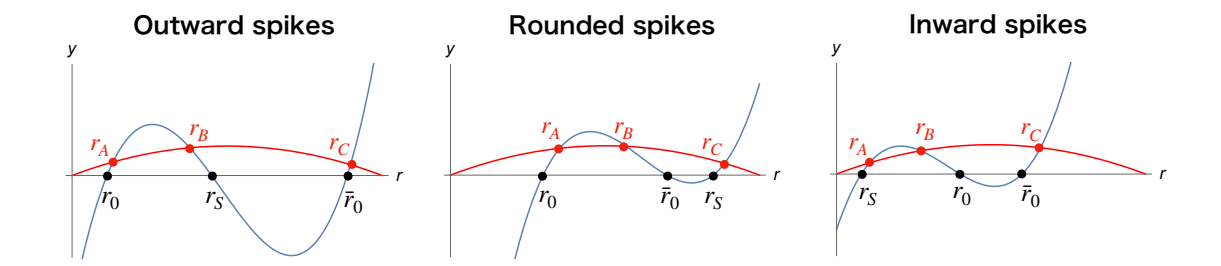


Figure D.1: The blue curves are $y=(r-r_S)\left(r^2-r+\frac{C^2}{\omega^2}\right)$, which intersect with the r-axis at $r=r_0,\bar{r}_0,r_S$. The red curves are $y=\nu^2r_Sr(1-r)$. The intersection points of the blue and red curves are the three solutions $r_{A,B,C}$ of Eq. (D.10). In the limit $\nu\to 0$, the three solutions approach to r_0,\bar{r}_0,r_S , and the solutions in Sec. 4.3 are reproduced. For example, when $r_0< r_S<\bar{r}_0$, finite ν solutions with $r_A< r_B< r_S< r_C$ are reduced to the outward spike solutions.

Then, we conclude that

$$r'^{2} = 4r(1-r)\rho'^{2} = \frac{4N^{2}\lambda^{2}(1+\omega^{2})r_{S}^{2}}{C^{2}} \cdot \frac{r^{2}(1-r)^{2}}{(r_{S}-r)^{2}} \cdot \left[r^{3} + \widetilde{F}(r)\right], \tag{D.7}$$

where $\widetilde{F}(r)$ is a quadratic polynomial defined by

$$\widetilde{F}(r) = \frac{1}{1+\omega^2} \left[-\left((1+\omega^2) + (1-\nu^2) \right) r^2 + (1-\nu^2) r + \frac{C^2}{\lambda^2 \nu^2} F(r) \right]. \tag{D.8}$$

This reproduces Eq. (5.30) by identifying $r_{A,B,C}$ with three solutions for $r^3 + \widetilde{F}(r) = 0$.

D.2 J = 0 limit

Finally, we discuss the limit where the internal charge vanishes J=0. First, the internal velocity ν and the internal space dependence ψ' of the string have to vanish to reproduce the solutions in Sec. 4.3. In particular, Eq. (5.29) shows that this is achieved in the limit

$$(\lambda - \omega)^2 \ll \nu^2 \ll 1. \tag{D.9}$$

Note that ψ' diverges if we take the limit $\nu^2 \ll (\lambda - \omega)^2 \ll 1$ instead. Then, let us study properties of $r_{A,B,C}$ for $\lambda = \omega$ with a finite ν . Under this assumption, the defining equation $r^3 + \widetilde{F}(r) = 0$ of $r_{A,B,C}$ is reduced to

$$(r - r_S)\left(r^2 - r + \frac{C^2}{\omega^2}\right) = \nu^2 r_S r (1 - r),$$
 (D.10)

where note that $r_S = (1 + \omega^2)^{-1}$ in the limit $\lambda = \omega$. If we further take the limit $\nu \to 0$, one of $r_{A,B,C}$ coincides with r_S . Therefore, the double pole at $r = r_S$ and one of three zeros collide and form a single pole at $r = r_S$, which is identified with a single pole of ρ'^2 at $\rho = \rho_1$ shown in Eq. (4.35).

To see how the limit $\nu \to 0$ reproduces the three classes of solutions in Sec. 4.3, let us parameterize the two solutions $r=r_0, \bar{r}_0$ for $r^2-r+\frac{C^2}{\omega^2}=0$ as

$$r_0 = \sin^2 \rho_0, \quad \bar{r}_0 = \sin^2(\frac{\pi}{2} - \rho_0) = \cos^2 \rho_0,$$
 (D.11)

where ρ_0 is identified with that in Sec. 4.3. Notice that we can employ this parameterization without loss of generality since $r_0 + \bar{r}_0 = 1$. Also, in order for r_0 and \bar{r}_0 to be real, $0 \le r_0 \bar{r}_0 = \frac{C^2}{\omega^2} \le \frac{1}{4}$ has to be satisfied, under which we can choose ρ_0 such that $0 \le \rho_0 \le \frac{\pi}{2}$. The classification in Sec. 4.3 is then rephrased as

- $r_0 < r_S < \bar{r}_0$: outward spike solutions,
- $r_0 < \bar{r}_0 < r_S$: rounded spike solutions,
- $r_S < r_0 < \bar{r}_0$: internal spike solutions.

As depicted in Fig. D.1, the outward spike solutions and rounded spike solutions are obtained in the limit $\nu \to 0$ of solutions with the ordering $r_A < r_B < r_C$, whereas the internal spike solutions are obtained from those with $r_S < r_A < r_B < r_C$.

Bibliography

- [1] J. Scherk and J. H. Schwarz, Dual Models for Nonhadrons, Nucl. Phys. B 81 (1974) 118–144.
- [2] T. Yoneya, Connection of Dual Models to Electrodynamics and Gravidynamics, Prog. Theor. Phys. 51 (1974) 1907–1920.
- [3] E. D'Hoker and D. H. Phong, Loop Amplitudes for the Fermionic String, Nucl. Phys. B 278 (1986) 225–241.
- [4] E. D'Hoker and D. H. Phong, Multiloop Amplitudes for the Bosonic Polyakov String, Nucl. Phys. B 269 (1986) 205–234.
- [5] A. Strominger and C. Vafa, *Microscopic origin of the Bekenstein-Hawking entropy*, Phys. Lett. B **379** (1996) 99–104 [hep-th/9601029].
- [6] Supernova Cosmology Project Collaboration, S. Perlmutter et al., Measurements of Ω and Λ from 42 high redshift supernovae, Astrophys. J. 517 (1999) 565–586 [astro-ph/9812133].
- [7] Planck Collaboration, N. Aghanim et al., Planck 2018 results. VI. Cosmological parameters, Astron. Astrophys. 641 (2020) A6 [1807.06209], [Erratum: Astron.Astrophys. 652, C4 (2021)].
- [8] W. J. Percival, B. A. Reid, D. J. Eisenstein, N. A. Bahcall, T. Budavari, J. A. Frieman, M. Fukugita, J. E. Gunn, Ž. Ivezić, G. R. Knapp, R. G. Kron, J. Loveday, R. H. Lupton, T. A. McKay, A. Meiksin, R. C. Nichol, A. C. Pope, D. J. Schlegel, D. P. Schneider, D. N. Spergel, C. Stoughton, M. A. Strauss, A. S. Szalay, M. Tegmark, M. S. Vogeley, D. H. Weinberg, D. G. York and I. Zehavi, Baryon acoustic oscillations in the Sloan Digital Sky Survey Data Release 7 galaxy sample, Monthly Notices of the Royal Astronomical Society 401 (01, 2010) 2148–2168 [https://academic.oup.com/mnras/article-pdf/401/4/2148/3901461/mnras0401-2148.pdf].
- [9] J. M. Maldacena and C. Nunez, Supergravity description of field theories on curved manifolds and a no go theorem, Int. J. Mod. Phys. A 16 (2001) 822–855 [hep-th/0007018].
- [10] S. B. Giddings, S. Kachru and J. Polchinski, Hierarchies from fluxes in string compactifications, Phys. Rev. D 66 (2002) 106006 [hep-th/0105097].
- [11] S. Kachru, R. Kallosh, A. D. Linde and S. P. Trivedi, *De Sitter vacua in string theory*, Phys. Rev. D **68** (2003) 046005 [hep-th/0301240].

[12] V. Balasubramanian, P. Berglund, J. P. Conlon and F. Quevedo, Systematics of moduli stabilisation in Calabi-Yau flux compactifications, JHEP **03** (2005) 007 [hep-th/0502058].

- [13] I. Bena, M. Grana and N. Halmagyi, On the Existence of Meta-stable Vacua in Klebanov-Strassler, JHEP 09 (2010) 087 [0912.3519].
- [14] I. Bena, A. Buchel and O. J. C. Dias, Horizons cannot save the Landscape, Phys. Rev. D 87 (2013), no. 6, 063012 [1212.5162].
- [15] I. Bena, M. Graña, S. Kuperstein and S. Massai, *Tachyonic Anti-M2 Branes*, JHEP **06** (2014) 173 [1402.2294].
- [16] I. Bena and S. Kuperstein, Brane polarization is no cure for tachyons, JHEP 09 (2015) 112 [1504.00656].
- [17] I. Bena, J. Blåbäck and D. Turton, Loop corrections to the antibrane potential, JHEP **07** (2016) 132 [1602.05959].
- [18] J. Blaback, U. H. Danielsson and T. Van Riet, Resolving anti-brane singularities through time-dependence, JHEP **02** (2013) 061 [1202.1132].
- [19] F. F. Gautason, D. Junghans and M. Zagermann, Cosmological Constant, Near Brane Behavior and Singularities, JHEP **09** (2013) 123 [1301.5647].
- [20] A. K. Kohara, E. Ferreira and T. Kodama, pp interactions in extended air showers, EPJ Web Conf. 99 (2015) 10002 [1410.8467].
- [21] B. Michel, E. Mintun, J. Polchinski, A. Puhm and P. Saad, Remarks on brane and antibrane dynamics, JHEP 09 (2015) 021 [1412.5702].
- [22] U. H. Danielsson, F. F. Gautason and T. Van Riet, Unstoppable brane-flux decay of $\overline{D6}$ branes, JHEP **03** (2017) 141 [1609.06529].
- [23] D. Cohen-Maldonado, J. Diaz, T. van Riet and B. Vercnocke, *Observations on fluxes near anti-branes*, JHEP **01** (2016) 126 [1507.01022].
- [24] D. Cohen-Maldonado, J. Diaz and F. F. Gautason, *Polarised antibranes from Smarr relations*, JHEP **05** (2016) 175 [1603.05678].
- [25] J. Moritz, A. Retolaza and A. Westphal, Toward de Sitter space from ten dimensions, Phys. Rev. D 97 (2018), no. 4, 046010 [1707.08678].
- [26] S. Sethi, Supersymmetry Breaking by Fluxes, JHEP 10 (2018) 022 [1709.03554].
- [27] U. H. Danielsson and T. Van Riet, What if string theory has no de Sitter vacua?, Int. J. Mod. Phys. D 27 (2018), no. 12, 1830007 [1804.01120].
- [28] G. Obied, H. Ooguri, L. Spodyneiko and C. Vafa, *De Sitter Space and the Swampland*, 1806.08362.

[29] S. K. Garg and C. Krishnan, Bounds on Slow Roll and the de Sitter Swampland, JHEP 11 (2019) 075 [1807.05193].

- [30] H. Ooguri, E. Palti, G. Shiu and C. Vafa, Distance and de Sitter Conjectures on the Swampland, Phys. Lett. B 788 (2019) 180–184 [1810.05506].
- [31] A. Higuchi, Forbidden Mass Range for Spin-2 Field Theory in De Sitter Space-time, Nucl. Phys. B 282 (1987) 397–436.
- [32] H. J. de Vega and N. G. Sanchez, A New Approach to String Quantization in Curved Space-Times, Phys. Lett. B 197 (1987) 320–326.
- [33] H. J. de Vega and N. G. Sanchez, Quantum Dynamics of Strings in Black Hole Space-times, Nucl. Phys. B 309 (1988) 552–576.
- [34] F. Combes, H. J. de Vega, A. V. Mikhailov and N. G. Sanchez, Multistring solutions by soliton methods in de Sitter space-time, Phys. Rev. D 50 (1994) 2754–2768 [hep-th/9310073].
- [35] H. J. de Vega, A. L. Larsen and N. G. Sanchez, Semiclassical quantization of circular strings in de Sitter and anti-de Sitter space-times, Phys. Rev. D 51 (1995) 6917–6928 [hep-th/9410219].
- [36] H. de Vega and I. Egusquiza, Planetoid string solutions in (3+1) axisymmetric space-times, Phys. Rev. D **54** (1996) 7513–7519 [hep-th/9607056].
- [37] J. M. Maldacena, The Large N limit of superconformal field theories and supergravity, Int. J. Theor. Phys. 38 (1999) 1113–1133 [hep-th/9711200], [Adv. Theor. Math. Phys.2,231(1998)].
- [38] S. Gubser, I. Klebanov and A. M. Polyakov, A Semiclassical limit of the gauge / string correspondence, Nucl. Phys. B 636 (2002) 99–114 [hep-th/0204051].
- [39] A. A. Tseytlin, Review of AdS/CFT Integrability, Chapter II.1: Classical AdS5xS5 string solutions, Lett. Math. Phys. 99 (2012) 103–125 [1012.3986].
- [40] D. E. Berenstein, J. M. Maldacena and H. S. Nastase, *Strings in flat space and pp waves from N=4 superYang-Mills*, JHEP **04** (2002) 013 [hep-th/0202021].
- [41] S. Frolov and A. A. Tseytlin, Semiclassical quantization of rotating superstring in AdS(5) x S**5, JHEP **06** (2002) 007 [hep-th/0204226].
- [42] J. A. Minahan, Circular semiclassical string solutions on AdS(5) x S(5), Nucl. Phys. B 648 (2003) 203–214 [hep-th/0209047].
- [43] S. Frolov and A. A. Tseytlin, Multispin string solutions in AdS(5) x $S^{**}5$, Nucl. Phys. B **668** (2003) 77–110 [hep-th/0304255].
- [44] S. Frolov and A. A. Tseytlin, *Rotating string solutions: AdS / CFT duality in nonsupersymmetric sectors*, Phys. Lett. B **570** (2003) 96–104 [hep-th/0306143].

[45] J. Engquist, J. A. Minahan and K. Zarembo, Yang-Mills duals for semiclassical strings on $AdS(5) \times S(5)$, JHEP 11 (2003) 063 [hep-th/0310188].

- [46] G. Arutyunov, J. Russo and A. A. Tseytlin, Spinning strings in AdS(5) x S**5: New integrable system relations, Phys. Rev. D 69 (2004) 086009 [hep-th/0311004].
- [47] A. L. Larsen and A. Khan, Novel explicit multispin string solitons in AdS(5), Nucl. Phys. B **686** (2004) 75–84 [hep-th/0312184].
- [48] S. Ryang, Folded three spin string solutions in AdS(5) x S**5, JHEP **04** (2004) 053 [hep-th/0403180].
- [49] M. Kruczenski and A. A. Tseytlin, Semiclassical relativistic strings in S**5 and long coherent operators in N=4 SYM theory, JHEP **09** (2004) 038 [hep-th/0406189].
- [50] M. Kruczenski, Spiky strings and single trace operators in gauge theories, JHEP 08 (2005) 014 [hep-th/0410226].
- [51] S. Ryang, Wound and rotating strings in AdS(5) x S**5, JHEP **08** (2005) 047 [hep-th/0503239].
- [52] I. Y. Park, A. Tirziu and A. A. Tseytlin, Semiclassical circular strings in AdS(5) and 'long' gauge field strength operators, Phys. Rev. D 71 (2005) 126008 [hep-th/0505130].
- [53] D. M. Hofman and J. M. Maldacena, Giant Magnons, J. Phys. A 39 (2006) 13095–13118 [hep-th/0604135].
- [54] N. Dorey, Magnon Bound States and the AdS/CFT Correspondence, J. Phys. A **39** (2006) 13119–13128 [hep-th/0604175].
- [55] T. McLoughlin and X. Wu, Kinky Strings in AdS(5) X S**5, JHEP 08 (2006) 063 [hep-th/0604193].
- [56] H.-Y. Chen, N. Dorey and K. Okamura, Dyonic giant magnons, JHEP 09 (2006) 024 [hep-th/0605155].
- [57] G. Arutyunov, S. Frolov and M. Zamaklar, Finite-size Effects from Giant Magnons, Nucl. Phys. B 778 (2007) 1–35 [hep-th/0606126].
- [58] J. A. Minahan, A. Tirziu and A. A. Tseytlin, Infinite spin limit of semiclassical string states, JHEP 08 (2006) 049 [hep-th/0606145].
- [59] M. Spradlin and A. Volovich, Dressing the Giant Magnon, JHEP 10 (2006) 012 [hep-th/0607009].
- [60] N. P. Bobev and R. C. Rashkov, Multispin Giant Magnons, Phys. Rev. D 74 (2006) 046011 [hep-th/0607018].
- [61] M. Kruczenski, J. Russo and A. A. Tseytlin, Spiky strings and giant magnons on S**5, JHEP 10 (2006) 002 [hep-th/0607044].

[62] K. Okamura and R. Suzuki, A Perspective on Classical Strings from Complex Sine-Gordon Solitons, Phys. Rev. D 75 (2007) 046001 [hep-th/0609026].

- [63] S. Ryang, Three-spin giant magnons in AdS(5) x S**5, JHEP 12 (2006) 043 [hep-th/0610037].
- [64] R. Ishizeki and M. Kruczenski, Single spike solutions for strings on S^{**2} and S^{**3} , Phys. Rev. D **76** (2007) 126006 [0705.2429].
- [65] A. E. Mosaffa and B. Safarzadeh, Dual spikes: New spiky string solutions, JHEP 08 (2007) 017 [0705.3131].
- [66] H. Hayashi, K. Okamura, R. Suzuki and B. Vicedo, Large Winding Sector of AdS/CFT, JHEP 11 (2007) 033 [0709.4033].
- [67] R. Ishizeki, M. Kruczenski, M. Spradlin and A. Volovich, Scattering of single spikes, JHEP 02 (2008) 009 [0710.2300].
- [68] A. Mikhailov and S. Schafer-Nameki, Sine-Gordon-like action for the Superstring in AdS(5) $x S^{**}5$, JHEP **05** (2008) 075 [0711.0195].
- [69] A. Jevicki, K. Jin, C. Kalousios and A. Volovich, Generating AdS String Solutions, JHEP 03 (2008) 032 [0712.1193].
- [70] M. Kruczenski and A. A. Tseytlin, Spiky strings, light-like Wilson loops and pp-wave anomaly, Phys. Rev. D 77 (2008) 126005 [0802.2039].
- [71] A. Jevicki and K. Jin, *Solitons and AdS String Solutions*, Int. J. Mod. Phys. A **23** (2008) 2289–2298 [0804.0412].
- [72] J. L. Miramontes, Pohlmeyer reduction revisited, JHEP 10 (2008) 087 [0808.3365].
- [73] S. Ryang, Conformal SO(2,4) Transformations for the Helical AdS String Solution, JHEP **05** (2008) 021 [0803.3855].
- [74] M. C. Abbott and I. V. Aniceto, Vibrating giant spikes and the large-winding sector, JHEP **06** (2008) 088 [0803.4222].
- [75] R. Ishizeki, M. Kruczenski, A. Tirziu and A. A. Tseytlin, *Spiky strings in AdS(3) x S1 and their AdS-pp-wave limits*, Phys. Rev. D **79** (2009) 026006 [0812.2431].
- [76] T. J. Hollowood and J. L. Miramontes, Magnons, their Solitonic Avatars and the Pohlmeyer Reduction, JHEP **04** (2009) 060 [0902.2405].
- [77] A. Jevicki and K. Jin, Moduli Dynamics of AdS(3) Strings, JHEP 06 (2009) 064 [0903.3389].
- [78] A. Tirziu and A. A. Tseytlin, Semiclassical rigid strings with two spins in AdS(5), Phys. Rev. D 81 (2010) 026006 [0911.2417].

[79] M. Kruczenski and A. Tirziu, Spiky strings in Bethe Ansatz at strong coupling, Phys. Rev. D 81 (2010) 106004 [1002.4843].

- [80] T. Noumi, T. Takeuchi and S. Zhou, String Regge trajectory on de Sitter space and implications to inflation, 1907.02535.
- [81] M. Kato, K. Nishii, T. Noumi, T. Takeuchi and S. Zhou, Spiky strings in de Sitter space, JHEP 05 (2021) 047 [2102.09746].
- [82] M. Froissart, Asymptotic Behavior and Subtractions in the Mandelstam Representation, Phys. Rev. **123** (Aug, 1961) 1053–1057.
- [83] Y. Jin and A. Martin Phys. Rev. B **135** (1964) 1375.
- [84] A. Martin, Extension of the axiomatic analyticity domain of scattering amplitudes by unitarity. 1., Nuovo Cim. A 42 (1965) 930–953.
- [85] S. Weinberg, Critical Phenomena for Field Theorists, pp. 1–52. Springer US, Boston, MA, 1978.
- [86] C.-S. Chu and D. Giataganas, Thermal bath in de Sitter space from holography, Phys. Rev. D 96 (2017), no. 2, 026023 [1608.07431].
- [87] H. de Vega, A. Larsen and N. G. Sanchez, Infinitely many strings in de Sitter space-time: Expanding and oscillating elliptic function solutions, Nucl. Phys. B **427** (1994) 643–668 [hep-th/9312115].
- [88] M. Hazumi et al., LiteBIRD: A Satellite for the Studies of B-Mode Polarization and Inflation from Cosmic Background Radiation Detection, J. Low Temp. Phys. 194 (2019), no. 5-6, 443–452.
- [89] Y. Kazama, S. Komatsu and T. Nishimura, Classical Integrability for Three-point Functions: Cognate Structure at Weak and Strong Couplings, JHEP 10 (2016) 042 [1603.03164], [Erratum: JHEP 02, 047 (2018)].
- [90] Y. Kazama and S. Komatsu, Three-point functions in the SU(2) sector at strong coupling, JHEP 03 (2014) 052 [1312.3727].
- [91] J. Caetano and J. Toledo, χ -systems for correlation functions, JHEP **01** (2019) 050 [1208.4548].
- [92] Y. Kazama and S. Komatsu, On holographic three point functions for GKP strings from integrability, JHEP 01 (2012) 110 [1110.3949], [Erratum: JHEP 06, 150 (2012)].
- [93] R. A. Janik and A. Wereszczynski, Correlation functions of three heavy operators: The AdS contribution, JHEP 12 (2011) 095 [1109.6262].
- [94] M. S. Costa, R. Monteiro, J. E. Santos and D. Zoakos, On three-point correlation functions in the gauge/gravity duality, JHEP 11 (2010) 141 [1008.1070].

[95] K. Zarembo, Holographic three-point functions of semiclassical states, JHEP **09** (2010) 030 [1008.1059].

- [96] M. Gary, S. B. Giddings and J. Penedones, Local bulk S-matrix elements and CFT singularities, Phys. Rev. D 80 (2009) 085005 [0903.4437].
- [97] T. Okuda and J. Penedones, String scattering in flat space and a scaling limit of Yang-Mills correlators, Phys. Rev. D 83 (2011) 086001 [1002.2641].
- [98] J. Penedones, Writing CFT correlation functions as AdS scattering amplitudes, JHEP **03** (2011) 025 [1011.1485].
- [99] S. Raju, New Recursion Relations and a Flat Space Limit for AdS/CFT Correlators, Phys. Rev. D85 (2012) 126009 [1201.6449].
- [100] M. S. Costa, V. Goncalves and J. Penedones, Conformal Regge theory, JHEP 12 (2012) 091 [1209.4355].
- [101] J. Maldacena, D. Simmons-Duffin and A. Zhiboedov, Looking for a bulk point, JHEP **01** (2017) 013 [1509.03612].
- [102] P. Haldar and A. Sinha, Froissart bound for/from CFT Mellin amplitudes, SciPost Phys. 8 (2020) 095 [1911.05974].
- [103] D. Meltzer, AdS/CFT Unitarity at Higher Loops: High-Energy String Scattering, JHEP **05** (2020) 133 [1912.05580].
- [104] S. Komatsu, M. F. Paulos, B. C. Van Rees and X. Zhao, *Landau diagrams in AdS and S-matrices from conformal correlators*, JHEP **11** (2020) 046 [2007.13745].
- [105] D. Chandorkar, S. D. Chowdhury, S. Kundu and S. Minwalla, Bounds on Regge growth of flat space scattering from bounds on chaos, 2102.03122.
- [106] N. Arkani-Hamed and J. Maldacena, Cosmological Collider Physics, 1503.08043.
- [107] N. Arkani-Hamed, P. Benincasa and A. Postnikov, Cosmological Polytopes and the Wavefunction of the Universe, 1709.02813.
- [108] C. R. Frye and C. J. Efthimiou, Spherical Harmonics in p Dimensions, 1205.3548.